NTNU – Trondheim
Norwegian University of
Science and Technology

Permeability, Growth and Morphology of Coastal Ice

Site Study in Van Mijenfjorden, Svalbard

Bård Blæsterdalen

MSc in Physics
Submission date: May 2015
Supervisor: Patrick Joseph Espy, IFY

Norwegian University of Science and Technology
Department of Physics

Preface

This thesis is the fulfillment of my master's degree in Physics at NTNU (the Norwegian University of Science and Technology). The entire work connected to the thesis has been conducted on Svalbard during the two spring semesters of 2014 and 2015. The writing and programming was done at UNIS (the University Centre in Svalbard), and the collection of data on the sea ice in Van Mijenfjorden. The experiments done in the field were conducted together with David Wrangborg and Carl Magnus Vindegg, who were working with their PhD and MsC theses, respectively. The experiments were done as a part of the SAMCoT (Sustainable Arctic Marine and Coastal Technology) project. This thesis would be suitable reading for engineers and scientists working with sea ice, but attempts have been made to make it understandable for students down to bachelor level within Arctic Technology and Geophysics.

By the end of my master's, there are several who deserve acknowledgments. First of all, I will thank my supervisors, Patrick Joseph Espy, Aleksey V Marchenko and Knut Vilhelm Høyland. I'm most grateful to Knut, who has provided very helpful feedback during the whole process, and also because he saved me from the dungeons of NTNU, sending me to the stunning island of Spitsbergen instead.

A special thank to the two Arctic cowboys Calle and David, whom I had the pleasure to work with during half a year of field-trips to Svea, and to Store Norske Spitsbergen Grubekompani which provided excellent food and lodging when we stayed there. Thanks also to the University Centre in Svalbard for two and a half years of academical rock 'n roll towards the end of my studies. Last but not least, I will mention the people in and around Barrack 4, and our nine Alaskan huskies, those who made the time after school hours something to remember for a lifetime.

I will end this preface by quoting Kjell Reidar Hovelsrud, who has spent more than 20 years as a trapper on Svalbard, and therefore knows what he is talking about (unfortunately it is in untranslatable Norwegian):

> *"Det er forskjell på teori og pakk-is."*

Longyearbyen, May 15th, 2015

Bård Blæsterdalen

Abstract

Coastal ice includes the parts of the sea ice that are stressed and deformed by tidal motion; the *ice foot* (the inner part that is frozen to the ground) and the *hinge zone* (the zone where cracking occurs due to tidal elevation of the floating ice). This thesis presents in situ measurements of first-year coastal ice conducted in a sound close to the head of the fjord Van Mijenfjorden, Svalbard, in the period between January and May 2014. During in total 6 field trips measurements of temperature, salinity, density, thickness and freeboard were done both on the coastal ice and on the free-floating ice. The latter was done at a point 200 m offshore.

Temperature oscillations with periods similar to the tides and amplitudes up to 0.5°C were found inside the ice in the hinge zone during a 10-days period, indicating a high permeability of the ice. Since the ice there was grounded at low tide and floating at high tide, the water level was constantly varying relative to the ice and could thereby drive a column of brine/seawater up and down through the ice cover. This observation corresponded well with the calculated average permeabilities, which were much higher before the temperature oscillations occurred ($2.3 \cdot 10^{-11}$ m^2) than after they had disappeared ($1.1 \cdot 10^{-11}$ m^2).

Freeboard and surface water measurements discovered buckling of the ice in the lower parts of the hinge zone, which varied with the tide. In May, the ice was clearly buckled at high tide and stretched out at low tide. Creation of new ice inside the tidal cracks, caused by inflow of water during the tidal cycle, and thermal expansion are factors suggested to cause elongation of the ice sheet. Since the shortest distance between two points is a straight line, the ice is more likely to be buckled at high tide than at low tide when it is lowered in the middle of the sound.

Maximum recorded amount of surface water was 18 cm, and through the season at least 20 cm of superimposed ice had been accumulating on the ice in the lower parts of the hinge zone. During cold periods, growth rates in the different parts of the ice varied; the ice foot was hardly growing at all, the free-floating ice was growing in moderate rates, whereas in the hinge zone the maximum growth was very high. The largest recorded ice thicknesses were 84 cm in the free-floating ice and 171 cm in the hinge zone. In the lower parts of the hinge zone the average ice temperatures were warmer than in the free-floating ice. Both the rapid growth and the temperature differences are expected to be caused by frequent flooding of the ice in the lower parts of the hinge zone, which often resulted in creation of a new layer of ice on top of the original layer. The release of latent heat connected to this process, in addition to direct heating by the warmer surface water, is believed to be the main reason for the warmer ice.

Also along the shore, large spatial variations in ice thickness were observed; two shore-perpendicular sections going across the hinge zone, 11 m from each other, showed that the maximum ice thickness differed with 70 cm. Mean salinities in the ice foot were relatively low, varying from 0.6 to 1.2 ppm, whereas in the hinge zone they varied between 4.9 and 7.2 ppm. In the free-floating ice, average salinities between 4.7 and 6.6 ppm were recorded.

Sammendrag

Kystis inluderer de delene av havisen som er stresset og deformert av tidevannsbevegelser; *landkallen* (den innerste delen, som er frosset fast i bakken) og *den aktive sonen* (sonen hvor isen sprekker opp på grunn av hevning og senkning av den flytende isen). Denne oppgaven presenterer feltbaserte målinger av kystis som er mindre enn ett år gammel, innerst i Van Mijenfjorden på Svalbard i tidaperioden Januar-Mai 2014. Iløpet av i alt 6 arbeidsøkter felt ble temperatur, salinitet, tetthet, tykkelse og fribord målt, både i kystisen og på et punkt 200 m fra land.

Temperaturevariasjoner med en periode lik tidevannsbølgen ble funnet i isen nær land. De var tydelige i rundt ti dager før de forsvant, og er en indikasjon på høy permeabiltet. Siden isen lå på grunn ved lavvann og var flytende ved høyvann der hvor dette ble målt, var vannivået konstant varierende i forhold til til isen og kunne dermed drive en søyle av saltlake/sjøvann opp og ned gjennom isen. Dette en observasjon som korrelerte godt med utregninger av gjenomsnittspermeabilitet, hvilke gav mye høyere verdier før temperaturvariasjonene ble synlige ($2.3{\cdot}10^{-11}$ m^2) enn etter at de forsvant ($2.3{\cdot}10^{-11}$ m^2).

Fribord- og overflatevannsmålinger viste at isen var bøyd nederst i den aktive sonen, slik at noen deler hadde fribord, mens andre hadde overflatevann. Denne bøyningen varierte med tidevannsnivået. I Mai var isen tydelig bøyd ved høyvann og strekt ut ved lavvann. Kontinuerlig dannelse av ny is inni tidevannsprekkene, forårsaket av tilsig av havvann, i tillegg til termal ekspansjon er foreslåtte faktorer som er troende til å utvide isen og dermed skape økt spenn, og derav bøyning. Det at isen vil "henge" ved lavvann og være horisontal ved høyvann er også et moment som tilsier at trykket vil være høyere ved høyvann.

Det ble målt opptil 18 cm overflatevann og tilsammen minst 20 cm isvekst oppover (dvs. is dannet av overflatevann) i nedre deler av den aktive sonen. I kalde perioder ble det målt varierende vekstrater; landkallen endret seg omtrent ikke i det hele tatt, den flytende isen vokste i moderat tempo mens i den aktive sonen ble høye vekstrater målt. Istykkelser på opptil 171 og 84 cm ble målt i henholdsvis den aktive sonen og den flytende isen. I den aktive sonen var temperaturene typisk varmere enn i den flytende isen. Den raskere veksten og den høyere temperaturen er sannsynligvis resultatet av overflatevann og isvekst oppover med resulterende varmekondusjon, både direkte og via frigjort latent varme, inn i isen.

Også paralellt med kysten ble det observert varierende istykkelser; to seksjoner som gikk normalt på kysten, 11 m fra hverandre, gav maksimale istykkelser som varierte med 70 cm. Gjenomsnitssaliniteter i landkallen var relativt lave og varierte mellom 0.6 og 1.2 ppm. I den aktive sonen ble saliniteter mellom 4.9 og 7.2 funnet, mens i den flytende isen ble gjennomsnittsaliniteter på mellom 4.7 og 6.6 funnet.

Contents

List of Figures

List of Tables

Chapter 1

Introduction

In recent years the scientific world has generally agreed that the Arctic sea ice is diminishing, observing significant decreases both in extent and thickness (Ragner, 2008). This trend is some places associated with great problems, such as the removal of an important arena for transportation or hunting in the winter season. Also, the sea ice decrease may be self-enhancing due to the related lowering of surface albedo in previously ice covered waters, causing radiation to be absorbed by the ocean rather than reflected back into the atmosphere (Notz, 2009). However, the decrease also opens possibilities. At present, the industry connected to production of hydrocarbons is pushing increasingly longer into Arctic regions. Although the burning of fossil fuels is considered to be the major cause of global warming (Johannessen et al., 2003), this evolution is likely to continue in the future, and will require both offshore and coastal structures which can resist ice forces. If the observed trend of decreasing sea ice extent in the Arctic is continuing, the northern sea routes will eventually become commercially viable. One such route is commonly known as the *Northeast Passage*, going through the waters north of Russia and being a shortcut that may bring about a revolution in sea trade between Europe and East Asia, saving up to 50% of the travel distance compared to the currently used shipping routes via Suez or Panama (Ragner, 2008). Increased use of the northern sea routes will further raise the need for ice resisting harbors and ships, and demand more knowledge about sea ice as a material.

The Arctic coastline is a zone between land and sea which is a focus of human activity, a rich band of biodiversity, critical habitat, and an area of high productivity. In general, erosion rates along the arctic coasts have increased along the past 30 years (Instanes et al., 2005), and this zone is threatened many places. The decreasing sea ice extent, letting waves erode the shores without being hampered by coastal sea ice, in combination with thawing of the permafrost which is holding the soil together, is expected to be major reasons for this evolution (Lantuit and Pollard, 2008). On the other hand, sea ice can cause damage on coastal structures and on the shoreline itself as the loads related to ice movement onto land (called *ivus* in inuit) can be considerable (Kovacs and Sodhi, 1980). Such loads are typically caused by wind and/or water drag forces on the ice, but also thermal expansion can lead to an ice cover moving onshore or against structures during spring warm up. Coastal protection is designed and constructed to avoid erosion and to protect man-made structures. This design will depend on coastal ice conditions, and more knowledge on the topic would therefore be an important part of protecting the arctic shores in a warming climate. At the moment, there are several unanswered questions connected to how coastal ice affects erosion and how it acts on coastal structures.

Many formulas have been developed to calculate growth rate of free-floating sea ice, both empirical and analytical. Several of them are presented in e.g. Løset et al. (1998). However, when it comes to sea ice in the shore area, the growth situation becomes more complicated due to frequently occurring surface water, tidal cracking of the ice, the fact that a part of the ice (the *ice foot*) usually is frozen to the shore and other factors. These factors are likely to cause formulas made to describe free-floating ice to be rather far from the truth.

The study of form and structure of coastal ice - its *morphology* - includes determination of how the ice in the shore area moves and grows. This is one of several topics described in this thesis on which the existing knowledge is sparse. The movement of the coastal ice is related to stresses in the ice sheet, which in some studies from Van Mijenfjorden were found to correlate with the tidal cycle (Caline and Barrault, 2008; Moslet and Høyland, 2003). However, other studies concluded that the stresses did not correlate with the tide, but were induced by thermal expansion of the ice (Teigen et al., 2005; Barrault and Høyland, 2007). The expansion would typically be due to warmer air and/or surface water causing the ice to heat.

Permeability of sea ice has seen little attention over the years, but is still an important parameter as it controls the persistence of surface melt ponds (Freitag and Eicken, 2003), and thereby the surface albedo of the ice. This is in turn a major factor governing the melt of sea ice (Fetterer and Untersteiner, 1998). As permeability controls transport of liquids through the ice, it also affects the biological sea-ice communities (Cota et al., 1987), the consequences of oil pollution (Nelson, 1981) and salt fluxes within the ice cover (Cox and Weeks, 1975).

The sparseness of knowledge about permeability, growth and morphology of coastal ice is the motivation factor for this study. Its goal is more specifically to describe how the data was collected, and to determine magnitude and possible driving mechanisms for each one of the three parameters mentioned above.

This thesis summarizes a fieldwork conducted in the fjord Van Mijenfjorden, Svalbard through most of the ice season 2014, starting in January and ending in May. It describes how measurements of several key variables of coastal ice were carried out, and presents a selection of the collected data sets. Finally, the various types of data are merged in a discussion dealing with coastal ice growth, movement and permeability.

Chapter 2

Literature Review

2.1 Terminology

An overview of the coastal zone is given in Fig. 2.1. In earlier works, the nomenclature describing coastal features is not always the same. In this thesis, the definitions given in WMO (1970) are used as a basis. In cases when they were found not to be sufficient, definitions from other papers are used. The most relevant terms and definitions used in this thesis are listed below:

Anchor ice: Submerged ice attached or anchored to the bottom, irrespective of the nature of its formation.
Coastal bluff: The transition between the marine shoreline and the upland. In USACE (2002), a bluff is defined as "a high, steep bank or cliff". Although the coastal bluff referred to in this thesis is not very high, I have used it to define the border between ice of sea origin and dry land/snow, which is the landward end of the ice foot.
Coastal ice: The zone of the sea ice that is affected by the boundary conditions at the shore (as proposed by Caline (2010)). In this thesis, more specifically, the term is defined as the part of the ice that is including the *ice foot* and the *hinge zone*.
Coastal zone: The transition zone where the land meets water, the region that is directly influenced by marine and lacustrine hydrodynamic processes. It extends offshore to the continental shelf break and onshore to the first major change in topography above the reach of major storm waves. On barrier coasts, it includes the bays and lagoons between the barrier and the mainland (USACE, 2002).
First-year ice: Ice that is less than one year old and is between 30 and 200 cm thick (Weeks, 2010).
Free-floating ice: Ice that is floating freely with the tide (unlike the ice foot and the ice in the hinge zone). In this thesis the term has been used to define the ice outside the outer tidal crack.
Freezing degree-day (FDD): A measure of the deviation of the mean daily temperature from a given standard, usually 0°C. For example, one day with an average temperature of -5°C represents 5 freezing degree-days (USACE, 2002). The term is further explained in Section 2.6.
Grease ice: A later stage of freezing than *frazil ice* when the crystals have coagulated to form a soupy layer on the surface. Grease ice reflects little light, giving the sea a matt appearance (WMO, 1970).
Hinge zone: The zone of the coastal ice where tidal cracks occur (Caline, 2010).
Ice cake: Any fairly flat piece of sea ice less than 20 m across. If it is less than 2 m across, it is called a small ice cake.

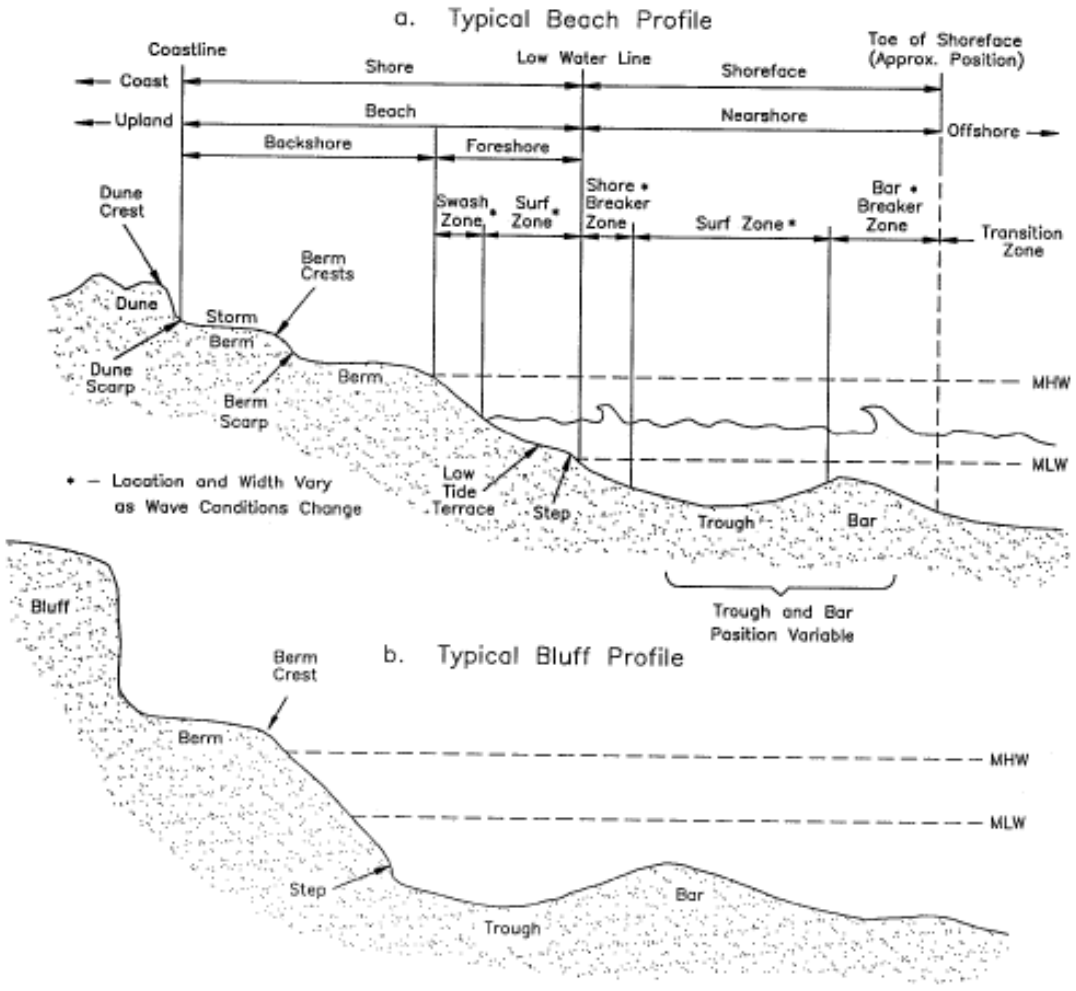

Figure 2.1: *Overview of the coastal zone (USACE, 2002).*

Ice foot: A narrow fringe of ice attached to the coast, unmoved by tides and remaining after the fast ice has moved away (WMO, 1970). It is determined as the ice frozen to the shore when gradual freezing of sea water from tide and wave spray occurs early in the winter season (Gabrielsen et al., 2008).

Landfast ice: Also called *fast ice*. Sea ice which forms and remains fast along the coast, where it is attached to the shore, to an ice wall, to an ice front, between shoals or grounded icebergs. Vertical fluctuations may be observed during changes of sea-level. Fast ice may be formed in situ from sea water or by freezing of floating ice of any age to the shore, and it may extend a few meters or several hundred kilometers from the coast. Fast ice may be more than one year old and can then be prefixed with the appropriate age category (old, second-year, or multi-year).

Level ice: Region of ice with relatively uniform thickness (ISO, 2010). In this thesis, the term is used to characterize ice with thicknesses deviating with less than 5 cm within 2 m horizontal distance. It is the parts of the free-floating ice with relatively even thicknesses, thus leaving out the segment of it that is closest to the hinge zone.

Nilas: Can be divided into two types: dark and light nilas. *Dark nilas* is a thin, less than 5 cm thick elastic crust that develops from subsequent downward growth. As nilas thickens (between 5 and 10 cm), it becomes somewhat lighter in color and is termed *light nilas* (Weeks, 2010).

Pancake ice: Predominantly circular pieces of ice from 30 cm to 3 m in diameter, and up to about 10 cm in thickness, with raised rims due to the pieces striking against one another. It may be formed on a slight swell from grease ice, shuga or slush or as a result of the breaking of ice rind, nilas or -under severe conditions of swell or waves- of young ice. It also sometimes forms at some depth at an interface between water bodies of different physical characteristics, from where it floats to the surface. Its appearance may rapidly cover wide areas of water.
Shore: The shore extends from the low-water line to the normal landward limit of storm wave effects. Where beaches occur, the shore can be divided into two zones: the backshore and the foreshore (USACE, 2002).
Shuga: An accumulation of spongy white ice lumps, a few centimetres across; they are formed from grease ice or slush and sometimes from anchor ice rising to the surface (WMO, 1970).
Superimposed ice: Ice that forms on top of the primary ice. It is caused by flooding of the ice cover from any imaginable water source. If there is snow on the ice surface, snow ice may form (Michel and Ramseier, 1971).
Slush: Snow that is saturated with water on the ice surface, or as a viscous mass floating in water after heavy snowfall (USACE, 2002).
Snow ice: Ice formed by refreezing flooded snow creating an ice layer that bonds firmly to the top surface of a floe.
Tidal cracks: Cracks in the sea ice outside the ice foot caused by tidal movements of the floating ice.
Young ice: Sea ice types possessing thicknesses between 10 and 30 cm. Young ice is the transition stage between nilas and first-year ice (Weeks, 2010).

2.2 Sea Ice in the Arctic

The Arctic basin and its adjacent seas are bordering Russia, Canada, USA, Norway and Greenland (Denmark), covering an area of around $14 \cdot 10^6$ km^2 (Untersteiner, 1975). During winter, the majority of this area is covered with ice and at the most the ice thickness can exceed 3 m. An exception is the south-western parts of the Barents sea between northern Norway and Svalbard, where large areas are more or less ice free all year. Due to the warming effect of the northern branch of the Gulf Stream, the climate in both the ocean and the atmosphere is warmer in these areas compared to similar latitudes elsewhere in the Arctic. In September, after a summers melt, the ice extent in the Arctic is usually at a minimum with an ice cover extent of about $8 \cdot 10^6$ km^2. Satellite data indicate a decrease of about 3% per decade in the annual sea ice extent from 1978 to 1999 (Johannessen et al., 1999). Comiso et al. (2008) argue for a steepening trend in September sea ice extent based on a statistically-significant difference in linear regression slopes, showing a reduction of about 3% per decade in the period 1979-1996 compared to 10.7% in the period 1996-2007. The decrease is, at least partly, due to a warming climate in the Arctic regions (Stroeve et al., 2012), which could further be related to natural temperature fluctuations. However, the human impact on the global climate system is likely the major cause (Johannessen et al., 2003).

2.3 Ice Formation in Arctic Fjords

The molecular structure of water is one oxygen atom bonded to two hydrogen atoms (Weeks, 2010). When water reaches freezing temperature, each hydrogen atom is attracted to its neigh-

boring oxygen atom and thus, when freezing starts, the water molecules connect to each other by weak, so-called *hydrogen bonds*. The oxygen atom is surrounded by four molecular orbits which have a somewhat higher electron density, and thereby a negative charge. Two of these are occupied by positively charged hydrogen atoms before the freezing starts. When the freezing occurs, the other two are being connected to hydrogen atoms which are parts of other water molecules. When several molecules are connected, they make a crystal system characterized by four axes: three a-axes in the so-called *basal plane* with 120° between them, and the c-axis which is perpendicular to this plane (Weeks, 2010). A theoretical figure of the molecular structure of ice is shown in Fig. 2.2. For normal seawater, crystallization usually starts from a foreign nuclei (also called *seed*) such as snow crystals or solid impurities when the water is cooled down to or slightly below its freezing point (Michel, 1978). If no such particles are present in the solution, the freezing will start spontaneously when the water is sufficiently supercooled to make the water molecules combine and form an ice embryo from which the ice starts to grow. The molecular lattice of ice is more open than for water, where the molecules are packed closer to each other, making ice less dense than liquid water.

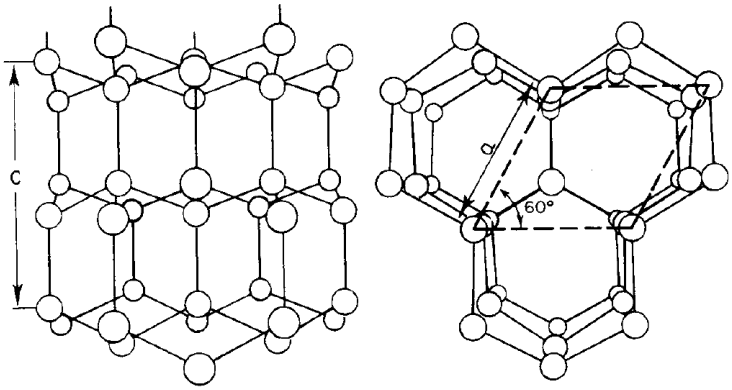

Figure 2.2: *The molecular structure of ice, seen perpendicular to the c-axis (left) and along the c-axis (right). The lines between the oxygen atoms represent the hydrogen bonds which contain one hydrogen atom each (Michel, 1978).*

In waters with some turbulence (due to e.g. waves), which normally is the case in Arctic fjords, the first layer of ice to form is called *primary ice*. Once the ice particles have started to form, the c-axis of the grains are oriented randomly since they are moved by wave action before they freeze together. The result is creation of *granular ice*, ice consisting of small crystals with a diameter of about 1-5 mm (Michel and Ramseier, 1971).

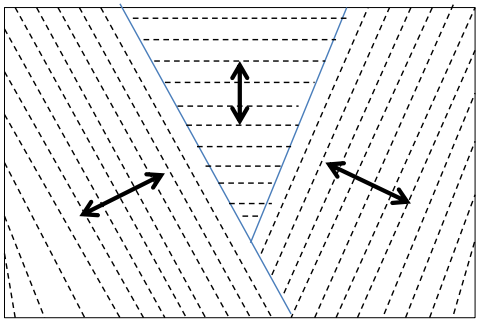

Figure 2.3: *Crystals with horizontal basal planes are being wedged out. The arrows indicate the c-axis direction, and the blue lines the orientation of the basal plane.*

The growth rate along the basal plane is orders of magnitudes faster than along the c-axis (Rosenberg and Tiller, 1957). The grains with vertically oriented c-axes will stop growing along the basal plane as soon as they meet other grains at, or close to, the water

surface; they are 'wedged out' by the vertically oriented crystals (Fig. 2.3). Thus the *secondary ice*, the ice below the transition zone where wedge out occurs, will have horizontally oriented c-axes and can be classified as *columnar ice*. The columnar grains will have a diameter between 1 and 20 mm (Michel and Ramseier, 1971). The transition zone typically extends between 10 and 20 cm from the ice surface.

Sea water is essentially a mixture of fresh water and salt. Salinity is a measure of the salt content of the water, and one way to express it is by its absolute salinity with the unit [g kg^{-1}], which is usually regarded as the same as the unit [ppt] (parts per thousand). Typical salt content in the waters around Svalbard is around 34 g kg^{-1}, meaning that in one kilogram of fresh water, 34 grams of salt is dissolved. The freezing temperature will be lower the more saline the water gets, and for water with a salinity of 34 ppt (=34 g kg^{-1}) it is around -1.8°C. When referring to salinities in sea ice, two terms the most commonly used. The *bulk salinity* is defined as the salinity of a completely melted sea ice sample, and is not to be confused with the *brine salinity*, which is the salinity of the brine itself (Notz, 2005).

When sea water freezes, salt is expelled since the salt molecules does not fit into the molecular lattice of ice. The pure ice grows along its basal plane into plates of fresh ice with a width less than 0.5 mm. After some time, plates with the c-axis oriented in the same direction grow together in groups to form an ice crystal (Kovacs, 1997). Most of the salt is drained out of the icy layer, as the water gets heavier the more saline it is. However, some of the salt is being trapped between the platelets in the crystal in pockets of water with high salinity called *brine*. The pockets are called *brine pockets*. The amount of brine entrapped in the ice and the size of the crystals vary with growth rate (Weeks and Ackley, 1986). At the ice-water boundary, both in the brine pockets and at the bottom of the ice layer, the water is normally at its freezing point, and thereby in phase equilibrium with the ice. When the ice continues to grow, the brine becomes cooled down to below its freezing point and some of it will freeze, making the pockets smaller and the brine even more salty (Notz, 2005). Thus, as shown in Fig. 2.4 and further elaborated in Section 2.5, the ice/brine weight ratio will increase as the ice gets colder. If the brine pockets stays connected through channels or so-called *drainage tubes*, brine drainage can occur through these (Kovacs, 1997). However, due to the same process as for the brine pockets, cooling of the ice would make these tubes decrease in volume and possibly close entirely.

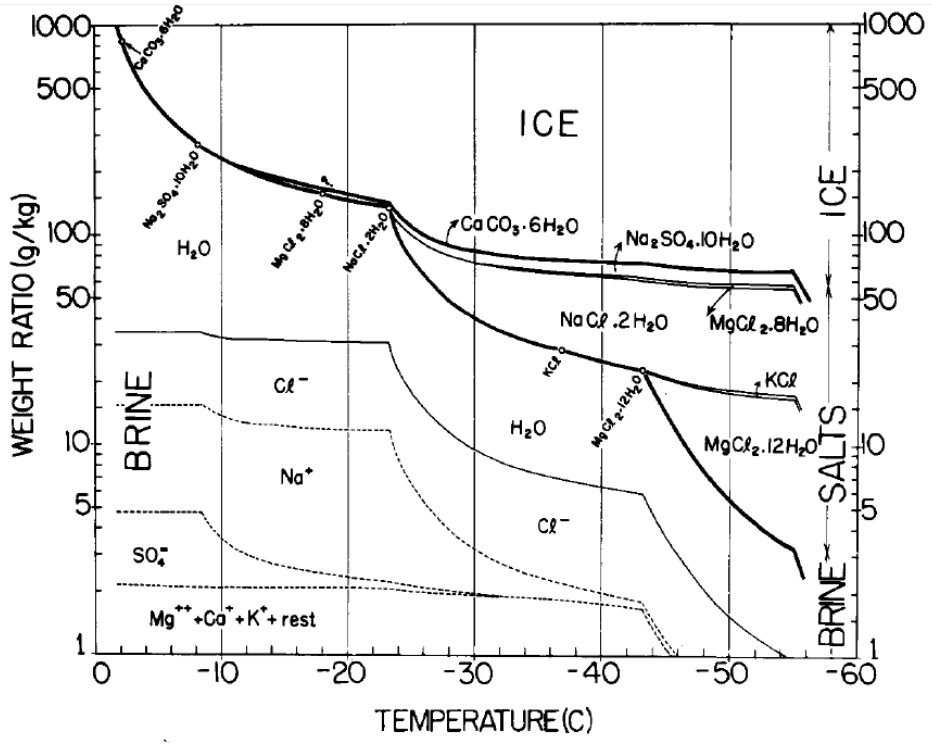

Figure 2.4: *The phase diagram for sea water with a salinity of 34.325 ppt, showing the fractions of brine, solid salts and pure ice at different temperatures, as presented by Assur (1958).*

2.4 Desalination Processes

Several processes have been suggested as important for the loss of salt from sea ice. By results from analytical and numerical studies, as well as from experiments from laboratory and field, Notz and Worster (2009) concluded that the only processes contributing to any measurable net loss of salt were *gravity drainage* and *flushing*. Gravity drainage occurs due to convective overturning of brine within the ice, since the brine at the top of the ice will be more dense than the brine further down, assuming cooling from above. The process is dependent on the permeability (featured in Section 2.5) of the ice; if the permeability is low, there will not be possible for the brine to move appreciably. Flushing is ”washing-out” of salty brine by fresher surface melt water during summer. By summer, the ice is normally warm, and thereby permeable, which is a necessity also for this process. The water is driven trough the ice by overhead pressure (Notz and Worster, 2009).

C-shaped salinity profiles are often observed in sea ice (Notz, 2005), related to high bulk salinities in the top and bottom layers, compared to in the intermediate layer. A relatively large amount of salt is entrapped in the top part of the ice as the growth often is rapid there, leaving less time for the salt to be drained out of the mushy layer by buoyancy-driven convection. The ice on top is then cooled down to low temperatures as the ice continues to grow, leading to lowering of the permeability and reduced desalination. In the layers further down, the growth is slower and less salt is being entrapped in the ice. Since the ice is normally warmer and more permeable here than in the top layer, gravity drainage is likely to lead salty brine downwards, further decreasing the salinity in the intermediate layer. In the bottom layer, sea water/brine is present between the platelets of ice which have not yet frozen completely together. Thus, this layer gets a relatively

high bulk salinity. By the end of the season, when the ice stops growing, the permeable layer of unconnected ice platelets (which often is termed *skeleton layer*) disappears, often together with the high bottom salinities (this was observed by Høyland (2009)).

As stated in Notz and Worster (2009), multiple C-profiles can form as the convection connected to gravity drainage reduces brine salinity in the convective region. The reduced salinity will lead to freezing and could lower the permeability enough to stop the convection. The result is a low-salinity layer on top of a layer of high saline ice. Only if the salty (and permeable) layer underneath is thick enough, the convection could start anew.

2.5 Permeability

Permeability can be defined as a property of a porous medium which allows advection of fluid through the connected pathways along their geometry. Darcy's empirical law describes the linear relationship between discharge and driving force, and is written

$$u = \frac{k}{\eta}\nabla p, \tag{2.1}$$

with specific discharge u measured in [m s^{-1}], pressure gradient ∇p in [N m^{-3}], permeability k in [m^2] and dynamic viscosity η in [kg m^{-1} s^{-1}] (Freitag and Eicken, 2003).

One way to determine the permeability of sea ice is applying Eqn. 2.1, obtaining the needed variables by direct measurements through so-called *blind hole tests*. Briefly, such a test is done by drilling a hole almost through the ice and measuring how fast seawater seeps into the hole. By blind hole tests, Freitag and Eicken (2003) found permeabilities in the Siberian and the central Arctic to range between 10^{-11} and 10^{-8} m^2. Another way to do it is by the method described below; assuming that the pure ice and the brine exist in thermal equilibrium, and that the fraction of solid salts in the ice can be neglected (which was found by Cox and Weeks (1983) to be reasonable in most cases), one can, by measuring the bulk salinity and temperature of an ice core, calculate brine content and then permeability of the sea ice.

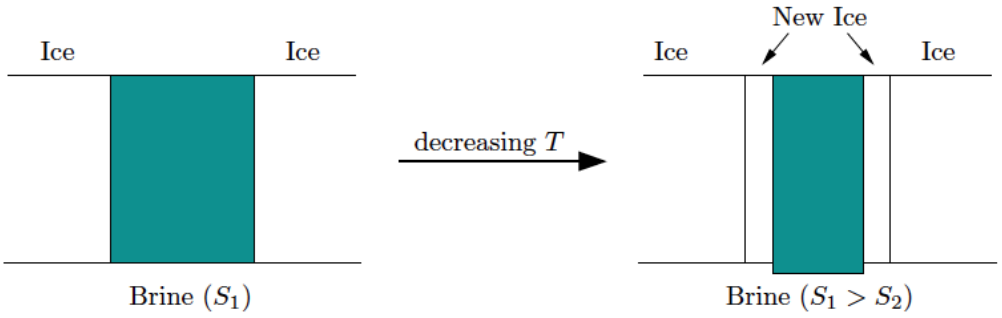

Figure 2.5: *When sea ice is cooled down, the brine gets higher salinity and lower volume. It is lowering its freezing point and thereby maintaining phase-equilibrium (Notz, 2005)*

As described in Eicken and Salganek (2010), the brine salinity can be approximated for temperatures above -23°C as

$$S_{br}(T) = \left(1 - \frac{54.11}{T}\right)^{-1} \cdot 1000ppt, \tag{2.2}$$

where T is in [°C], and [ppt] is an abbreviation for *parts per thousand*. The brine content of a sea ice sample can then be expressed as (Cox and Weeks, 1983):

$$(1 - \phi) = \frac{S_{bu}}{S_{br}(T)}, \tag{2.3}$$

where ϕ is the solid weight fraction, S_{bu} denotes the bulk salinity and $S_{br}(T)$ the brine salinity.

The solid mass (mass of freshwater ice) per mass of sea ice can be expressed by

$$\phi = \frac{m_{solid}}{m_{liquid} + m_{solid}}. \tag{2.4}$$

This relationship as well as the brine salinity $S_{br}(T)$ is dependent on the temperature of the sea ice, since some of the liquid will change to solid when the local temperature falls (and the other way around, see Fig. 2.5), to maintain phase-equilibrium. The salinity of the brine, and thereby its freezing temperature will fall, so the brine always stays at freezing temperature (Notz, 2005). Finally, the permeability k is given by:

$$k = 10^{-17}[(1 - \phi) \cdot 1000]^{3.1} \cdot m^2. \tag{2.5}$$

Equation 2.5 is an empirical equation based on measurements in young sea ice (Freitag (1999); Notz and Worster (2009)). It should be noted that because gas content of the ice is not included in the equations above, calculations of permeability in ice that is grounded close to shore during parts of the tidal cycle, would give too low values in cases when the brine channels are filled with air and not with brine.

2.6 Stefan's Solution

A simple and often used model for calculation of ice growth is Stefan's Law (Eqn. 2.7). The major assumption in the model is that all the energy that is released as a new layer of ice with thickness dh freezes, is conducted up through the ice (with thickness h) and out of the surface:

$$-\lambda \frac{\Delta T}{h} = \rho l \frac{dh}{dt}. \tag{2.6}$$

The equation above can be solved and expressed as follows (Stefan, 1891, as cited by Høyland (2009)):

$$h_i^2 = h_{i,0}^2 + \omega \frac{2\lambda}{\rho l} FDD, \tag{2.7}$$

where h_i and $h_{i,0}$ are the current and the initial ice thicknesses, λ is the thermal conductivity, ρ is the ice density, ΔT is the temperature difference between the ice surface and bottom ($= T_f - T_a$) and l is the latent heat. ω is an empirical constant to account for simplifications in the model, such as an insulating snow cover on top of the ice that would cause the temperature on the ice

surface (which is often not accessible) to differ from the air temperature T_a. FDD is the amount of freezing degree days, and can be defined as

$$FDD = \int_{t_0}^{t} max(0, (T_f - T_a))dt \tag{2.8}$$

where T_f if the freezing temperature of seawater and T_a is the air temperature. In the equations above the following is assumed: The water below the ice is at its freezing point ($T_{water} = T_f$), that no radiation or other factors are heating up the ice from within, that the temperature profile through the ice sheet is linear and that the ice surface temperature is known if not using the ω constant to account for it.

2.7 Formation of Coastal Ice

Figure 2.6 shows parts of the ice that are frequently referred to in this thesis. Coastal ice is in this thesis defined as the *ice foot* and the *hinge zone*, which are subject to different growth mechanisms than the *free-floating ice*, where growth rate often can be approximated by Stefan's solution (described in Section 2.6). As there exist little published information dealing with formation and growth of the coastal ice, the following two sections, which aim to draw a picture of the creation of the ice foot and the hinge zone, are based mainly on observations done during the winter of 2006/2007.

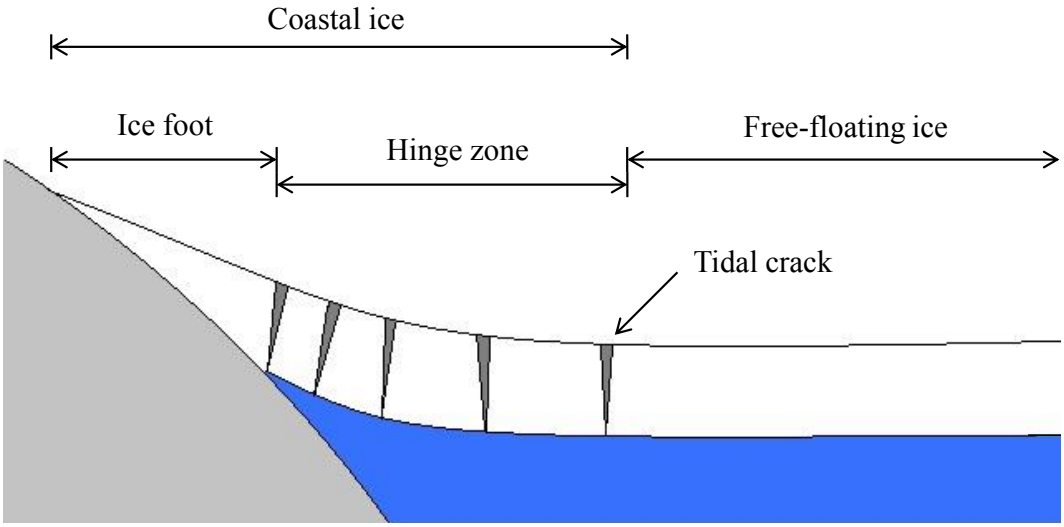

Figure 2.6: *Illustration showing the different parts of the coastal and the free-floating ice. To the left in the figure is the ice foot, frozen onto land. In the middle is the hinge zone, the zone in which the tidal cracks are located. To the right is the free-floating ice (most of it is often also called 'level ice', see Section 2.1), going from the hinge zone and continuing offshore. The grey area represents the beach/sea bottom, and the blue area water.*

2.7.1 The Ice Foot

An early explanation of the creation of the ice foot is, as given by Bentham (1934), that by ebb tide, water left in ponds and puddles on the beach freezes. During the following high tide, not

all of this ice melts and successive tides will hence build up a rim of ice along the shore. The paragraph below, complementing Bentham's observations, is based on Caline (2010). It describes the development of the ice foot around Longyearbyen harbor and at the tip of Barryneset (the location and relevance of the peninsula Barryneset are given in Section 3.3).

The first stage, before the sea froze over, was creation of an ice cap on the beach by freezing of sea water spray, swash and moisture. The lower end of the ice cap reached almost down to the medium high water level. When the sea started to freeze, and pancake ice developed on the surface, deposition of pancakes on the beach formed a berm that by spray, swash and moisture got consolidated within a few days. After the sea ice had formed, wind and tidal forces broke loose an ice cake which was pushed partly onshore. After some time the ice cake was cemented to the ground and had become a part of the ice foot. As the ice cover grew thicker, it got grounded during most of the tidal cycle at the same time as the area connecting it to the ice foot became larger. Eventually it broke, making a crack that defined the border between the ice foot and ice that was moving due to tidal action (the hinge zone). Later in the season, the ice foot did not grow significantly, since it was no longer affected by water or moisture other than in the form of snow. Caline also stated that size of the ice foot is dependent on the time interval between the first sea ice appears until the sea freezes over, since it is in that period it grows the most (Caline, 2010).

After the ice foot breaks up in spring, according to Nansen (1922, as cited by Wadhams, 1981), some remnants of it will still be buried in the beach sediments, and hence it is playing an important role for coastal erosion.

2.7.2 The Ice in the Hinge Zone

Gabrielsen et al. (2008) observed the development of the ice that eventually became the hinge zone outside the tip of Barryneset. This section is based on their findings.

Until mid-December, floating pancake ice covered the sea and the ground was ice-free below mean sea level. By the end of December, a layer of ice that was connected to the shore covered the sea. At first, this layer followed the tide, but by January it had become thicker and got partly frozen into the ice foot and the sea bottom, and did not move with the same amplitude as the tide anymore. As it was partly frozen to the beach, it became flooded close to shore by high tide, leading to formation of superimposed ice. Investigations of the superimposed ice revealed that it was of the type granular, and was found to be very porous. In the end of January, the ice thickness around one meter outside the innermost tidal crack was 0.8 m, and in the end of February it was 1.6 m. Outside the hinge zone the ice was much thinner, with a thickness of 0.6 m by the end of February.

Chapter 3

Site

3.1 Svalbard

Svalbard is an archipelago situated in the north-western Barents sea, between Northern Norway and the North Pole. It is under Norwegian sovereignty, but several nations are doing scientific research and other work on and in the waters around the archipelago. The main island is Spitsbergen, which is where the administrative capital Longyearbyen is located (Thuelsen, 2014). Longyearbyen was built as a mining town, but today science and tourism represent the income for a large part of its inhabitants. There is also a Russian mining settlement called Barentsburg, an international research station in Ny-Ålesund, a Norwegian mining camp in Svea and a Polish research station in Hornsund (Sysselmannen, 2012). Compared to other areas at the same high latitudes, Svalbard has a relatively mild climate thanks to the earlier mentioned warm ocean currents flowing from the Atlantic ocean and passing the western coast of Spitsbergen.

3.2 Van Mijenfjorden

Van Mijenfjorden is a fjord located at 77°N 15°E, on the west coast of Spitsbergen. A map of Spitsbergen and Van Mijenfjorden is shown in Fig. 3.1a. The natural environment of a large part of the areas on the Arctic shelf can be characterized by relatively small water depths, long ice season, frequent wind, low air temperatures, tides with current velocities up to 1 m/s and small water level variations, regions with seasonal permafrost and variable river runoff (Marchenko et al., 2009). This can be said to be fairly typical for the Van Mijenfjorden area as well. The mouth of Van Mijenfjorden is almost closed off by the narrow island Akseløya which gives shelter from ocean swell and reduces circulation of seawater, thus giving favorable ice growth conditions in the fjord. Close to the head of the fjord lies the Norwegian coal mine Svea Nord, run by Store Norske Spitsbergen Grubekompani (the Norwegian Coal Mining Company). The fjords relatively stable freezing patterns as well as easy logistics thanks to the norwegian coal mine, makes it a favorable place for studies on sea ice. Since 1979 the quay infrastructure at Kapp Amsterdam close to the mining camp has been the object of several studies (Caline, 2010). A review of measurements of ice conditions in Van Mijenfjorden and Sveabukta from 1998 to 2006 was given by Høyland (2009), stating that ice typically covers the fjord from December/January until June/early July.

3.3 Barryneset

The investigations described in this thesis were conducted on the sea ice outside Barryneset, which is a headland located in the inner part of Van Mijenfjorden. It stretches out from the north-western shore into Sveasundet, which is the sound that connects the shallow inner basin Braganzavågen with the deeper Sveabukta and the rest of the fjord (see Fig. 3.1b). The shortest distance from the tip of Barryneset to Littrowneset, a headland on the opposite side of Sveasundet, is around 690 m (Caline, 2010). The tip of Barryneset has been subject to several studies on coastal ice, and in 2006 a small cabin (commonly nicknamed 'Fabrice Cabin', after Fabrice Caline who was the first to use it) was installed there, providing electricity, shelter and heat. In 2006, the tip had been formed with angular corners and covered with geosyntetic bags. When we arrived, however, erosion had rounded the tip, and smoothened the beach profile into a gently ascending slope going from the waterline up to a small bluff a few meters from the cabin. The gently inclined beach slope seemed to continue into the water, without any significant bumps or edges on the sea bottom. The cabin itself had been moved around 17 m inland since 2008 (see Section 4.2), probably because of a retreat of the entire tip of Barryneset.

In Sveasundet, the ice season is normally longer than in the deeper parts of the fjord. Typically, the sea freezes over between November and January, the ice reaches its maximum thickness in mid-May and breaks up between the middle of June and the middle of July. Maximum ice thicknesses in the period between 1998 and 2006 was measured to be between 0.72 and 1.3 m (Høyland, 2009). As stated in Caline (2010), it was found, based on a discussion with a person that used to work in Svea in the 1980's, that anchor ice may occur in Sveasundet, which in some parts is rather shallow. This was later confirmed by Wrangborg et al. (2013). As Sveabukta is approximately perpendicular to the rest of the fjord, which in turn is protected by ocean swell by the island Akseløya, the waves in the sound are essentially wind-generated. The tidal range in Svea was found by Caline (2010) to be 1.13 m on average. Caline also stated that the wind in Svea seldom is stronger than 15 m/s, and about 40% of the time, it is blowing from north-northeast. As typical for the Arctic climate, the snow cover in Svea seldom gets thicker than a few decimeters due to a combination of little precipitation and frequent wind.

A rule of thumb is that the tide in Longyearbyen has the same range, and is one hour ahead of the tide in Svea (Caline, 2010).

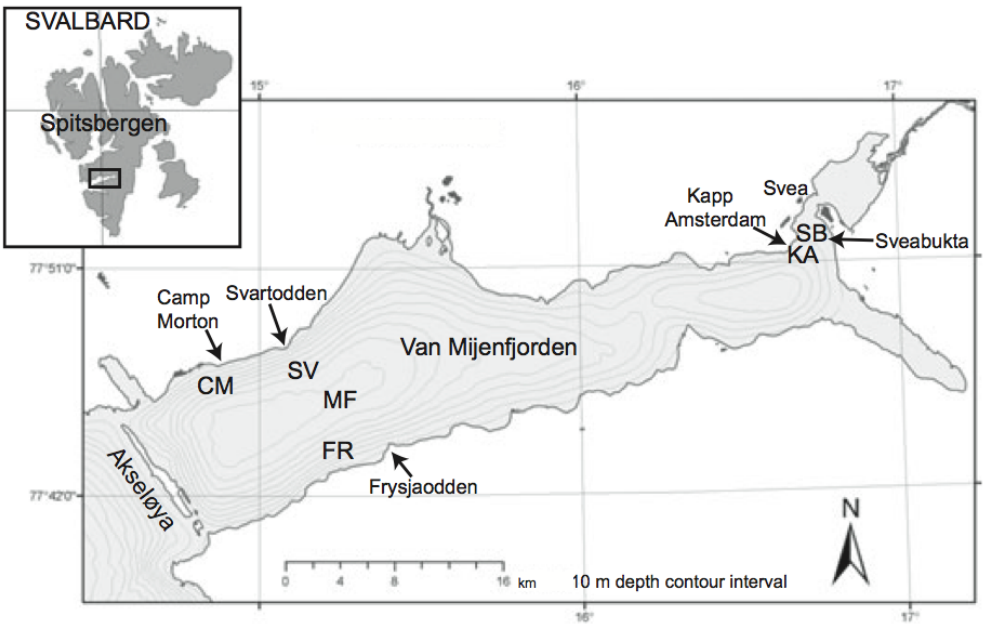

(a)

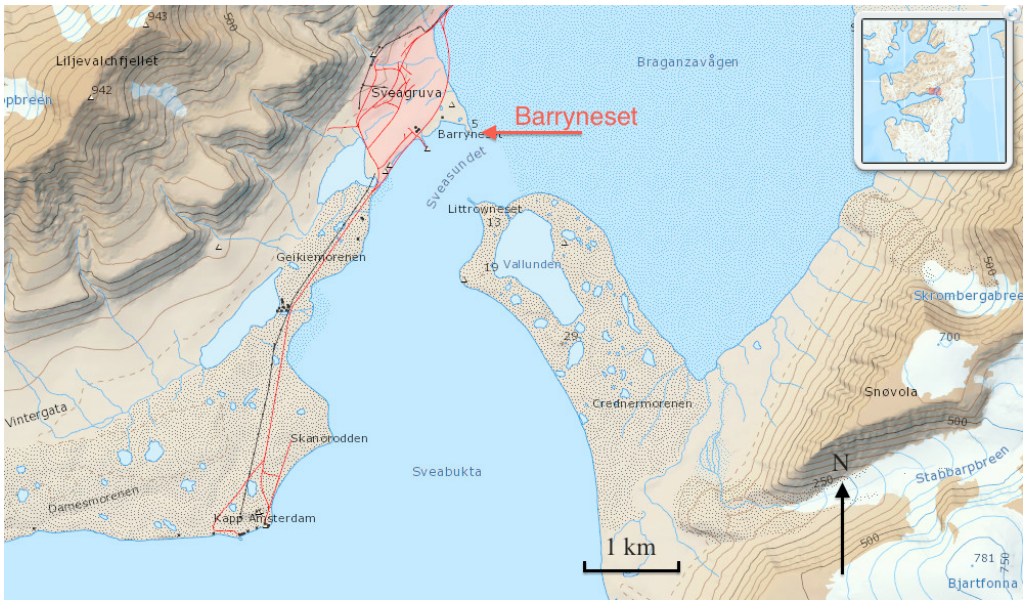

(b)

Figure 3.1: *Maps of Van Mijenfjorden in different scales. Barryneset, where the fieldwork took place, is close to Svea which can be found in the top right corner of the map in figure (a) (Høyland, 2009). Figure (b) is a zoomed-in map pointing out Barryneset's location and the surrounding area (NPI, 2014).*

Chapter 4

Instrumentation and Site Investigations

4.1 Field Trips

The discussed results were obtained during a field campaign run by UNIS (the University Centre in Svalbard) as a part of the SAMCOT (Sustainable Arctic Marine and Coastal Technology) project. It was conducted during the spring semester 2014, starting the 30th of January and ending the 10th of May. In this time period in total 6 excursions were conducted by Carl Magnus Vindegg, David Wrangborg and myself. Each field trip was starting and ending at UNIS in Longyearbyen, with transportation by snowmobiles to and from Svea where accommodation in the mining camp was provided by Store Norske Spitsbergen Grubekompani. The field trips lasted between two and four days depending on the required work with instruments and measurements on the ice outside Barryneset. An overview of the field trips, showing the parts of the work that are most relevant for this thesis, is given in Table 4.1. In addition to the investigations described below, pressure and tilt measurements were conducted throughout the whole spring. Laser scanning of the ice surface was done several times and on the last field visit, two time-lapse cameras were mounted on the roof of the cabin at Barryneset to get photos of the ice break-up. As we were only three persons participating in the fieldwork, most tasks were done as a team although each one of us was responsible for getting certain measurements relevant to our own work done.

The work on the ice was conducted mainly on three different locations: the hinge zone, Site 1 and Site 2. As shown in Fig. 4.1, Site 1 was located just outside the outer tidal crack in the hinge zone, and Site 2 around 200 m off the tip of Barryneset. It should be noted that before March 13, Site 1 was located between Crack 4 and Crack 5, around 2.5 m closer to shore. It is called ”Old Site 1” when referred to in the text. A more detailed map of Site 1 and the hinge zone is shown in Fig. 4.2.

A major problem (but also an interesting finding) was the large amounts of surface water and the creation of superimposed ice between the outer part of the hinge zone and Site 2. Between February 20 and March 12, ca 20 cm superimposed ice had accumulated on the ice, and various amounts of surface water was present on top of it throughout this third field trip. The observation was based on the fact that all the instruments both at Site 1 and 2 with cables were submerged in ice, even if most of them were placed on top of pallets, which in turn were lying on top of the snow cover just to avoid problems related to surface water. Figure 4.3 shows surface water around the stress sensor at Site 1 at February 19. It was a laborious task removing loggers, adjusting thermistor strings and replacing pressure sensors with all the cables connected to them.

A mixture of brute force and precision was required to cut away the ice without causing damage to the instrumentation. After this event, more actions were taken to avoid future problems; loggers were placed on dry land if it was possible, or on top of double pallets which in turn was laid on top of the snow cover. Cables were elevated high above the ice, connected with duct tape to standing plastic poles. The thermistor strings were elevated so that the upper sensor still was well above ice surface. The biggest problem was the pressure sensors, which had to be inserted at a certain depth in the ice. In that case we could only reinstall the sensors at the correct depth, elevate the cables and loggers, and hope that the ice would not continue to grow upwards.

Table 4.1: *An overview of the field trips, including the measurements most relevant for this thesis.*

Trip	Time period	What was done	Comments
1	30.01 - 01.02	-Ice cores collected at Site 1 and Site 2. -DGPS measurements of tidal cracks and sensors. -Seabird (water pressure and temperature) sensor deployed outside Site 1.	Surface water at Site 1 during high tide.
2	19.02 - 20.02	-Ice cores collected at Site 1, Site 2, hinge zone and ice foot. -Thermistor strings inserted at Site 1, Site 2 and in the hinge zone. -DGPS measurements of tidal cracks and sensors.	Ca 15 cm surface water between Site 1 and Site 2, several loggers had been flooded since last visit.
3	12.03 - 14.03	-Ice cores collected from Site 1, Site 2, hinge zone (at high and low tide) and ice foot. -The thermistor string at Site 1 relocated and both strings at Site 1 and Site 2 elevated. -DGPS measurements of tidal cracks and sensors. -Cross-section of the hinge zone.	Ca 20 cm superimposed ice had accumulated at Site 1 since last visit. High amounts of surface water present.
4	30.03 - 03.04	-Ice cores collected at Site 1 and Site 2. -New thermistor string inserted between Crack 4 and Crack 5 (close to ”old” Site 1). -DGPS measurements of tidal cracks and sensors.	Supervision of Bachelor students. High amounts of snow had accumulated.

		-2 different cross-sections of the hinge zone, and one shore-parallel section taken.	
5	24.04 - 25.04	Ice cores collected at Site 1 and Site 2. -DGPS measurements of tidal cracks. -Cross-section of the hinge zone.	
6	10.05 - 11.05	-Ice cores collected from Site 1, Site 2, Hinge zone (at high and low tide) and ice foot. -DGPS measurements of instruments and key points. -Cross-section of the hinge zone. 2 time-lapse cameras mounted on the cabin. -All instruments retrieved from the ice.	High amounts of surface water both at Site 1 and Site 2.

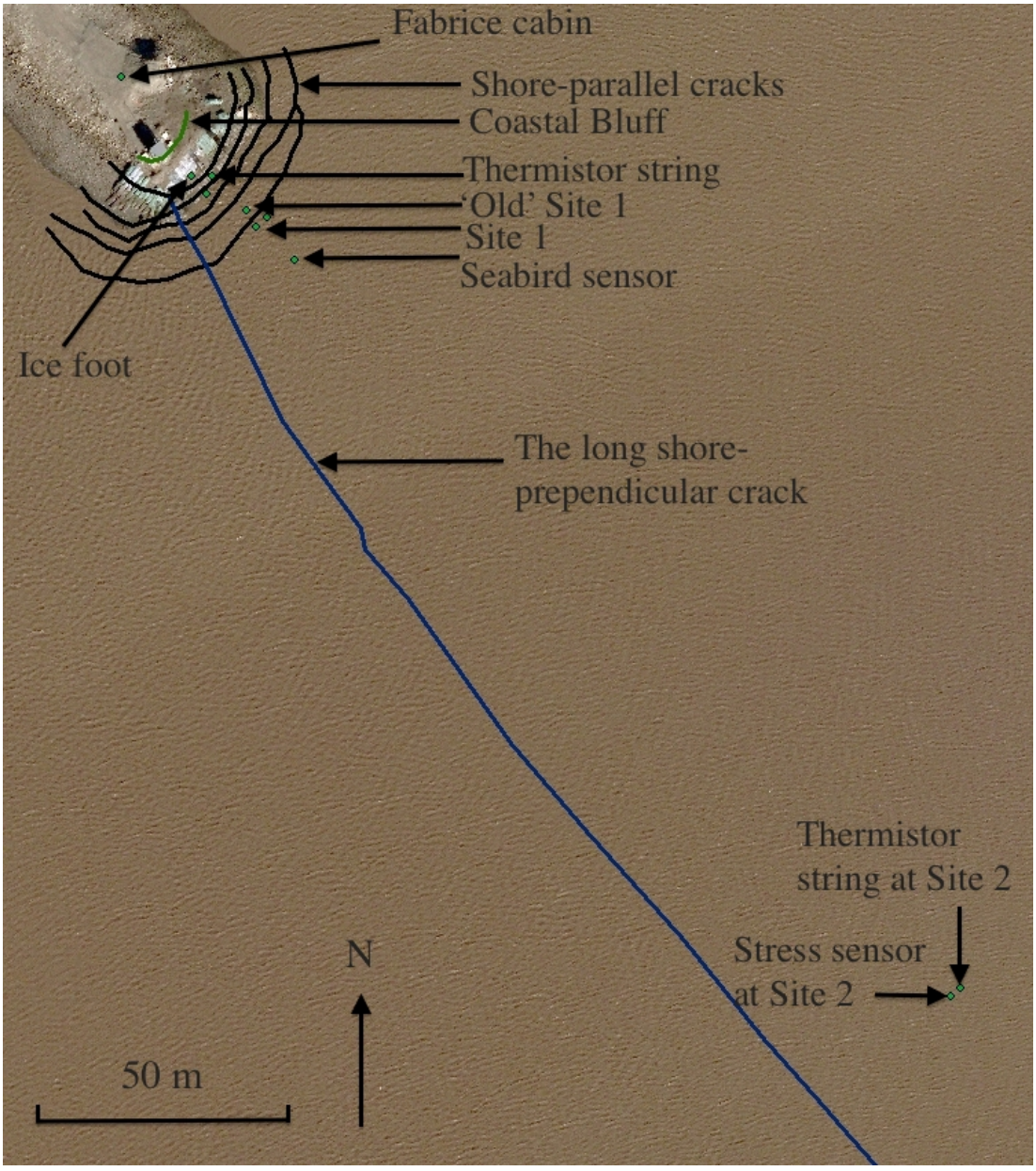

Figure 4.1: *Overview of the study area with positions of instruments and tidal cracks, mapped using DGPS data and the ArcMap software. The tip of Barryneset is seen in the top left corner. The aerial photo was taken in the ice-free season, on a day when the water was turbid.*

4.2 Differential GPS

A Leica DGPS 1200 model was used to map the tidal cracks, positions of all instruments deployed on the ice, and other key points. Such mapping was done on most of the field trips, to get as good as possible overview of the site (see Table 4.1). The DGPS consists of a rover unit that was used to measure positions, and a base unit that was placed at a point with a known, exact position and altitude. This point was situated some hundred meters inland of the cabin on Barryneset. The base unit determines how the measured GPS-positions deviate from the the ”true” position during the survey period, and thereby one can compensate for any atmospheric disturbances of the satellite signal and get much more exact results than from an ordinary GPS device. The DGPS has an accuracy of order 1 cm in the horizontal plane, while in the vertical plane it is somewhat poorer (Caline, 2010).

When mapping the tidal cracks, the points were measured on top of the snow as directly as possible above the crack. The distance between each measured point usually varied between 0.2 and 3 m depending on the crack pattern. If the crack was changing direction, the distance was short, and if the crack was relatively straight a longer interval was used. When measuring positions of instruments, a position directly above the instrument sensor was measured. The Rover unit was held in position for about 5 seconds at each point while mapping the tidal cracks and instruments. When positions on stakes were taken to determine any horizontal movement of the ice, it was held in position for about 15 seconds to get a higher accuracy. It was also tried to map the surface of Section 1 using the DGPS, holding the rover unit in place on fixed points on the ice for at least 15 seconds, both at high and low tide. However, the vertical accuracy of the measurements was not good enough for this purpose (see Appendix C).

In order to correct the measured GPS-data, post-processing was done using the Leica Geo Office Combined software delivered by Leica Geosystems. This is the stage when data from the base unit was used to correct the GPS-coordinates collected with the rover unit. Plotting was done using ArcMap version 10.1. An aerial photo from 2008 was used as a background map for the plotting, as it was found to be the most detailed and updated map available. However, Fig. 4.2 shows that the map is not entirely correct, the coastal bluff is now where the cabin (which obviously was moved later) was situated at the time the map was made.

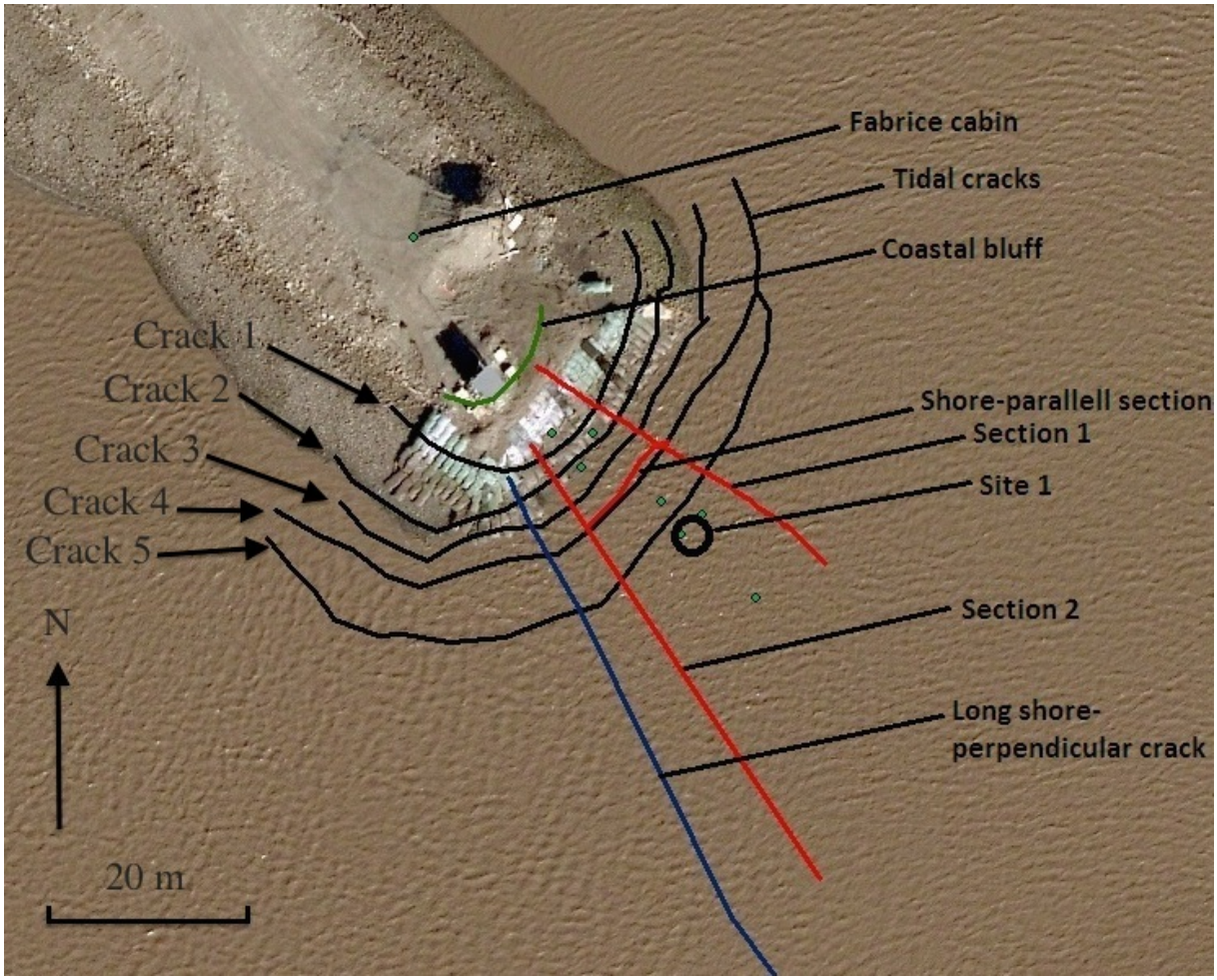

Figure 4.2: *Map made using DGPS data showing tidal cracks (black), the coastal bluff (green) and the three different sections (red).*

4.3 Weather Observations

Except rough, sporadic wind and temperature observations, no weather measurements were done by us during this field campaign. Air temperature data from Svea weather station was downloaded from eKlima, a web portal that gives free access to the climate database of the Norwegian Meteorological Institute (eKlima (2014)). The weather station was located at Svea Airfield, 700 m northwest of Barryneset.

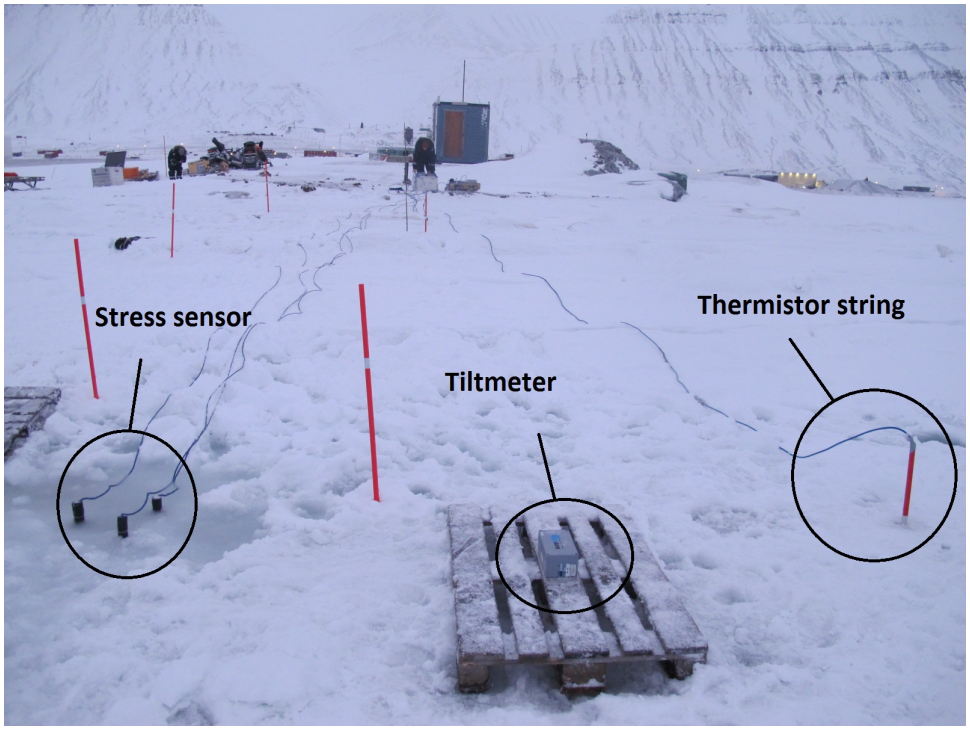

Figure 4.3: *Site 1 with instrumentation. Barryneset and the cabin in the background, February 19*

4.4 Thermistor Strings

The temperatures throughout the ice were measured by 4 thermistor strings from EBA Engineering Consultants Ltd, each connected to an Ultra-Logger Data storage unit from Lakewood Systems ltd. Before the strings were inserted, the recordings were checked by putting the strings in a bucket filled with a mixture of ice cubes and water, witch thereby should keep a temperature close to $0\,^{\circ}\mathrm{C}$. All the strings gave correct values within an error interval of $\pm 0.05\,^{\circ}\mathrm{C}$. On February 20, three strings were inserted vertically through the ice at Site 2, Site 1 and in the hinge zone between Crack 1 and Crack 2. On March 30, another string was inserted in the same way in the hinge zone between Crack 4 and Crack 5.

The positions of the strings are shown in Fig. 4.4. To protect the sensors and keep the strings straight, they were all fitted into red plastic sticks of the same type as the ones used to mark positions on the ice. Another advantage with using the sticks was that they made it possible to withdraw or adjust the strings without having to cut them out of the ice. It was possible, with some force, to rotate the stick and thereby loosen it before pulling it up. All strings except the one at Site 1 had their logger connected directly to them, so the logger would lie on the ice or on a pallet next to the sensors. As shown in Fig. 4.3 the string on Site 1 was installed with a long connector cable that reached the cabin, so that the logger could be kept inside. The intention was to avoid damage to the logger due to weather and surface water. Each string had 16 temperature sensors in total, and on the strings at Site 1 and 2 they were all spaced 10 cm from each other. On each of the two strings in the hinge zone, the upper sensor was located about 0.5 m away from the others while the rest were spaced 10 cm from each other. They were all programmed to record data with a period of 30 minutes.

The strings inserted in the floating ice (at Site 1 and Site 2) were inserted so that the height from the upper sensor down to the ice surface was approximately 60 cm. The string inserted in the upper part of the hinge zone (between Crack 1 and Crack 2) was inserted with the lower sensor levelled with the ice bottom, since the ice there was expected to be grounded at low tide. The lower string in the hinge zone was inserted with 50 cm distance from the second sensor to the ice surface. Due to high amounts of surface water that had partly become superimposed ice, the strings at Site 1 and 2 had to be elevated 20 cm on March 13. The surface water had submerged a connector on the extension cable between the Site 1-string and the logger, and corrupted all data after March 2. The cable was removed and the string was reinstalled 2.5 m away from its original position, on the outer side of Crack 5, with the logger placed on the snow surface next to it.

On every field visit, data was downloaded from the loggers and the memory reset, as the memory of the loggers got ca 60% full after 3 weeks when they were recording data every 30 minutes. The thermistordata was plotted using MATLAB, taking into account the vertical adjustments of the strings at Site 1 and Site 2. The data from the string at Site 1 before and after it was moved 2.5 m horizontally was plotted together, as the ice and water conditions were expected to be more or less the same.

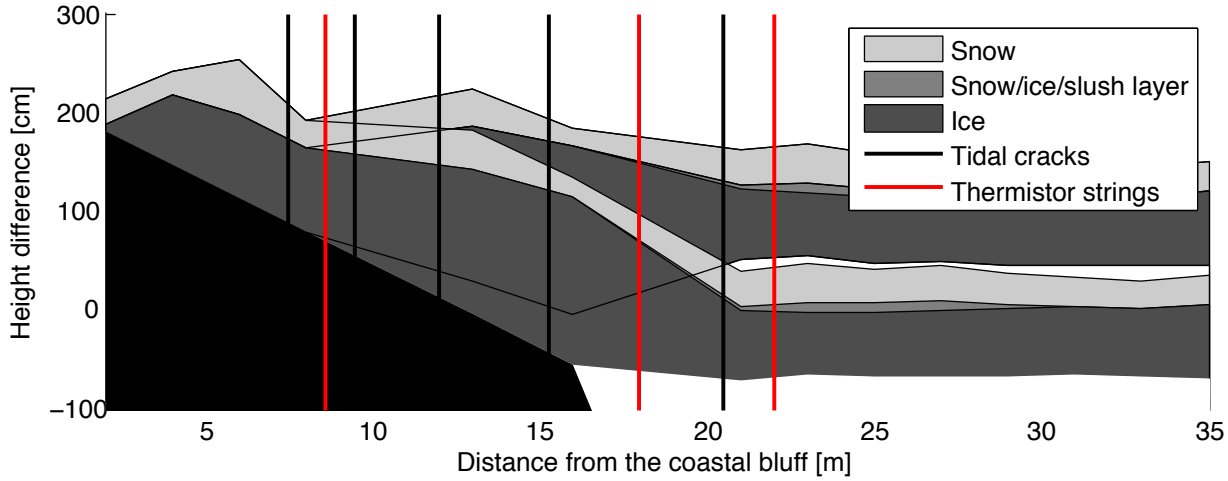

Figure 4.4: *Plot of the ice in the hinge zone from April 24, showing the distance from the coastal bluff to the tidal cracks and the three innermost thermistor strings. Crack 1 is the leftmost on the figure, and the rightmost thermistor string is at Site 1.*

4.5 Ice Cores

On every field trip, ice cores were collected at Site 1 and Site 2, whereas in the hinge zone, cores were collected on February 19, March 13 and May 11 (see map in Fig. 4.1). The cores collected in the hinge zone and in the ice foot were collected close to Section 1 (shown in Fig. 4.2). The cores from Site 1 and Site 2 were taken up to 3 m from the stress sensors and the thermistor strings, but not closer than 1 m to avoid disturbance of data. In the ice foot and the hinge zone, every new core was drilled around 0.5 m away from where cores had previously been collected.

A Kovacs Mark 3 ice drill from Kovacs Enterprise was used to extract the ice cores, connected to a Hitachi DH 36DAL 36 Volt power drill. The Kovacs drill could take cores with a length of up to one meter and had an inner diameter of 7.25 cm. If necessary, the connector between the barrel and the power drill could be extended to get samples from ice thicker than 1 meter. Two blades on the inside of the barrel prevented the ice cores from falling out when it was lifted out of the ice.

When the drill had been removed from the ice with an ice core inside it, it was important to extract the core from the Covacs barrel as quick as possible to avoid freezing of the core onto the inner walls, which would make it impossible to remove without heating the whole system. The samples were cut into approximately 10 cm thick pieces and put into plastic boxes or plastic bags as soon as the core was extracted from the ice. Also in this phase it was important to work quickly, since brine drainage from the core before it was stored in a sampling box would give lower salt and density values than in reality. The length of each piece and number of the box/plastic bag were carefully written down. In some cases, if the ice core was broken or was very long (the ice in the hinge zone was almost 2 m thick at the most), the cores were sometimes cut into longer or shorter pieces than 10 cm to reduce the workload in the laboratory and to make it easier to measure the volume of every piece. If the core was to be used for thin section measurements, every piece was oriented with the upper end towards the lid of the cup. While in Svea, the samples were stored outdoors. Back at UNIS, they were stored in a cold room at temperatures lower than -15 $^{\circ}$C before they were to be measured.

After a core had been removed, ice thickness, snow depth, amount of slush/snow-ice and freeboard/amount of surface water was measured. The measurements were done so that the total thickness of snow, snow-ice and slush would give the distance from the ice surface to the top of the snow layer, while any surface water was measured separately and independent of the other three parameters. Since the height of the snow surface always was larger than the amount of surface water, measurements of the latter would mean a layer of slush equivalent to, or larger than it. When Fabrice Caline measured surface water outside Barryneset in 2007, he placed tubes around the drilled holes to avoid flooding of the ice in the hinge zone (Caline, 2010). This was not used on this fieldwork, since no additional flooding was observed when the holes were drilled. Water level was not measured for the cores collected in the ice foot and between Crack 1 and Crack 2, as the distances from the ice surface down to the water surface (if any water was present in the hole at all) were long and often difficult to determine. This procedure of measuring snow, snow-ice, slush and freeboard also accounts for the cross-sections of the hinge zone (described in Section 4.6).

4.5.1 Salinity and Density Measurements

At UNIS, length, width and weight of every piece was measured, and the cores which were not to be used for thin sections were taken out of the cold lab to melt. The KernKB weight used had an accuracy of $\pm$ 0.1 g. The accuracy of the caliper used to measure length and width of each sample is $\pm$ 0.1 mm but since the surfaces of the ice samples often were quite irregular (broken pieces etc.), the accuracy of these measurements often became worse. Density was then calculated by dividing the weight of each sample by its size. The bulk salinity of the water from each melted sample was measured with a Mettler Toledo SevenGo SG7 pH/Conductivity meter with an accuracy of $\pm$ 0.5% of the measured value (Mettler-Toledo (2015)). Plotting of the data

was done using MATLAB.

4.6 Cross-Sections of the Hinge Zone

A Kovacs 2-inch drill connected to the Hitachi power drill was used to make vertical holes trough the ice with 2-4 m spacing along a straight line going from the coastal bluff onto the level ice. In the hinge zone, where the variations in ice were largest, holes were drilled with 2 m spacing, while on the level ice 4 m space was considered enough. The shore-perpendicular sections were at least 35 m long. It was necessary to drill all the way through the ice, also where it was grounded, and it was difficult to avoid any damage on the equipment; hitting rocks on the seabed under the ice proved to be very harmful for the drill bits. Where the ice was floating, a stick with a hook on it was used to determine the ice thickness, the hook made it possible to detect the bottom of the ice. Ice, snow, slush and snow-ice thicknesses were measured over each hole. A regular folding ruler was used. Freeboard or amount of surface water at each hole was measured both at low- and high tide, except in the hinge zone in the cases when the freeboard became larger than 35 cm. The distance from the coastal bluff to the outer point where the ice was found to be grounded (lying on the ground) was noted.

Sections at three different places were made (see Fig. 4.2). Section 1 was repeated four times, while Section 2 and the shore-parallel section were only made once with help from the UNIS bachelor students Anton Agafonov, Daria Ksenofontova and Kseniia Gorbunova, during their fieldwork in April. Plotting of data was done using MATLAB.

Since the measurements did not give any information about the topography of the beach or the sea floor, this was assumed when plotting the data to be a slope inclining with constant rate from the point where the ice was grounded at low tide up to the coastal bluff. The ice was plotted at high and low tide using the height difference found by pressure data from the Seabird sensor (Section 5.4).

4.7 Water Temperature and Pressure

To measure water level variations and temperature, a Seabird SBE 39 temperature and pressure gauge was used. The SBE 39 is a high-accuracy temperature and pressure recorder with internal battery and non-volatile memory, for deployments at depths up to 10 500 m (SBE-39, 2013). It can measure temperatures in the range of -5 to 35°C, and store 3 665 000 samples when logging temperature, pressure and time. The internal clock has an accuracy of ± 1 minute/year.

On the first fieldwork, the sensor was deployed on the sea bottom between Site 1 and Site 2, around 8 m off Crack 5. The position of the Seabird is shown in Fig. 4.1. Before it was installed, the sensor was fitted into a metal pipe to protect it and make it heavier so it would not move on the seafloor. In addition, it was moored with a heavy piece of metal. Using the Kovacs drill and an ice saw, a big enough hole was made in the ice and the sensor with the attached mooring was lowered by hand down to the sea bottom at around 3.5 m depth. The rope that was used to lower the sensor was threaded through a thin 1.5 m long metal tube with a metal crossbeam, which then was put into the hole so that the crossbeam rested on the ice surface. In this way the rope was protected while going through the ice, and easier to remove from the ice

by the end of the season when the hole had refrozen. Before leaving Longyearbyen, the Seabird had been programmed to record time, temperature and pressure with a period of one minute. While traveling between Longyearbyen and Svea by snowmobile, the Seabird was wrapped up in an insulating material so it would not freeze. After it had been removed, on May 11, data was downloaded and plotted using MATLAB. When the data was plotted it was assumed that a pressure difference of 1 decibar equals 1 m of sea level elevation/lowering.

Chapter 5

Results

5.1 Temperature Recordings

When the thermistor strings at Site 1, Site 2 and in the hinge zone were inserted, the weather had been unusually warm for the season with air temperatures close to $0^{\circ}\mathrm{C}$ for several weeks. Accordingly, the ice was in general warm and close to its freezing point all the way through. In the beginning of March the air temperatures sank, the ice became colder and the ice started to grow again. In the figures where ice temperatures are plotted with depth, the ice surface is used as the point of zero depth, as the freeboard was varying too much to be defined as a fixed value. The positions of the strings are shown in Fig. 4.1 and Fig. 4.4.

5.1.1 The Inner Thermistor String

In Fig. 5.1 temperature recordings from the thermistor string in the hinge zone are shown, through plots of temperature with time at three different depths in the ice in addition to air temperature recorded at the weather station at Svea airport (Fig. 5.1a), and plots of all 16 sensors in the string plotted with depth (Fig. 5.1b). There were considerable differences between the temperatures recorded at the weather station and those recorded by the upper sensors on the string, especially after the dark season had come to an end. Depths in Fig. 5.1a are given in cm *above* ice bottom, and the total ice thickness was measured to be around 90 cm with only small changes during the season. The lines showing ice bottom, snow and ice surfaces in Fig. 5.1b, are based on measurements done on March 30. It is worth noticing that while the ice thickness did not change appreciably, the layer of snow got around 50 cm thick later in the season.

When the string was inserted on the 20th of February, the ice temperature was close to the freezing point all the way through. In the end of February, when the air temperature sank, the temperature gradient in the ice increased. A day or two after this event, a wavelike response in temperature was visible at depths from the bottom and up to around 20 cm below the ice surface, as made more visible in Fig. 5.2. The period of the signal was roughly the same as the semi-diurnal tide. After some days the ice got colder and the signal disappeared, first in the upper part of the ice and around 5 days later it also faded out at the bottom without reappearing later in the season. Another plot showing the temperature oscillations between February 20 and March 10 is shown in Appendix A.1.

5.1.2 Site 1

Figure 5.3 shows the temperatures recorded at Site 1, and is plotted the same way as the recordings in the hinge zone. Depths in Fig. 5.3a are given in cm *below* the ice surface. Similar to the string in the hinge zone, the temperature was close to the freezing point the first weeks before it started to fall. However, compared to both the string in the hinge zone and the one at Site 2, it never got far from the freezing point. Below 30 cm depth, the ice temperature never got less than -2.8°C. Figure 5.3b shows the ice and snow thicknesses as recorded on March 13. Water level is not marked on the figure since the freeboard was varying too much to be mapped properly. In the period between the time when the string was inserted and March 13, the ice was growing at least 20 cm upwards and the string was elevated accordingly, as can be seen in Fig. 5.3b. Also after this event, the ice continued to grow upwards, but unfortunately the magnitude of the growth was not measured accurately. The lack of data in the period between 2 - 14 March was caused by flooding of the cables that connected the string to the data logger by surface water. On March 30, a new string was inserted between Crack 4 and Crack 5 (close to the ”old” Site 1). Its recordings were fairly similar to the string at Site 1, and are given in Appendix A.2.

5.1.3 Site 2

Figure 5.4 shows temperatures recorded at Site 2. The horizontal lines in Fig. 5.4b show the ice and snow surfaces as mapped on March 13, and it should be noted that the amount of snow increased drastically later in the season (up to about 50 cm) and that the ice became about 10 cm thicker. Similarly to the cases described above, the ice was warm all the way through until March 15 when the ice suddenly started to become colder. Around April 10, the temperature gradient was at its largest, and on May 10 the ice was again close to its freezing point at top and bottom with somewhat colder temperatures (around -3°C) in the intermediate layers.

Also here, the string was elevated on March 13 as the ice had grown about 15 cm upwards. However, after this event neither significant amounts of surface water nor superimposed ice was observed. Freeboard is not included in the plot, since it was varying throughout the season. Maximum freeboard measured at Site 2 was 4 cm and the minimum was 2 cm of surface water.

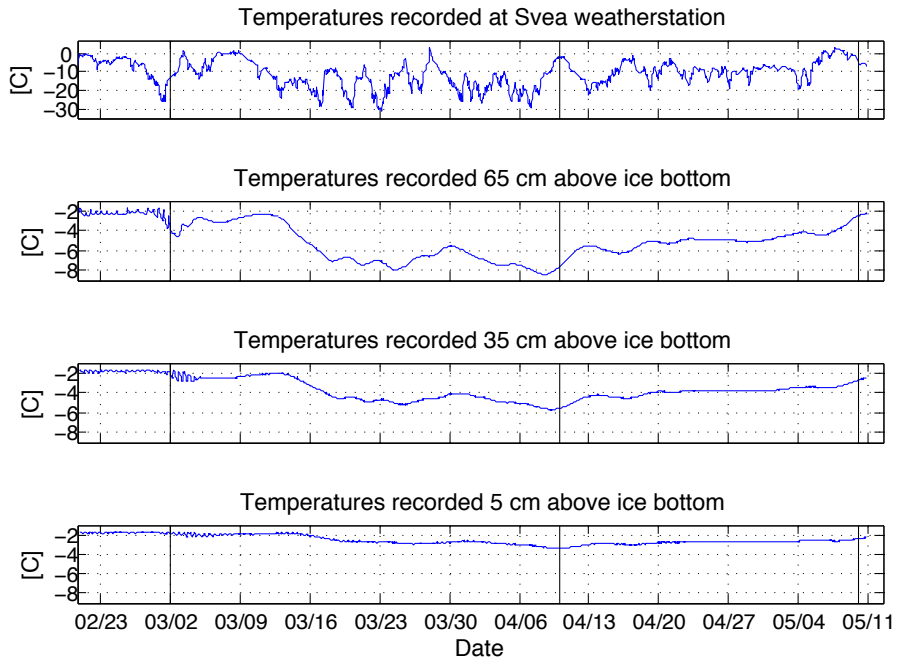

(a)

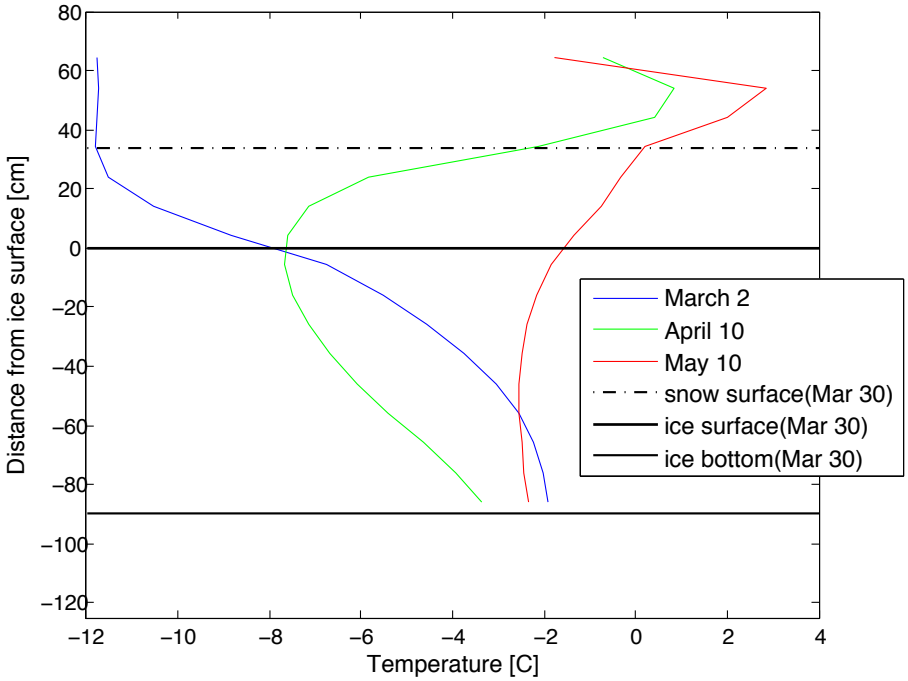

(b)

Figure 5.1: *Plots showing temperatures in the hinge zone between Crack 1 and Crack 2 during the whole season (a), with vertical profiles at three different times, March 2, April 10 and May 10 (b). The black vertical lines in Fig. (a) represent the times when the vertical temperature profiles in Fig. (b) originate.*

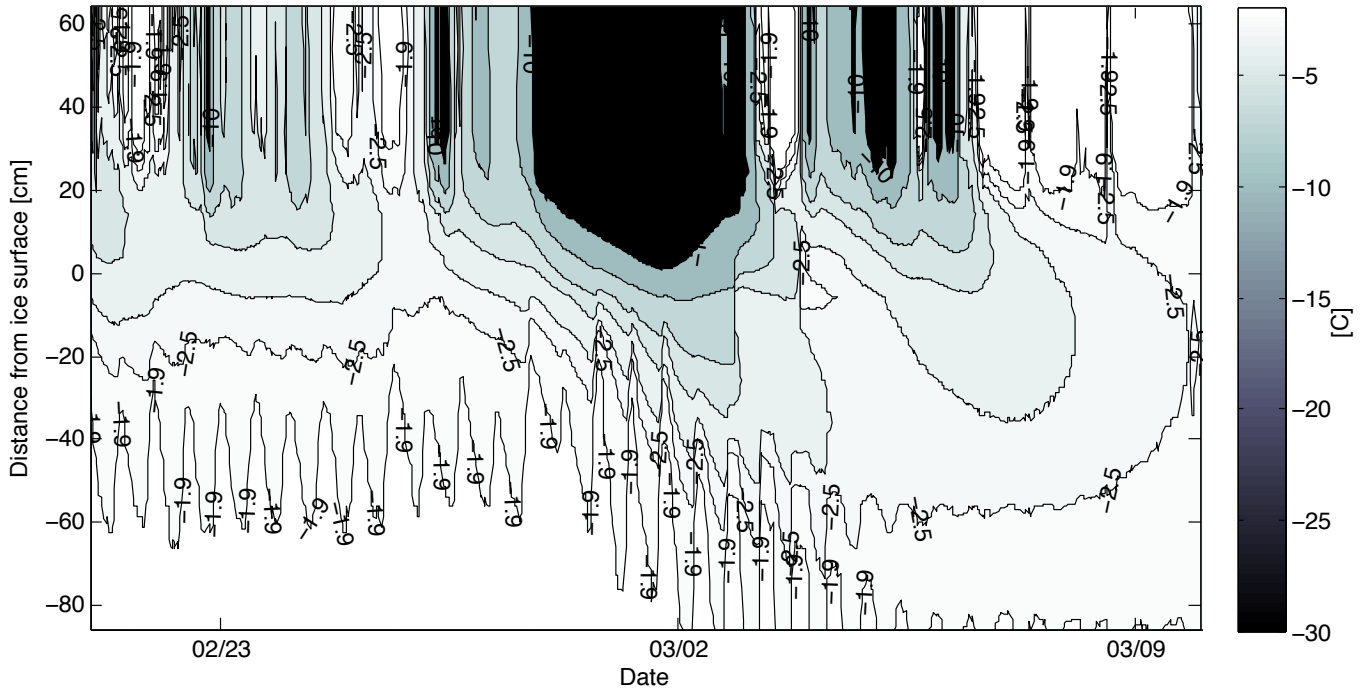

Figure 5.2: *Contour-plot showing the temperature distribution through the ice cover, between Crack 1 and Crack 2 in the period February 20-March 10. The ice thickness was 90 cm.*

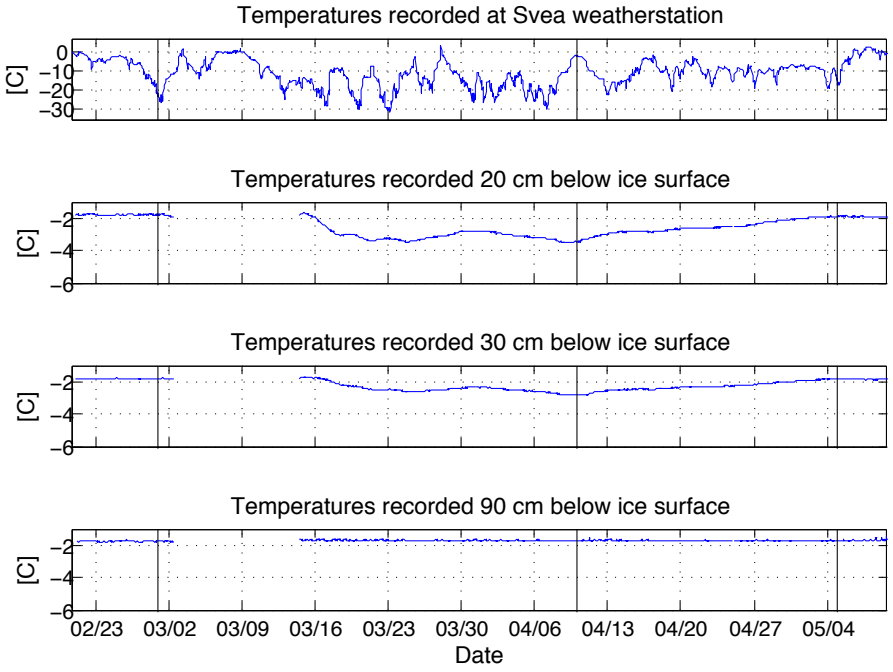

(a)

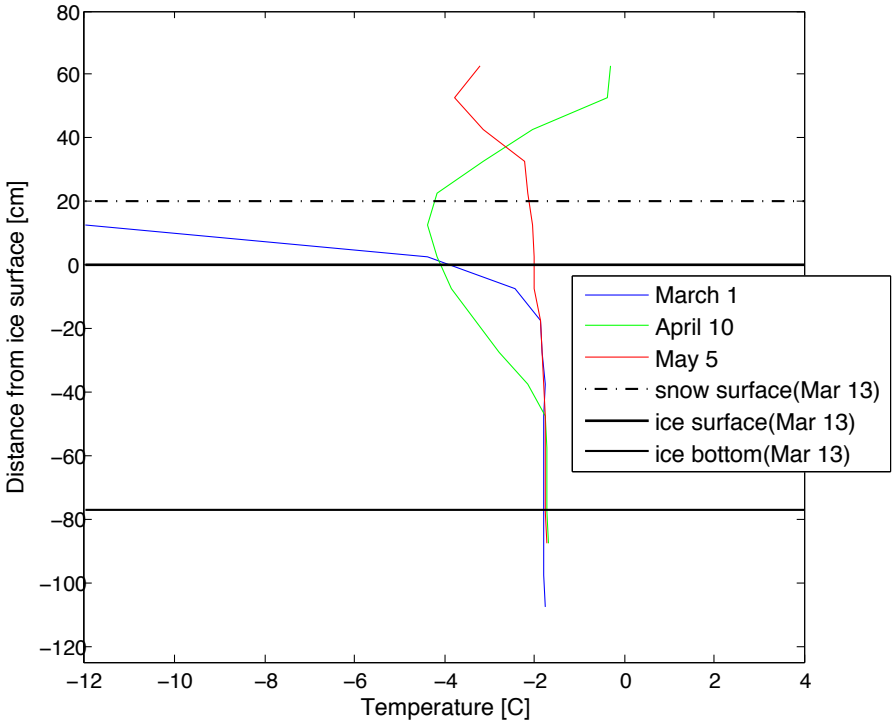

(b)

Figure 5.3: *Plots showing temperatures at Site 1 during the whole season (a), with vertical profiles at three different times, March 1, April 10 and May 5 (b). The black vertical lines in Fig. (a) represent the times when the vertical temperature profiles in Fig. (b) originate.*

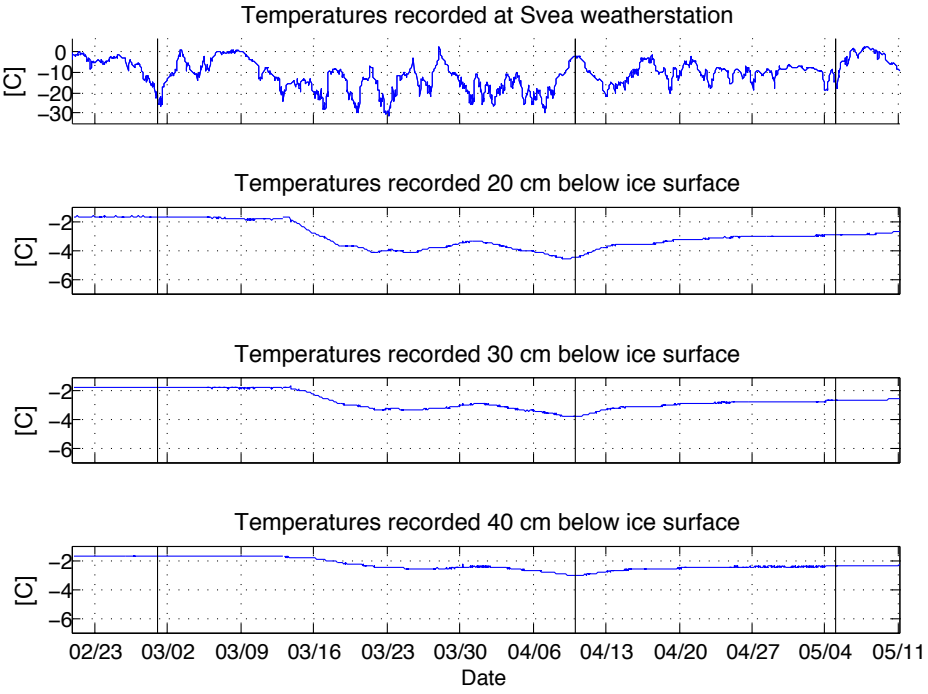

(a)

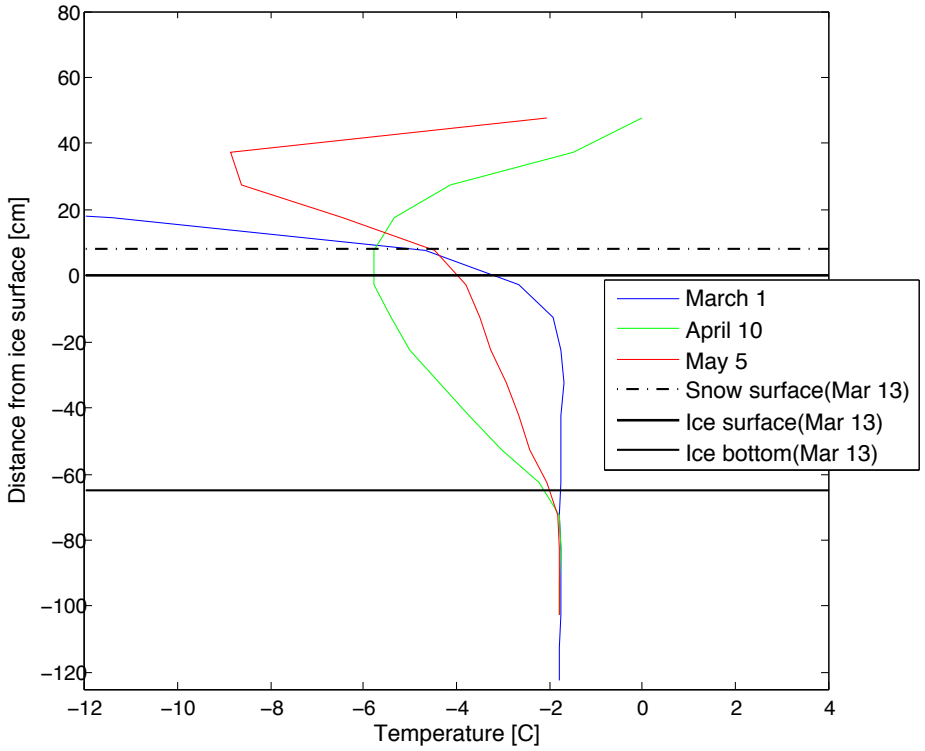

(b)

Figure 5.4: *Plots showing temperatures at Site 2 during the whole season (a), with vertical profiles at three different times, March 1, April 10 and May 5 (b). The black vertical lines in Fig. (a) represent the times when the vertical temperature profiles in Fig. (b) are made.*

5.2 Ice Cores

Of the numerous ice cores that were collected and analyzed during the fieldwork, the most relevant are presented in this chapter. Additional plots of density and salinity, are left for Appendix B.

Figure 5.5: *An ice core collected in the ice foot on March 13. The bottom of the core is towards left on the picture*

5.2.1 Ice Foot

The salinities in the ice foot were considerably lower than in the hinge zone and the floating ice, having mean values of around 1 ppm. Salinities from three different times are shown in Fig. 5.6. The core from February shows an increasing salinity towards the bottom with a maximum of 2.7 ppm at the bottom. The core from March had uniform salinities of around 0.8 ppm almost all the way through. The core from May had lowest salinities with around 0.5 ppm except at the bottom where it was 1.2 ppm. The length of the cores were varying. For all the cores, the ice at the bottom was mixed with sediments, and layers of the ice in the upper parts could often be classified as snow ice. A picture of one of the cores that were collected in the ice foot is given in Fig. 5.5, showing that the bottom part of the core is a mixture of sediments and ice. No floating water was found in any of the holes where the ice cores had been removed. It should also be mentioned that, unfortunately, tidal levels were not noted when collecting the cores in the hinge zone, and are therefore unknown.

5.2.2 Hinge Zone

Salinity: In the period between February 20 and March 13, an oscillating response in ice temperature was observed between Crack 1 and Crack 2 (see Fig. 5.2). One explanation of this phenomenon could be vertical motion of sea water driven by tidal forces. Although the temperature oscillations had almost disappeared at that time, cores for salinity and density measurements were taken on March 13 at high and low tide close to the thermistor string, in order to further

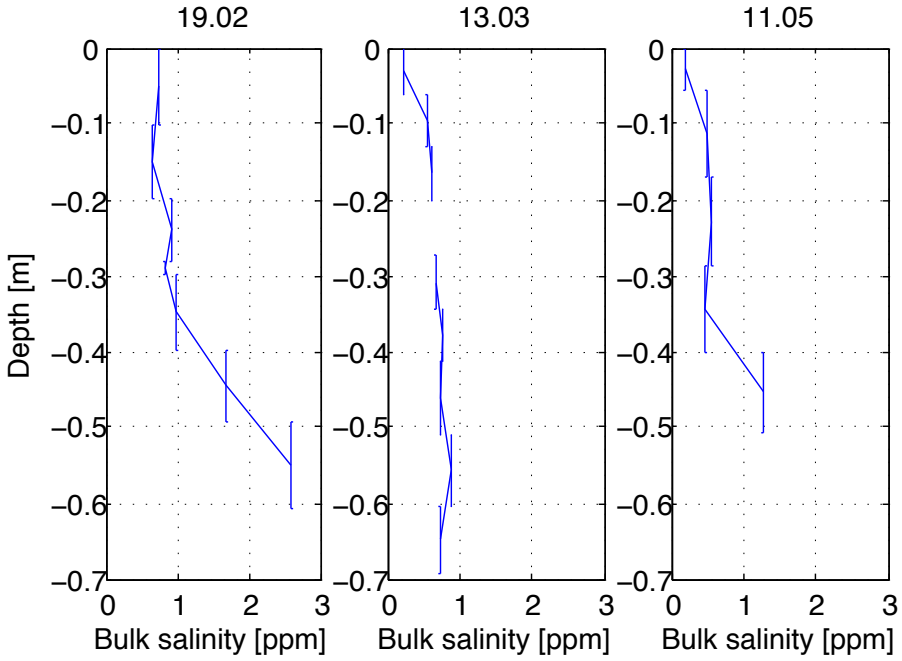

Figure 5.6: *Bulk salinity of three ice cores taken in the ice foot in February, March and May*

investigate this. The result is shown in Fig. 5.7. The cores were taken around 0.5 m from each other and both had low salinities in the top layers, around 0.3 ppm, which increased down to 0.7 m depth. The core that was collected at high tide had a salinity around 4 ppm which was slowly increasing from 0.5 to 0.7 m depth. In contrast, the core collected at low tide had lower salinties, around 0.4 ppm, down to 0.4 m before it increased rapidly and reached a 5.5 ppm peak at 0.7 m depth. In the lower 15 cm, the low tide-core had a salinity of 4 ppm while the core collected at high tide had a salinity around 1.7 ppm higher. Unfortunately, no measurements of water level were done when these cores were collected. However, the plots showing Section 1 at high and low tide (presented in Section 5.3.2) indicate that the water level between Crack 1 and Crack 2 was lower than the ice bottom by low tide, and reaching up to a level around 30 cm depth by high tide on March 13.

Density: Density measurements of the two cores are shown in Fig. 5.8. They both show a trend of low density in the topmost layer and increasing density towards the bottom. They have approximately the same mean values, 785 kg/m^3 at high tide and 789 kg/m^3 at low tide. However, the shape of the two curves differ from each other; the high tide profile has relatively constant densities at medium depths, around 785 kg/m^3, while the low tide profile shows a depression with less than 700 kg/m^3 at 0.55 m depth.

Permeability: Figure 5.9 shows plots of permeability from the hinge zone between Crack 1 and Crack 2, calculated using Eqn. 2.5 with the salinities measured in the core that was collected at *high tide* on March 13 (shown in Fig. 5.7), and temperatures from four different times. The reason why the dates were chosen were as follows: February 24 and March 12 were just before and after the event shown in Fig. 5.2, for which permeability was suggested an important

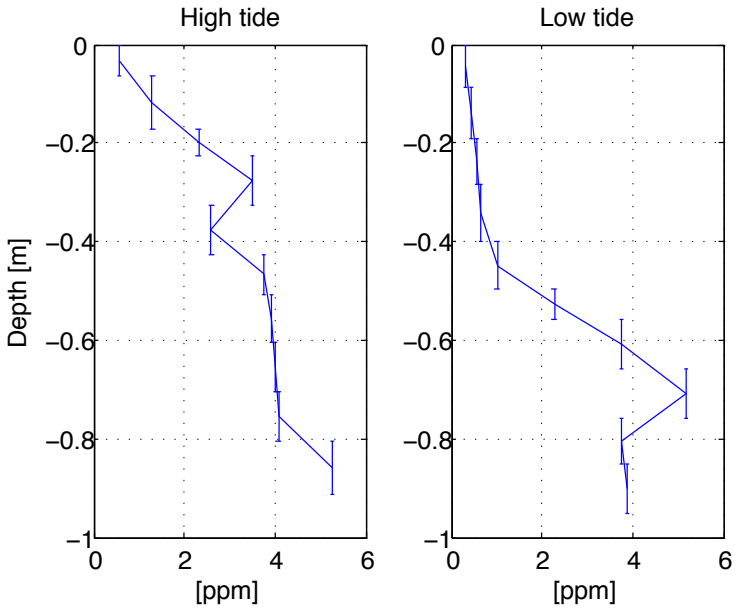

Figure 5.7: *Bulk salinity of two ice cores collected between Crack 1 and Crack 2 on March 13. The cores were taken at high and low tide.*

parameter. In the period around April 10 the ice was at its coldest, while in May the ice was warmer again, but no oscillations in temperature like those shown in Fig. 5.2 were observed. A comparison of permeability from these dates was therefore of interest. It should be noted that there did not exist any salinity profiles from the given location measured later in the season than March 13, so these had to be used despite the fact that a decrease or increase of ice salinity would influence the permeability.

As shown in Fig. 5.9 and Table 5.1, the highest average permeability of the four was found on February 24. This was just before the event when temperature oscillations in the ice was clearly visible. After the event, on March 12, the permeabilities had decreased considerably. On April 10 it was at its lowest, and on May 11 it had become higher again, although not as high as on February 24. In all the four profiles the permeabilities were increasing towards the bottom which also was the warmest and most saline part of the ice. In the lower 30 cm, the permeability never got higher than the values from February 24. The two profiles in Fig. 5.10 are calculated by

Table 5.1: *Key values of permeability in the hinge zone (Between Crack 1 and Crack 2) from four different dates. Note that the minimum values are given in order* 10^{-15}

	Permeability, k [m^2]			
Date	Mean	Minimum	Maximum	Note
February 24	$2.3{\cdot}10^{-11}$	$7.4{\cdot}10^{-15}$	$7.8{\cdot}10^{-11}$	Before temperature oscillations appeared
March 12	$1.1{\cdot}10^{-11}$	$0.7{\cdot}10^{-15}$	$5.9{\cdot}10^{-11}$	After the oscillations had disappeared
April 10	$0.2{\cdot}10^{-11}$	$1.1{\cdot}10^{-15}$	$1.2{\cdot}10^{-11}$	The ice was relatively cold
May 11	$0.9{\cdot}10^{-11}$	$169{\cdot}10^{-15}$	$3.4{\cdot}10^{-11}$	The ice was relatively warm

the same method, using temperatures from March 13, and the salinities measured in the two

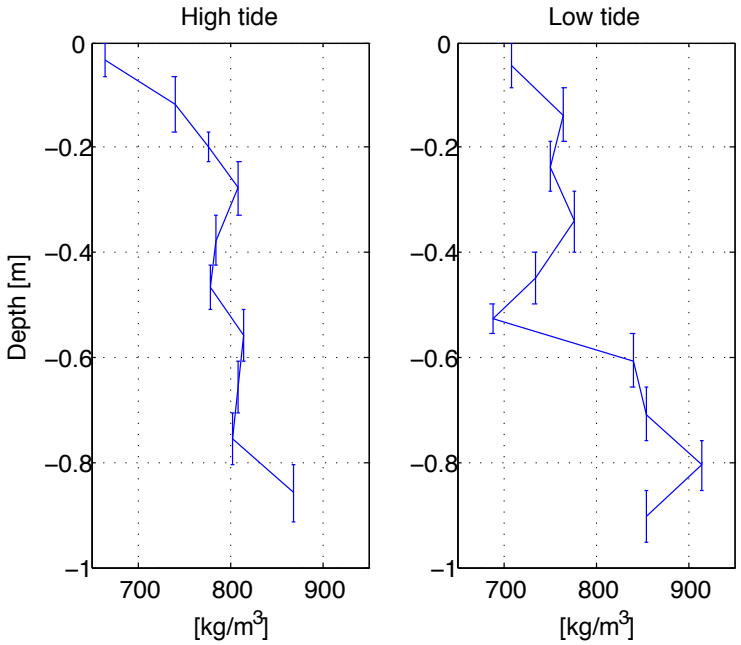

Figure 5.8: *Density measurements of the two ice cores that were collected between Crack 1 and Crack 2 on March 13*

cores collected at high and low tide on the same date. Key values are given in Table 5.2. At high tide, the maximum permeability was found in the bottom 10 cm, while at low tide the maximum permeability was found around 65 cm depth. Both minimum, maximum and mean permeabilities were found to be lower at low tide than at high tide.

Table 5.2: *Key values of permeability in the hinge zone from March 13, at high and low tide. Note that the minimum values are given in order* 10^{-15}

	k [m^2]		
	Mean	Minimum	Maximum
High tide	$1.2{\cdot}10^{-11}$	$0.7{\cdot}10^{-15}$	$6.0{\cdot}10^{-11}$
Low tide	$0.8{\cdot}10^{-11}$	$0.1{\cdot}10^{-15}$	$4.0{\cdot}10^{-11}$

5.2.3 Site 1

On March 13, Site 1 was moved 2.5 m away from the shore, to the other side of Crack 5, and so was also the location where the Site 1-cores were collected. The salinity profiles from Site 1, shown in Fig. 5.11, are drawing a zigzagging pattern in the beginning of the season, with two to three saline layers separated by fresher ice. On March 30, the salinity was decreasing with more than 2 ppm going from 0.25 m to 0.45 m depth, followed by a markedly 3 ppm increase going 15 cm further down. Contrary to the others, the core from March 30 had lower salinities in the bottom 15 cm of the ice, which were decreasing towards the bottom. In April and May the profile had smoothened out into a C-shaped curve, with higher salinities in the ice top and

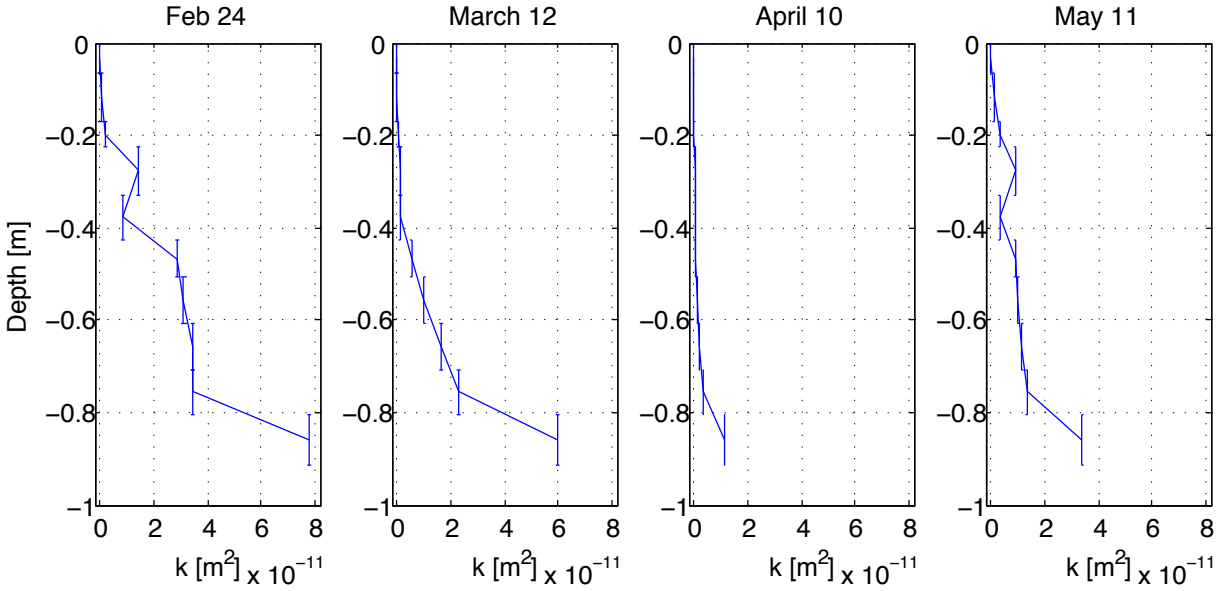

Figure 5.9: *Permeability (k) in the hinge zone, between Crack 1 and Crack 2 at four different times. The profiles are calculated using the salinities measured in the ice core that was collected at high tide on March 13, and temperatures from February 24, March 12, April 10 and May 11.*

bottom layers than in the middle of the ice cover. On May 9, the saline middle layer was not visible at all.

5.2.4 Site 2

Figure 5.12 shows the salinity measurements from cores collected close to Site 2. The measurements were for a while comparable to Site 1, with three layers of saline ice at the top, bottom and in the middle of the ice, separated by less saline layers. This form of the profile was visible between March 12 and May 9. Also here, the curves were getting more C-shaped towards the end season, but contrary to Site 1, the middle saline layer remained clearly visible until the last core was collected in May. As shown in Table 5.3 there is no big difference in mean salinity between Site 1 and 2, except somewhat higher values at Site 1. The mean values also show a trend of slight decrease in salinity from March to May.

Table 5.3: *Mean values of salinity [ppm].*

Location	Jan 30	Feb 19	March 12	March 30	April 24	May 9
Ice foot		1.2	0.6			0.6
Site 1	6.9	6.5	7.2	5.2	5.9	4.9
Site 2	6.6	4.7	6.5	5.8	6.3	5.3

5.2.5 Snow, Ice, Slush and Freeboard

Freeboard, snow- and ice thicknesses are shown in Tables 5.4 and 5.5. At Site 1, the freeboard varied with the tide, and since the values in Table 5.4 are from different parts of the tidal cycle,

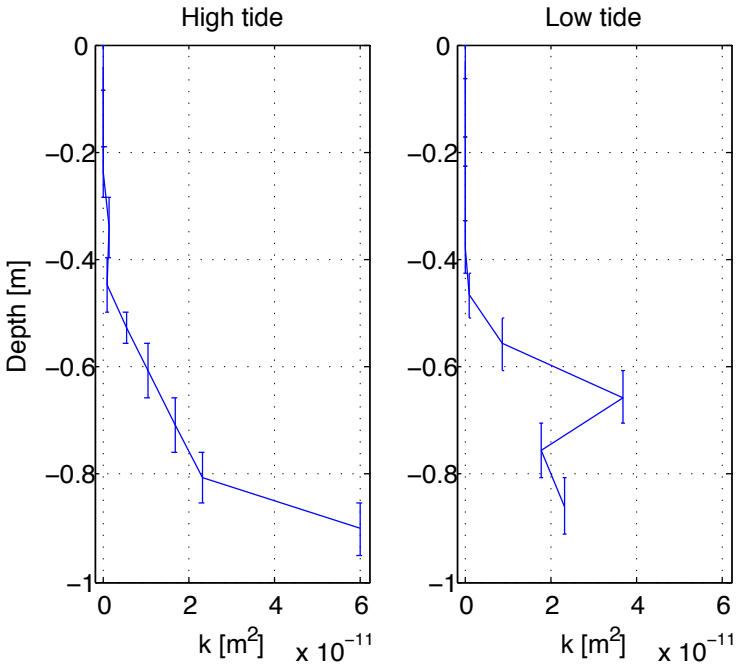

Figure 5.10: *Permeability (k) between Crack 1 and Crack 2, calculated using the temperatures recorded on March 13 with salinities measured at high and low tide on the same date.*

they are not representative and should be seen together with the results in Section 5.3. At Site 2 on the other hand, the freeboard seemed to be unaffected by the water level. At both sites, the measured amount of surface water (represented by negative freeboard values in the tables) was at its maximum on February 19. On this date, the ice thickness at Site 2 was at its lowest, after a decrease of 11 cm during less than three weeks. The ice at Site 1 on the other hand, had grown 5 cm in the same period. A rapid growth occurred at Site 2 during the next 3 weeks, and the ice there reached its maximum thickness on April 24, while at Site 1, the ice was growing at a relatively even rate through the season until May 9.

The growth rates at Site 1 and Site 2 were comparable, except the significant drop in ice thickness at Site 2 before February 19 and the following sharp increase before March 12. On February 19, the total thickness of snow/slush/snow ice at Site 1 was about twice as high as at Site 2.

Table 5.4: *Snow, ice, slush and freeboard at Site 1. Negative freeboard values mean surface water.*

Date	Snow [cm]	Slush/snow ice [cm]	Ice thickness [cm]	Freeboard [cm]
Jan 31	15	13	43	-6.5
Feb 19	6	36	55	-16.5
Mar 12	19	2	60	0
Mar 30	31	0	64	3
Apr 24	36	4	72	0
May 9	50	0	85	-18

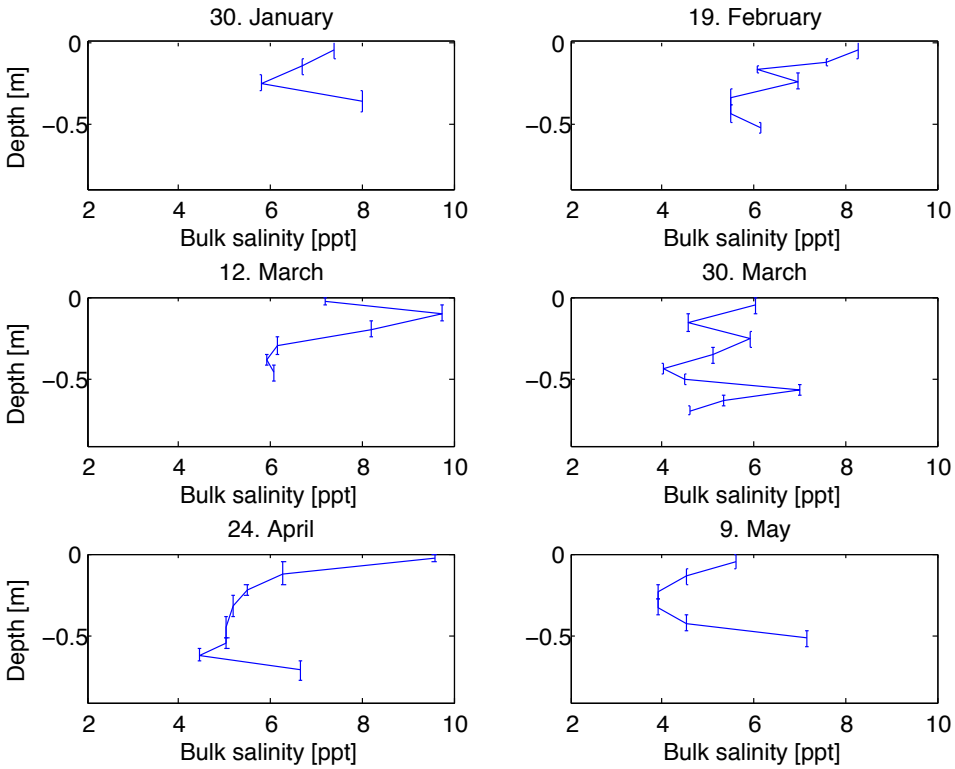

Figure 5.11: *Salinities at Site 1. The vertical bars show the height of each measured piece of the ice core.*

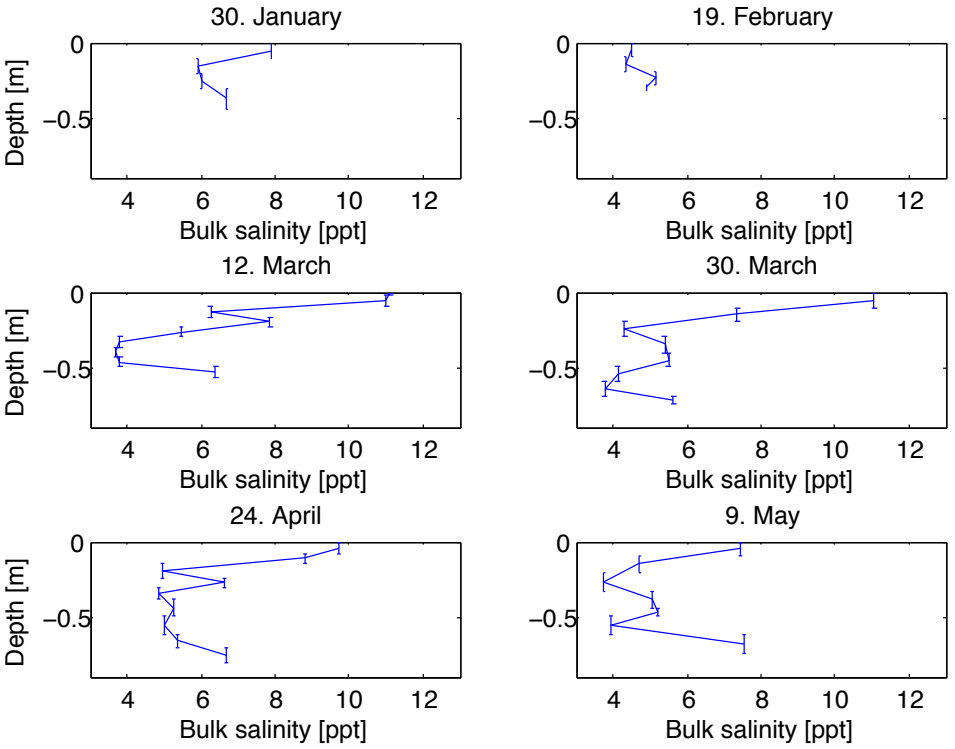

Figure 5.12: *Salinity measurements from Site 2. The vertical bars show the height of each measured piece of the ice core.*

Table 5.5: *Snow, ice, slush and freeboard at Site 2. Negative freeboard values mean surface water.*

Date	Snow [cm]	Slush/snow ice [cm]	Ice thickness [cm]	Freeboard [cm]
Jan 31	7	0	44	1.5
Feb 19	22.5	0	33	-12
Mar 12	19	2	65	4
Mar 30	25	0	66.5	1.5
Apr 24	22	0.5	78.5	2
May 9	42	0	77	0

5.3 Cross-Sections of the Hinge Zone

Section 1 was repeated four times between March 13 and May 10, it was stretching from the coastal bluff, through the hinge zone and out to the level ice. Table 5.6 gives locations of the different features and zones along Section 1.

Table 5.6: *Distance in meters from the coastal bluff to the shore-parallel cracks and to the sensors close to Section 1, measured on May 10. It also shows which parts of the sections that were defined as ice foot, hinge zone and free-floating ice.*

	Meters from the coastal bluff
Crack 1	7.5
Inner hinge-zone thermistor	8.6
Crack 2	9.5
Crack 3	12
Crack 4	15.3
Outer hinge-zone thermistor	18
”Old” Site 1	19.5
Crack 5	20.5
Site 1	22
Ice foot	0 - 7.5
Hinge zone	7.5 - 20.5
Free-floating ice	20.5 - 35

5.3.1 Ice Growth

Plots of ice thickness along Section 1 are shown in Fig. 5.13. In Table 5.7, key numbers from the different parts of the section are presented.

Ice foot: Inside Crack 1, the thicknesses measured on March 13 and April 24 were more or less the same ranging from 9 cm closest to the bluff, to around 80 cm close to Crack 1 with an average of around 60 cm. On March 31, the ice foot was measured to be much thinner on average (53.7 cm), and on May 10 an average thickness of 53.2 cm was recorded.

Hinge zone: In the hinge zone, which was located between 7.5 m and 20.5 m from the coastal bluff, the ice was found to be thicker than both in the ice foot and the free-floating ice. In the period when the sections were made, the ice in the hinge zone was growing quicker than the free-floating ice, and generally it had a smaller temperature gradient than both the free-floating ice and the ice foot (Section 5.1). The largest ice thickness along Section 1 was found on April 24, when the ice was 171 cm thick between Crack 4 and Crack 5.

The free-floating ice: Contrary to the hinge zone, the free floating ice was found to grow during most of the period when the sections were taken, reaching its maximum on May 10. Between April 24 and May 10 the mean ice thickness in the hinge zone decreased while it in the same period increased in the free-floating ice. Also at Site 2 the ice was growing most of

the period, although not as much as the ice in the outer 15 m of Section 1. Table 5.5 shows the evolution of ice thickness at Site 2.

Table 5.7: *Minimum, maximum and mean values of ice thickness along Section 1, given in cm.*

	Ice foot			Hinge zone			The free-floating ice		
Date	Min	Max	Average	Min	Max	Average	Min	Max	Average
Mar 13	9	88	63.5	57	115	93.5	54	61	63.6
Mar 31	24	110	53.7	65	127	100	58	70	57.7
Apr 24	9	86	62.7	72	171	124.5	64	75	69
May 10	9	75	53.2	70	145	106.7	66	84	74

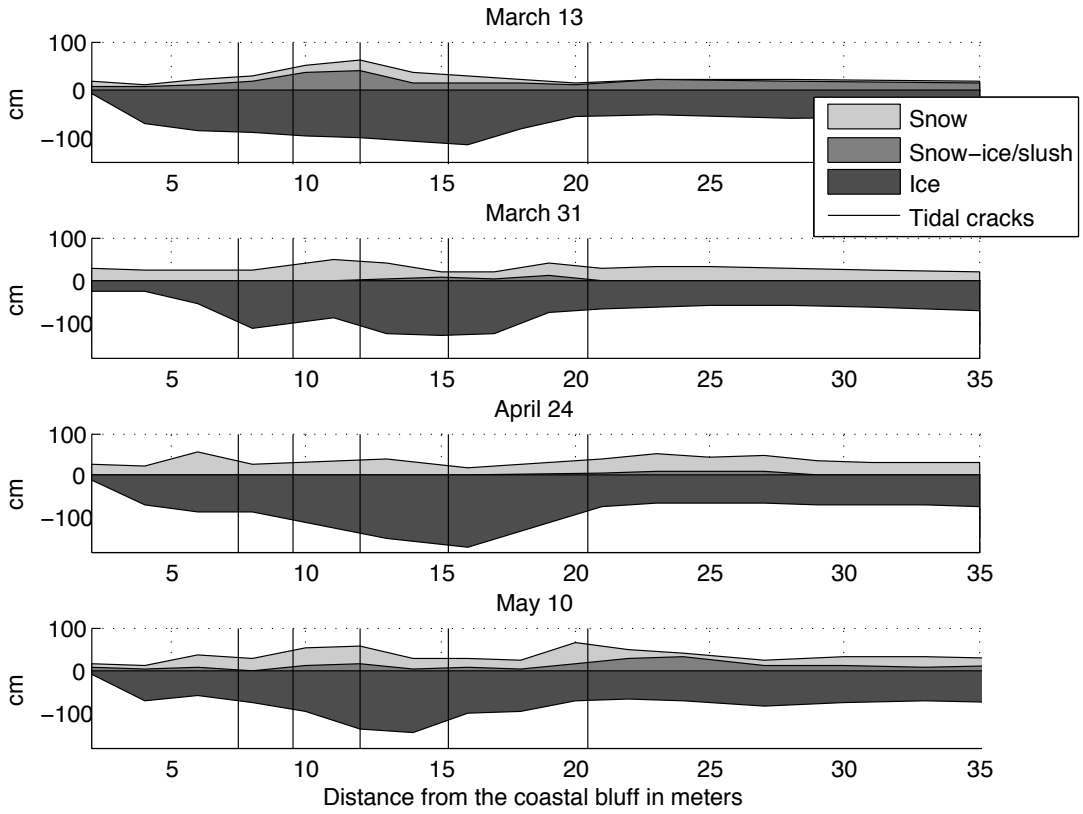

Figure 5.13: *Comparison of Section 1 taken at four different times, showing thicknesses of ice, snow-ice/slush and snow. The vertical lines represent the tidal cracks, where Crack 1 is the leftmost and Crack 5 is the rightmost line. Note that the axes are not in scale.*

5.3.2 Vertical Movement of the Ice

Figures 5.14 and 5.15 show plots of the ice at high and low tide relative to the water level. In Fig. 5.15, a plot of the ice at medium water level from April 24 is also shown. In all the profiles, except the one from April 24, considerable amounts of surface water were present between 15 and 25 m away from the coastal bluff. Tidal ranges, based on data from the Seabird sensor (Section 5.4), at the times when the sections were made are shown in Table 5.8.

Table 5.8: *Tidal ranges at the times when the sections were taken*

Date	Tidal range [m]
March 13	0.85
March 31	1.7
April 2	1.7
April 24	1.1
May 10	0.8

March 13: There was zero freeboard at high tide and up to 22 cm surface water at low tide between Crack 4 and Crack 5. The distance between the outer points where the ice was grounded at high and low tide was 4 m.

March 31: On March 31, the case was the opposite, with up to 20 cm surface water between Crack 4 and Crack 5 at high tide while the freeboard was close to zero at low tide. The distance between the points where the ice was grounded at high and low tide was 7 m.

April 24: The largest amount of surface water, 8 cm, was found outside Crack 5, three hours after low tide. At both high and low tide the freeboard was close to zero. The distance between the points where the ice was grounded at high and low tide was 8 m.

May 10: Contrary to the others, the profile from May 10 shows an elevation/buckling of the ice close to Crack 5 at high tide while it seemed stretched out at low tide. It should be noted that the points where the ice was measured were not the same in all the profiles, and that in all the profiles except the one from May 10, they were a meter or so away from Crack 5. Most surface water was found outside Crack 5, amounting to 28 cm at high tide and 26 cm at low tide. The distance between the points where the ice was grounded at high and low tide was 12 m.

The distance between the points where the ice was grounded at high and low tide was increasing throughout the spring, despite the fact that the tidal range was much smaller in May than in March and April.

5.3.3 Section 2 and the Shore-Parallel Section Along Crack 4

These sections were only made once, on April 2. They are referred to in Fig. 4.2 as ”Section 2” and ”Shore-parallel section”. A plot of Section 2 is shown in Fig. 5.16a. The ice thickness in the hinge zone was 197 cm at the most, 16 m from the coastal bluff. In comparison, this is 70 cm thicker than the highest ice thickness that was measured in Section 1 on March 31, two days earlier. The free-floating ice was around 60 cm thick, which is more or less the same as it was in Section 1. A buckling of the ice was clearly visible, both at high and low tide. At high tide, the ice had a freeboard of 23 cm, 18 m off the bluff. 6 m further out, at high tide, there was 22 cm surface water which decreased to a few cm thick layer which was present on the ice all the way out to where the section was ending. At low tide, the ice had a freeboard of 47 cm at a point 16 m from the bluff, and almost no surface water was present on the ice.

The 11 m long section taken along Crack 4, going from Section 2 to Section 1, is shown

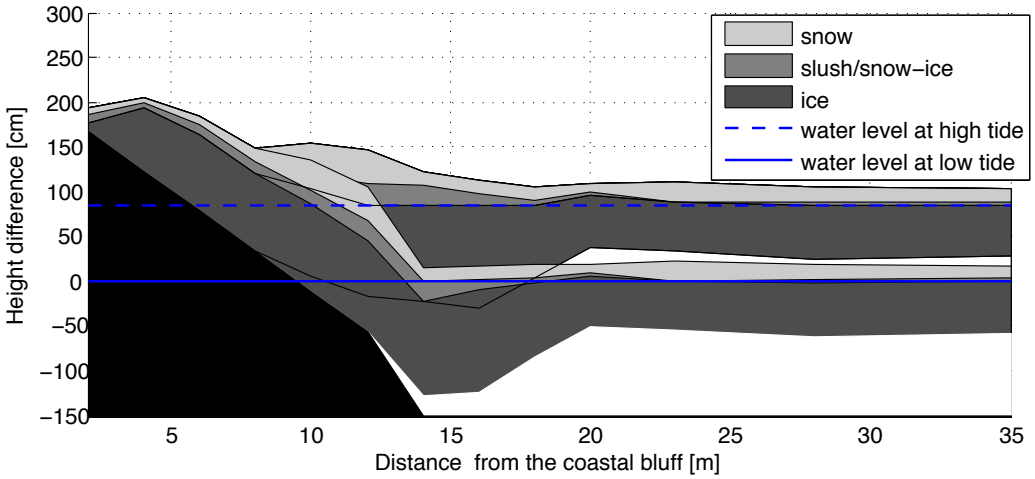

(a) *March 13*

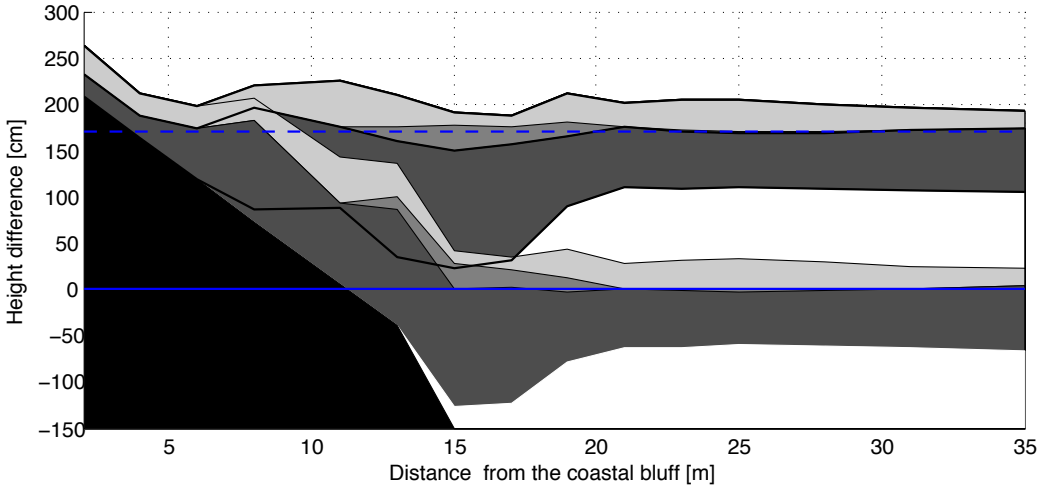

(b) *March 31*

Figure 5.14: *Section 1 taken on March 13 (a) and March 31 (b), at high and low tide. Note that the axes are not in scale.*

in Fig. 5.16b. It was taken 3 hours after high tide and shows a large variation along the shore, with ice thicknesses ranging from 197 to 107 cm. The maximum freeboard was 23 cm and the highest amount of surface water was 20 cm.

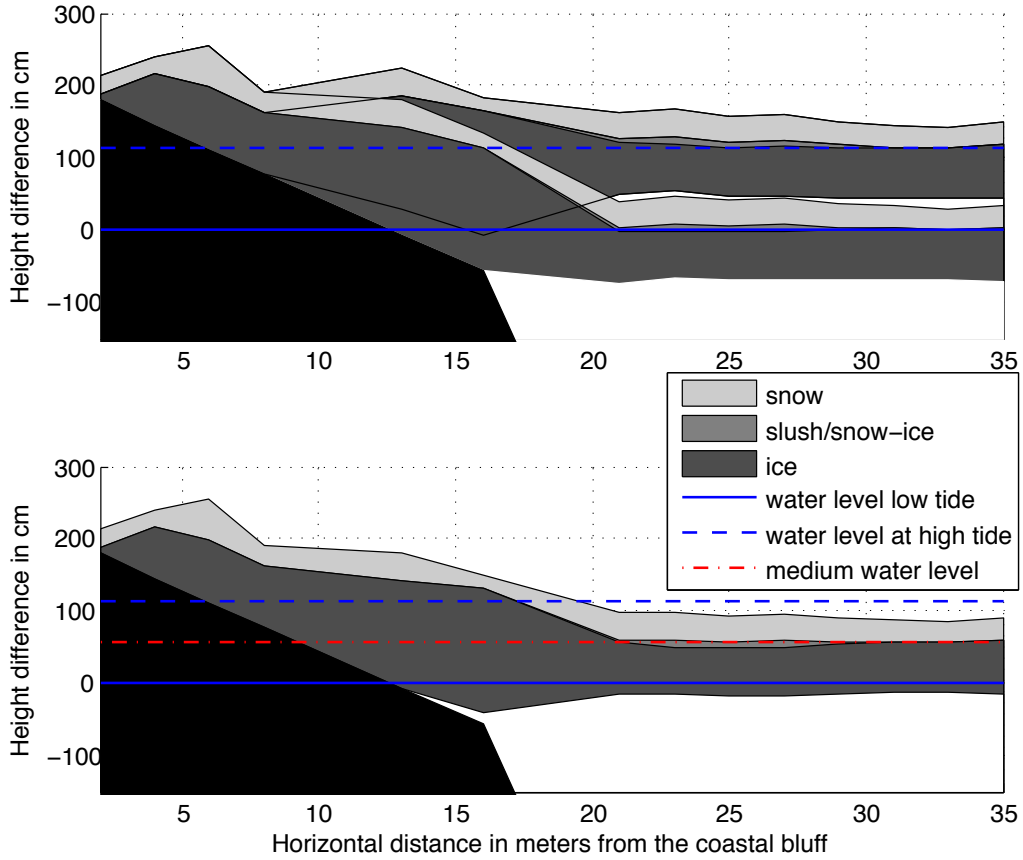

(a) *April 24. Plots of the ice at high and low tide (upper plot), in addition to three hours after low tide (lower plot)*

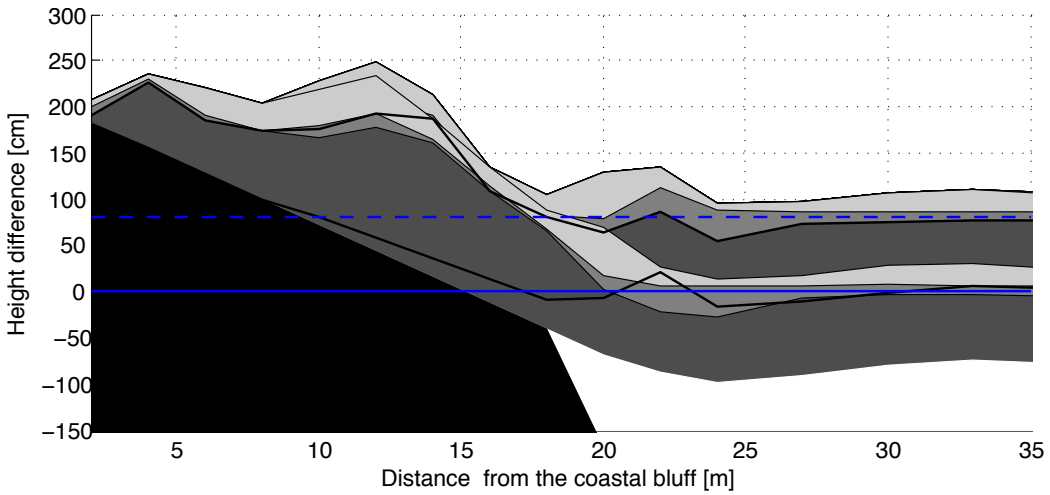

(b) *May 10*

Figure 5.15: *Section 1 taken at high, low and medium tide on April 24 (a), and at high and low tide on May 10 (b)*

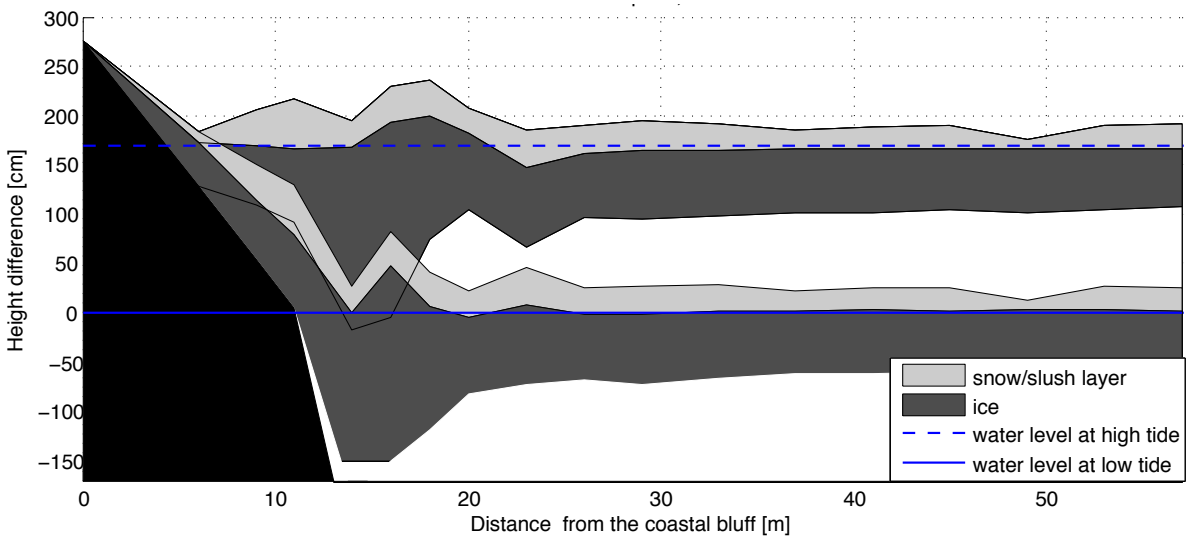

(a) *Section 2.*

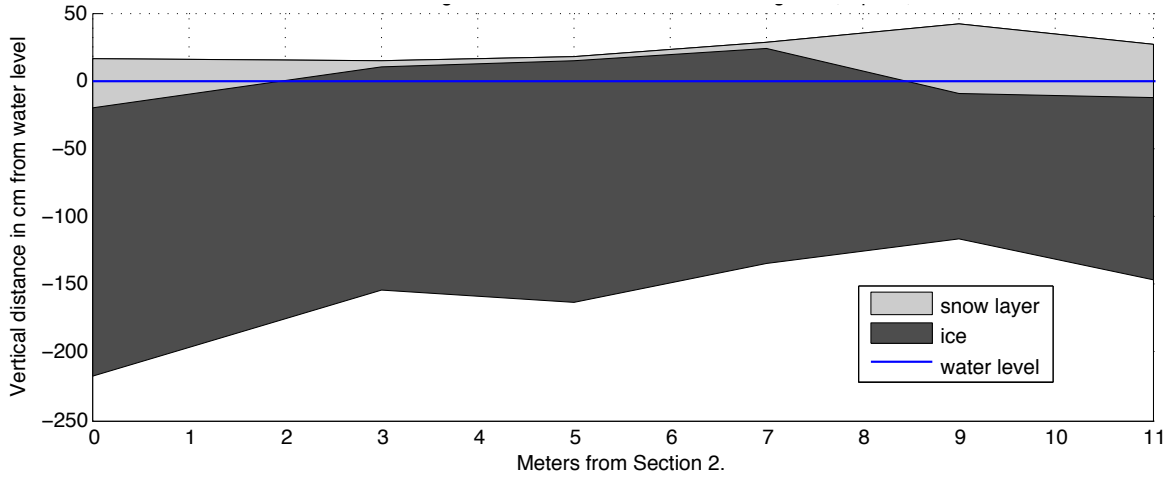

(b) *The shore-parallel section taken 3 hours after high tide, going between Section 2 (left side of the figure) and Section 1.*

Figure 5.16: *The two sections made on April 2, Section 2 (a) and the shore-parallel section (b)*

5.4 Water Temperature and Pressure

Plots of temperature (upper plots) and sea level variations are shown in Figs. 5.17 and 5.18 for two time intervals. The temperature plot in Fig. 5.17 is smoothed to make the seasonal trend more visible, although temperature fluctuations following the tidal movements like those shown in Fig. 5.18 were present most of the time. The water temperature was close to, or below -1.9°C throughout the season. The coldest temperature measured was -2.03°C and the maximum was -1.84°C. The water was relatively warm in late February, and a slightly decreasing trend until the end of April was observed before the temperature increased again in the beginning of May. In the period between April 11 and April 20, the water temperatures were slightly higher relative to the weeks before and after. The tidal range varied between 2.16 m at spring tide and 0.44 m at neap tide, with a medium range of 1.22 m.

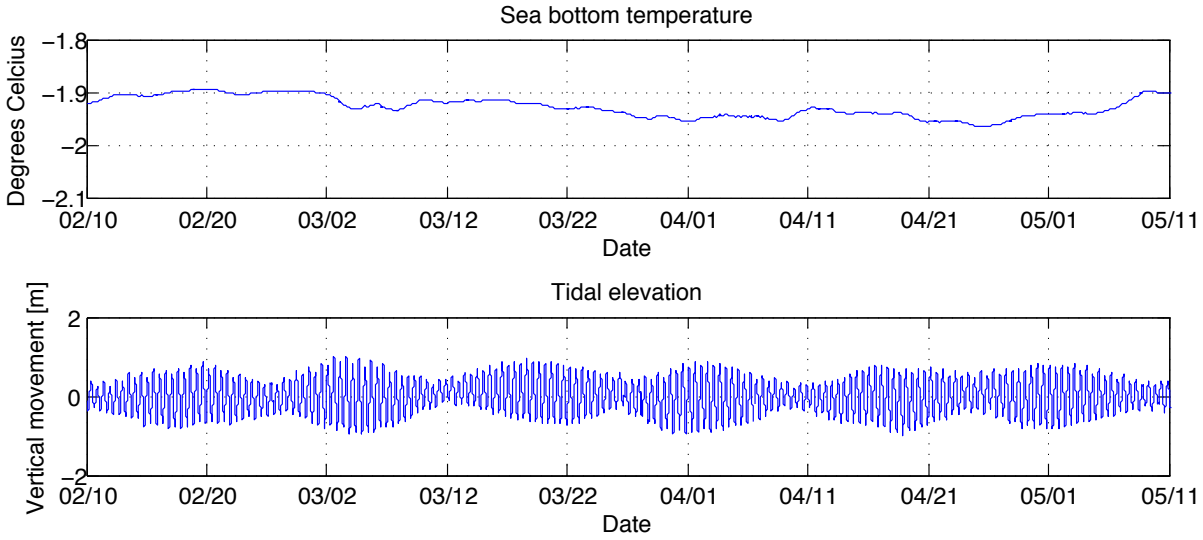

Figure 5.17: *Water temperatures and tidal variations through the whole period.*

Figure 5.18 is a non smoothed zoomed-in plot showing temperature and water level between March 29 and April 1. The temperatures oscillated with the tide and were around 0.1°C higher at high tide than at low tide. A tendency of a sharp increase in temperature just before the tide was at its highest followed by a slower decrease during ebb, low tide and flow is visible. This pattern was recognizable through the whole period, with some variations in amplitude and occasional irregularities.

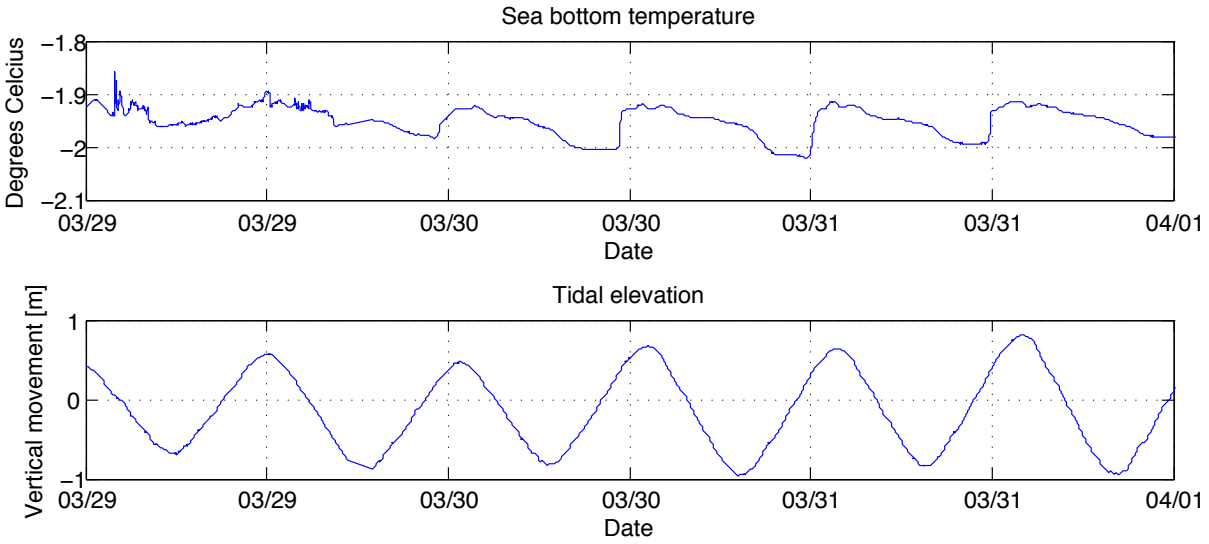

Figure 5.18: *Semi-diurnal oscillations in water temperature (upper plot) and sea level (lower plot). A trend of sharp increase in temperature around high tide was observed, followed by a slower decrease during ebb, low tide and flow.*

Chapter 6

Discussion

6.1 Permeability

By the end of February, the air temperatures sank considerably after the long period of warm weather was over. Oscillations in ice temperature with a period close to the semidiurnal tide were then clearly visible for some days (Figs. 5.2 and 6.1), between Crack 1 and Crack 2. A closer look at the temperature plots reveal similar oscillations, however with smaller amplitude, before the event. After the days with strong oscillations, the ice got colder and the signal disappeared completely, except in the bottom 5 cm of the ice. It is likely that this signal originated from water and tidal motions, since no such oscillations were observed in air temperature during the same period. Also, the change in ice temperature was quicker than the thermal properties of solid ice would allow such a signal to propagate from the top or the bottom of the ice without being smoothed out, or at least delayed, after penetrating more than 20 cm of ice. A plausible explanation of the disappearance of the signal is permeability differences of the ice before and after the event, due to the fact that warm ice is more permeable than cold ice (Cox and Weeks, 1983; Notz and Worster, 2009).

To further investigate this phenomenon, two ice cores were taken close to the thermistor string on March 13, just after the signal had disappeared. Salinity and density profiles from these cores are shown in Figs. 5.7 and 5.8, respectively. The salinity profiles differ from each other as the one taken at high tide was more uniformly distributed with depth, while the core taken at low tide was fresher at top with rapidly increasing salinities down to 0.7 m depth. Density profiles from the same cores revealed that at low tide, the density was low between 0.2 and 0.6 m depth, and high between 0.6 and 0.8 m, compared to high tide. The mean density was more or less the same for both of them. This might be indications of moving 'centers of gravity' for both salinity and density, moving up at high tide and down at low tide. The salinity profiles indicate a sinking column of brine in the upper layers of the ice while the water level was sinking - assuming that the brine in the top layers of the ice was replaced by air - causing the noticeable decrease in salinity between high tide and low tide. The density profiles agree, with higher densities at high tide than at low tide in the upper 60 cm of the ice. However, the trend observed in the cores could also have been caused by other factors, such as spatial variations in ice properties and errors in the density measurements. On March 13, the oscillating temperature signal had disappeared in all ice layers except at the lower sensor which was located about 5 cm above the ice bottom. A high permeability before the event could let the standing column of salt water/brine flow up and down through brine channels, drainage tubes and interconnected brine pockets, driven by tidal

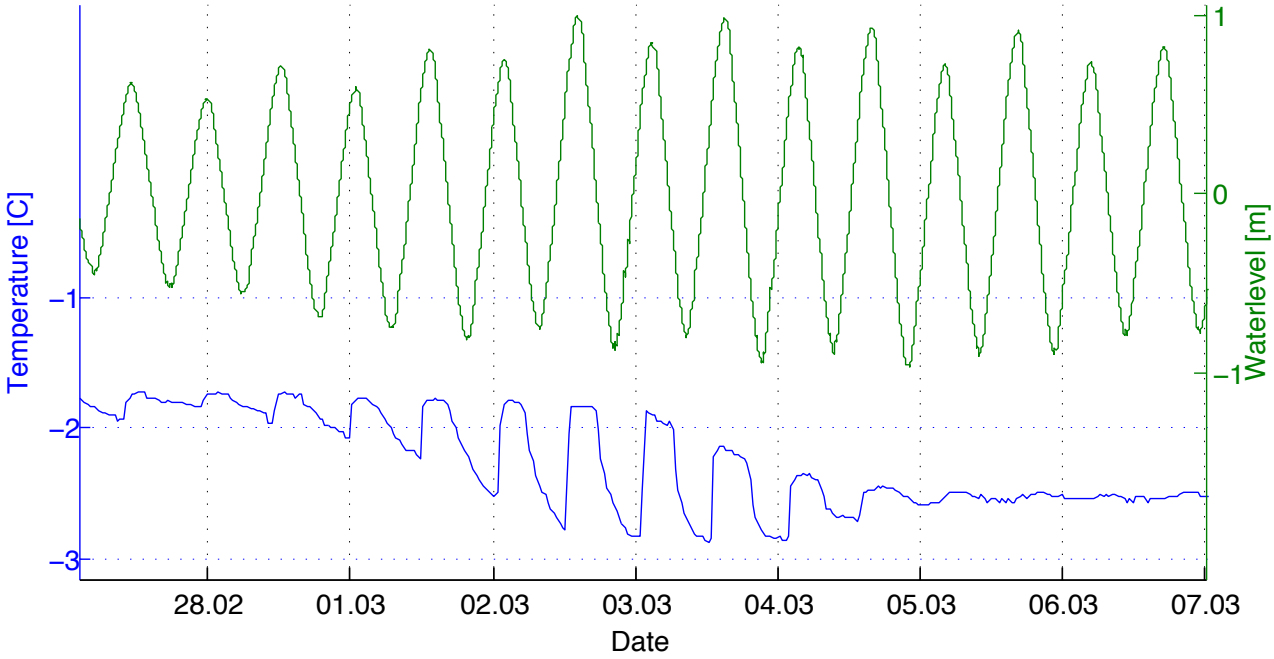

Figure 6.1: *Oscillations in water level (green curve) and temperatures recorded 35 cm above ice bottom (blue curve) plotted with time*

pressure variations, as illustrated in Fig. 6.2. Since the temperature signal correlated so well with the tide (see Fig. 6.1), without any significant delay between the rise in pressure and the rise in temperature, it is likely that a brine channel was located very close to or around the thermistor string. A larger distance between the string and the closest brine channel would mean a delayed temperature signal. As illustrated in Fig. 6.2, the temperature of the ice will not vary as much as the temperatures at a certain point within a brine channel.

As the ice was grounded most of the time, tidal motion of the sea water level would be relative to the ice - contrary to the free-floating ice - inducing the variations in pressure associated with this mechanism. Before the cooling of the ice, the water column would have a small temperature difference between top and bottom making the oscillations visible but small. After some days with air temperatures well below -15 °C, the water column would have a larger temperature gradient with colder water on top, making the temperature variation more visible. At a certain point, the brine channels would be closed off to keep thermal equilibrium in the ice-brine boundary, and the movement of the water column stopped.

The calculated permeabilities shown in Fig. 5.9 are in agreement with the discussion above, as the values from before the event of oscillating temperatures, from February 24, were found to be much higher than after the event, on March 12. Further, the figure shows that the permeabilities got very low later in the season, before increasing again in May. Although the permeability increased significantly in May, it never got higher than in February. This could be the reason why the oscillating temperature signal was not seen again, not even in May when the ice was almost at its freezing point. Another explanation could be that the formulas presented in Section 2.5 only take into account the volume of brine relative to the ice, without considering the pathways of brine channels. The brine channels that had been interconnected earlier in the season, were

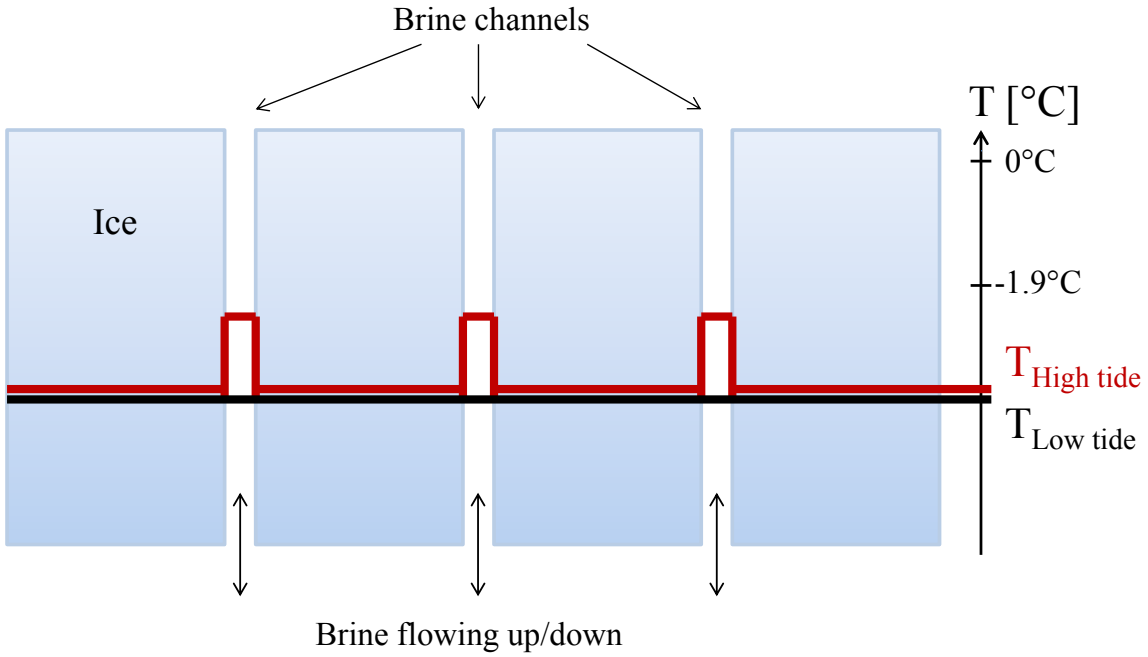

Figure 6.2: *Illustration of brine flow conducting heat within the ice cover, in the hinge zone where the ice is grounded at low tide and floating at high tide. At high tide the water level increases relative to the ice, and brine with warmer temperature than the ice is moved upwards through the brine channels.*

likely closed off in the cold period that followed. When the ice then got warmer, it might have happened that they were not connected again in such a way as to allow for brine or sea water effectively penetrating the ice cover like it (presumably) did before March 13 - even though the brine channels were widening corresponding to the relatively high calculated permeability in May.

Another scenario which is not taken into account by the formulas, is when the channels are filled with air and not with brine, which could have been the case in the topmost ice layers when the two cores were collected on March 13. The density profiles from the same cores are in agreement with the discussion above, indicating lower densities and thereby higher air content in the upper parts of the ice at low tide than at high tide. The two profiles of permeability (shown in Fig. 5.10) were more different than one should expect. Considering the ice temperature, which was not changing noticeably in the 6 hours between the two cores were collected, it is rather unlikely that the permeability would change appreciably during such a short time period. It is likely that the much lower permeabilities calculated at low tide is a result of brine being replaced by air in the upper parts of the core, and that the changed form of the profile is a result of constrictions in the brine channels and perhaps also spatial variations in the ice due to the fact that the two cores were collected around half a meter away from each other.

According to Cox and Weeks (1983), decrease in brine temperature should be related to an increase in brine salinity, so that the brine always stays close to its freezing point. In that case the temperature variations would be caused by absorption of latent heat as salty brine moves downwards and melts the warmer ice, and release of latent heat when less saline brine moves upwards and freezes. However, this is not necessarily the case. It can be compared with so-called

flushing of sea ice during spring time which happens when surface melt pond water, driven by pressure, percolates the ice matrix as discussed by Eicken et al. (2002). They observed flushing of the ice, but could not come up with an explanation as to why the almost fresh melt water that percolates into the ice does not refreeze in such a way that the ice becomes impermeable and further flushing becomes greatly reduced. It is reason to believe that the speed of the oscillations is too high to keep the moving brine/seawater in the channels in complete thermal equilibrium all the time.

6.2 Ice Growth and Melting

6.2.1 The Rapidly-Growing Ice in the Lower Parts of the Hinge Zone

The ice growth in the hinge zone proved to be different from the free-floating ice, as it was both growing faster and getting much thicker. The largest variations in ice thickness were seen around 5 m shoreward of Site 1, around Crack 4, while closer to land the ice thicknesses did not change significantly (see Fig. 5.13). On April 24, the maximum ice thickness recorded there was more than twice the maximum for the free-floating ice. The rapid growth is likely connected to the observed creation of superimposed ice. In general, surface water was observed more frequently in the hinge zone than in the free-floating ice. The thermistor string at Site 1, where surface water were found to be present most of the time, showed that the ice temperature was close to the freezing point almost all the time and never below -4 °C. In comparison, the temperature gradients at Site 2 and at the innermost string were in general much bigger, steadily increasing from top to bottom in periods when the air temperature had been low for several days. Three temperature profiles from April 7 is shown in Fig. 6.3, showing temperature gradients from the hinge zone, Site 1 and Site 2 after several days with cold weather. Freezing of surface water, with the associated release of latent heat, would keep the ice at its freezing point no matter how cold the air temperatures might be (as further discussed in Section 6.2.5). This would cause the ice at Site 1 to stay warm compared to the ice at Site 2 which would be cooled down from above. Similar findings were done outside Barryneset in 2007 by Gabrielsen et al. (2008), which explained the rapid growth close to shore as follows: ”The reasons are a greater heat transfer and the formation of superimposed ice”.

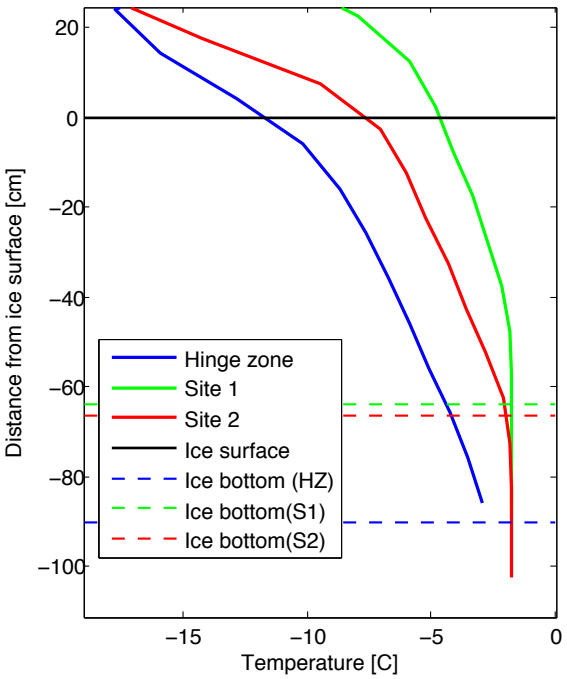

Figure 6.3: *Comparison of temperature profiles from the innermost string (see Fig. 4.4), the string at Site 1 and the one at Site 2, recorded on April 7. Before they were measured, the air temperatures had been around -20 °C for several days.*

Although surface water was observed regularly both around Crack 4 and at Site 1, the growth rate was much higher at Crack 4. A reason could be that Site 1 was flooded so regularly that the surface water did not have the time to freeze before being replaced or drained away. Less frequent flooding would result in enhanced cooling of the ice and more rapid creation of superimposed ice once it got flooded again. Also, the insulating layer of snow at Site 1 was in general thicker than at Crack 4, reducing the atmospheric cooling of the ice at Site 1. The ice within Crack 3 did not grow significantly after March 13, but was still thicker than the free-floating ice. Since the area of surface water seemed to move offshore during the season, it is reason to believe that this part of the ice had been subject to surface water and rapid growth earlier in the season, before the measurements were started. At a certain point, when it got thick enough, it would be too stiff and elevated too high above the ground to allow surface water to overflow it.

6.2.2 Spatial Variability

On March 31, Section 1 was taken for the third time. Two days later, on April 2, Section 2 and the shore-parallel section were measured. On those dates, the outer parts of both Section 1 and Section 2 showed ice thicknesses in the free-floating ice that were almost the same. However, in the hinge zone the case was the opposite, with considerable variations in ice thickness. The shore-parallel section, showed in Fig. 5.16b displays that close to Crack 4, the ice in Section 2 was 62 cm thicker than in Section 1. Key values of ice thicknesses are given in Table 6.1, further emphasizing the variations in ice thickness along the shore. An undulating beach surface could cause uneven distribution of surface water on the ice, and thereby enhancing the ice growth close to section 2. Caline (2010) stated that the shape of the beach slope would influence the tidal bending of the coastal ice, and thereby the formation of tidal cracks. This would in turn affect the surface water distribution. Another factor that might have had an effect on the growth is the long shore-perpendicular crack (shown in Figs. 4.1 and 4.2) which was located close to Section 2. This may also have been the reason for the fact that, at high tide, a layer of surface water was found on all of the free-floating ice along Section 2. In contrast, no surface water was present on the free-floating parts of Section 1 when it was mapped two days earlier. However, there are several other possible explanations of the uneven ice thicknesses, and more data is needed to be able to determine what exactly is the cause.

Table 6.1: *Key values of ice thickness along the shore-parallel section. It was going from Section 2 to Section 1, along Crack 4*

	Minimum	Maximum	Mean	Standard deviation (σ)
Ice thickness [cm]	107	197	156	32

6.2.3 Growth at Site 1

Salinity profiles from Site 1 indicated that a layer of more saline ice had developed on top of the original ice layer during the two weeks before March 30. The profile had the form of a double C,

instead of the ”normal” single C-shaped curve with more saline ice at the top and at the bottom of the ice than in the middle. On March 12, around 20 cm of surface water had been observed on the ice around Site 1, and it is likely that some of this surface water became superimposed ice as the air temperatures were well below freezing point in that period. Later in the season, ice growth at Site 1 slowed down and a single C-shaped salinity profile developed, probably due to either gravity drainage of brine - leading the salty layer downwards over time - or flushing, as a result of warm, permeable ice and pressure from the overhead surface water. The concept of occurrence and disappearance of double C-profiles is further discussed in Section 6.2.5.

6.2.4 Growth at Site 2

The double C-shaped profiles were also observed at Site 2. Similar to Site 1, it is likely that they originated from surface water which was observed at Site 2 to an amount of 15 cm on February 20. In the period between February 20 and March 12 the ice grew 32 cm at Site 2, and an extra C-profile had been created in the top 20 cm of the ice. The double C-profile at Site 2 did not smooth out to a single C similarly to what happened at Site 1, but remained relatively unchanged until May. An explanation could be that the ice at Site 2 was colder on average, leading to lower permeability and thereby less gravity drainage of brine. No surface melt ponds were observed on May 9 or before, so any brine flushing should not be expected.

6.2.5 Double C-Profiles of Salinity

A likely explanation of the salinity profiles from Site 1 and Site 2, which often were found to have the form of a double C, is that a new C-curve had been created on top of one that was already existing in the original ice cover, caused by a layer of saline surface water turning into superimposed ice. This correlated with the measurements of surface water, which was seen in large amounts in the beginning of the season both at Site 1 and Site 2. A suggested course of events leading to this is explained below, and illustrated in Fig. 6.4.

Cooled down by air, the layer of surface water will start to freeze. As for normal sea ice, the growth rate would typically be largest in the beginning, causing more salt to be entrapped in the topmost layer of superimposed ice than further down. The advancing, downwards moving ice-water boundary would expel salt, which then would heap up on top of the original ice cover. If the ”old” ice is colder than freezing temperature (which it normally is), heat transfer from the surface water to the ice would lead to heating of the ice and cooling of the water. The conduction of heat from the water to the ice would then happen in two stages. First, conduction of sensible heat from the water will be the governing mechanism. Later, in cases when the surface water is cooled down from below enough to start freezing, conduction of latent heat released in the process would cause further heating of the ”old” ice. In both cases, heating of the ”old” ice layer would occur either until the entire layer of surface water freezes, or until it reaches its freezing point. This might have been the reason why the ice at Site 1, which was flooded regularly, was staying close to its freezing point most of the season. The lowest layer of superimposed ice - the layer lying on top of the ”old” ice - is likely to get a relatively high salinity, since little or no salt would initially be expelled by gravity drainage as it is stopped by the surface of the original ice cover. Another reason for the high salinity in this layer could be that the water furthest down would get a high salinity due to the freezing which is happening simultaneously from the air/water interface and downwards, releasing brine with high density which sinks down to the

surface of the ”old” ice before it possibly freezes.

Eventually, if the original ice cover gets warm and the permeability high enough before all of the surface water has frozen, loss of salt by flushing through the original ice cover may occur. Over time, also gravity drainage can contribute to the brine drainage, smoothening out the two C-shaped salinity profiles, leading salt from the intermediate layers towards the bottom. The result would likely be a single C-profile, like the one that was observed at Site 1 towards the end of the season.

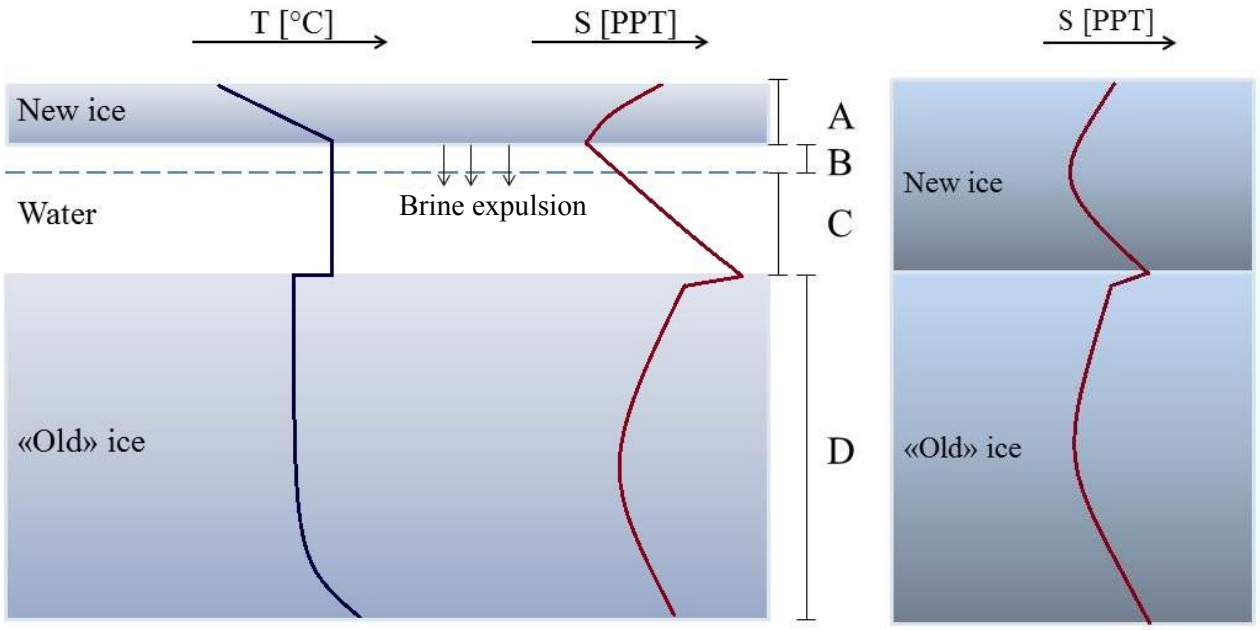

(a) *While the surface water is freezing*

(b) *After the surface water has frozen completely*

Figure 6.4: *Sketches illustrating the creation of a double-C shaped salinity curve.*
Figure (a): A layer of new ice (A) has started to grow on top of a layer of surface water. As its thickness increases (B), brine will be expelled from the advancing ice front into the remaining layer of water, (C), between the bottom of the new ice and the top surface of the ”old”, original ice layer (D), which has a C-shaped salinity profile already. The new ice that is forming will entrap high amounts of salt in the beginning, when the freezing is happening fast. In the intermediate layers of the new ice, the growth rate and thereby the salinity will be lower. Close to the surface of the ”old” ice layer where the water has a high salinity due to the earlier brine release, the salinity of the new ice will be high.
Figure (b): The result is a new C-profile being created on top of the old one.

6.2.6 Melting

In May the ice in the hinge zone had become thinner on average, while the free-floating ice had continued to grow since last field visit (Table 5.7). At that point the air temperatures had been warm for several days, the midnight sun was shining much of the time, and the water temperatures had become slightly warmer. Surface water was present on the ice all the way from

Site 1 to Site 2. Since the free-floating ice was still cold with temperatures down to -3 °C, and the ice at Site 1 and in the hinge zone were at the freezing point all the way through, one is led to the conclusion that while the ice in the hinge zone was melting, the free-floating ice had conserved negative thermal energy enough to continue freezing. Another mechanism enhancing the melting in the hinge zone could be oscillations of water/brine in the ice as elaborated in Section 6.1. Although no clear signs of such oscillations were observed in the temperature recordings, they could still have been there as the temperature of the ice and the column of brine would likely be essentially the same, and more or less constant with depth.

6.3 Bending of Ice Close to the Shore

In Chapter 5.3 plots of Section 1 at high and low tide from four different times are presented, in addition to Section 2 and the shore parallel section. The plots show ice thickness, amount of slush/snow ice, amount of snow, and freeboard.

All the sections show that the highest amounts of surface water were found in the outer part of the hinge zone. The zone where surface water was found, seemed to move offshore during the season. This might have been caused by ice growth; as the ice was growing during the season, the thickening could have made it stiffer and less bendable. Another mechanism which could stiffen the ice in the hinge zone is freezing of seawater in the tidal cracks, making the ”hinges” bend less smoothly. All sections except the one taken on April 24 shows buckling of the ice in the lower part of the hinge zone, resulting in changed freeboard or surface water. In the first section, which was collected on March 13, surface water was found at low tide but not at high tide. In the other sections - except the one from April, which was found not to be buckled at all - the highest amount of surface water was found at high tide. Pressure induced by tidal motions seemed to play a role, but also thermal expansion of the ice in the sound could have an effect on the buckling. As shown in Table 6.2, the ice was coldest on March 31 and April 24, before it got warmer again in May.

Table 6.2: *Mean ice temperatures at Site 1 and Site 2*

	March 13 [°C]	March 31 [°C]	April 24 [°C]	May 10 [°C]
Site 1	-1.92	-2.70	-2.34	-1.80
Site 2	-1.82	-3.93	-3.32	-2.7

The warming of the ice would make it expand, and could lead to an ice sheet with a size slightly larger than the width of the sound outside Barryneset (see also Section 6.3.1). It seems that the ice was ”stretched out” at low tide and compressed by high tide. Another explanation of the occurrence of surface water could be that the ice was partly frozen to the ground so it was flooded at high tide, as suggested by Gabrielsen et al. (2008). According to Vindegg (2014) who discussed stress measurements conducted outside Barryneset during the same period, the stress at Site 1 was highest at low tide while at Site 2 it was highest at high tide. As the stress sensors were placed close to the ice surface at around 20 cm depth (Vindegg, 2014), this may be indications of a pressure close to shore due to bending at low tide (see Fig. 6.5). Further, high pressures at Site 2 could occur either due to increased pressure across the entire sound at high tide - assuming no bending of the free-floating ice in any part of the tidal cycle - or that the

ice was grounded in the middle of the sound at low tide. In 2013, one year earlier, Wrangborg et al. (2013)) had found anchor ice 400 m off the tip of Barryneset (200 away from Site 2). Such a grounding of the ice could cause it to bend upwards, easing the pressures in the upper parts of the ice at low tide compared to at high tide. Although the ice was not found to be grounded at Site 2 at any point during the described fieldwork, anchor ice elsewhere in the sound may have given the same effect on the pressure recordings there. However, it is questionable whether anchor ice as far away as 200 m would have any appreciable effects on the stresses at Site 2.

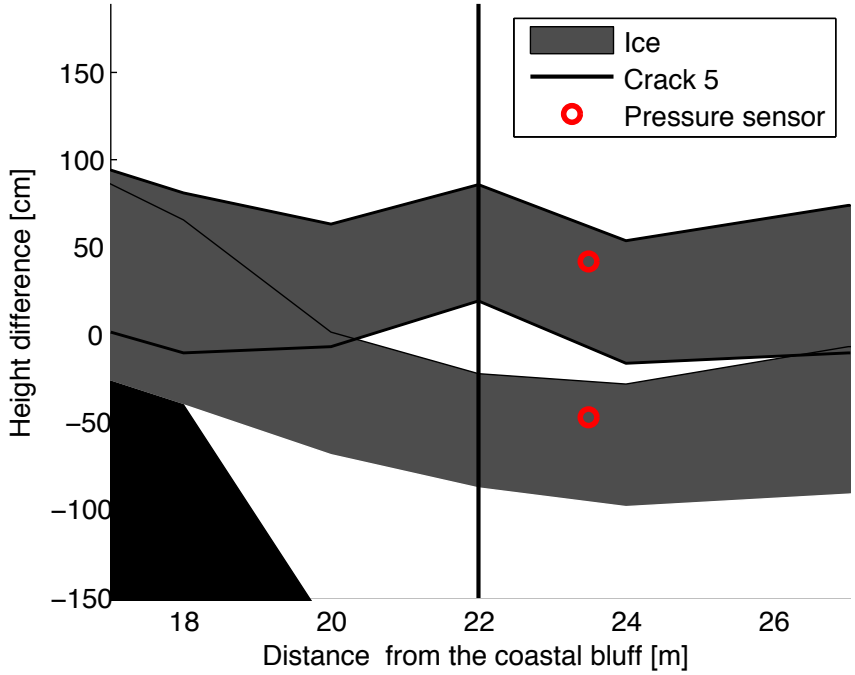

Figure 6.5: *Section 1 on May 10 (a zoomed-in and simplified version of Fig. 5.15 (b)), showing the ice and the position of the pressure sensor at Site 1 at high and low tide. At low tide the sensor, which was placed in the upper part of the ice, is expected to have been subject to compressive stress due to bending of the ice.*

As the tidal cracks were opening and closing twice every day due to tidal movement, it is likely that water could have flowed up through a crack and then, in contact with the colder ice, frozen. The newly formed ice would contribute to an extension of the ice in the hinge zone, increasing lateral pressures in the ice and pushing the ice in the lower parts of the hinge zone towards sea. This would further have led to an excess of ice in the sound, increasing through the season and adding up with the possible, already discussed, thermal expansion of the ice sheet. This could be an explanation as to why the most severe bending of the ice was observed in May, when the ice was both relatively warm and possibly had been subject to expansion through creation of ice in the tidal cracks all season.

Assuming that the ice cover across the sound can be looked upon as a coherent piece of material with constant extent, and that it is level at high tide and lowered in the free-floating part at low tide, there will be an excess of ice at high tide, since the shortest distance between two points is a straight line. This excess could be the reason for the high tide buckling that was observed in May. The concept is illustrated in Fig. 6.6, and further elaborated in Section 6.3.1.

Other factors like external forcing by wind or currents are also possible explanations of the phenomenon. Information on this topic is currently very sparse, if not non-existing.

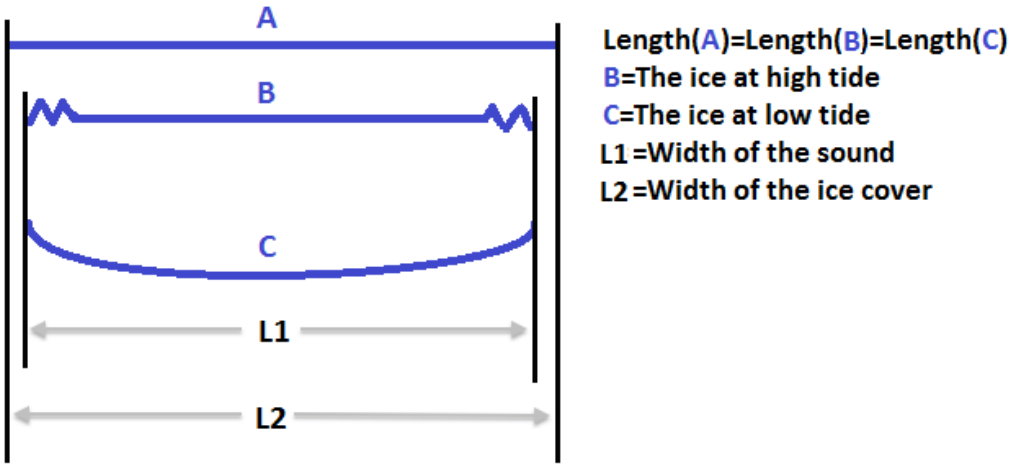

Figure 6.6: *Illustration of the ice with the buckling that was observed in May. Since the shortest distance between two points is a straight line, there will be an excess of ice at high tide*

6.3.1 Two Numerical Estimates

The calculations below consider the extent of the ice across Sveasundet along its narrowest cross-section.

Ice excess caused by tidal motion
To give an idea about length scales of the suggested excess of ice caused by tidal motion (illustrated in Fig. 6.6), the following rather simplistic calculation was done. It should be noted that in the calculation, the ice was not considered to be smooth like at low tide in the figure (Fig. 6.6, profile c), but rather as consisting of three straight parts connected with joints. It was assumed that:
-The free-floating ice had constant freeboard and extent all the time (no buckling or creep).
-The ice in the hinge zone was horizontal at high tide and lowered in the outer part at low tide.
-The hinge zone across the sound was similar to the one outside Barryneset.
-The entire ice sheet can be regarded as a continuous piece of material.
-The tidal elevation and the horizontal extent of the hinge zone can be looked upon as the two catheti in a right triangle, and the beach profile as its hypotenuse.

The *Pythagorean theorem* can be expressed

$$a = \sqrt{b^2 + c^2}. \tag{6.1}$$

Here, a, b and c are the three edges of a right triangle, where a is the hypotenuse. The horizontal distance from Crack 1 to Crack 5 was was 13 m, and the medium tidal range 1.22 m.

Equation 6.1, with b=1.22 m and c=13 m then gives

$$\sqrt{1.22^2 + 13^2} = 13.057,$$

meaning that from high to low tide, the length of the hinge zone-ice had to increase from 13 m to 13.057 m, with a difference of 5.7 cm. Since it was assumed that the same happened on the opposed side of the sound, the total value for the ice sheet would be twice as high. Hence, one can conclude that the ice sheet across the sound would have to be 11.4 cm longer at low tide than at high tide without being buckled.

Thermal expansion between March 31 and May 10
To estimate the magnitude of thermal effects, the following calculation was done. The conditions are listed below:
-From March 31 to May 10, the average ice temperature at Site 2 increased with about 1.2°C (Table 6.2).
-At its narrowest point, Sveasundet is 690 m wide (Caline, 2010).
-The coefficient of one-dimensional thermal expansion for sea ice close to 0°C is $52{\cdot}10^{-6}$ T^{-1} (Butkovich, 1959; Cox, 1983; Fukusako, 1990).
-It was assumed that the temperatures at Site 2 were representative for the whole ice sheet, that the ice can be looked upon as a continuous piece of material, and that the effects of pressure are negligible.

The coefficient of thermal expansion gives the fractional change in length per degree of temperature change. Linear thermal expansion of an ice sheet can thus be expressed as

$$\Delta L_{ice} = L_{ice}\alpha\Delta T, \tag{6.2}$$

where ΔL_{ice} is the changed length, L_{ice} is the length of the ice sheet in a particular direction, α is the coefficient of linear thermal expansion of sea ice, and ΔT is the change in temperature.

Using Eqn. 6.2 with the variables ΔT=1.2°C, L_{ice}=690 m and α=$52{\cdot}10^{-6}$ T^{-1}, one obtains a thermal expansion of the ice sheet across Sveasundet, ΔL_{ice}, of 4.3 cm.

Although being rather rough estimates, the calculations above show that both the effects of tidal elevation and thermal expansion give contributions in the order of cm to the ice extent, and should therefore not be neglected.

6.3.2 Cross-Sections - Evaluation of the Method

All four times Section 1 was taken, more or less similar ice thicknesses in the ice foot were measured, except on March 31 when the profile (shown in Fig. 5.14b) showed an ice foot that was thinner than the others. This is probably due to too shallow drilling, since such a big loss of ice in the ice foot after a period with relatively cold weather is not likely, nor is it likely with a substantial growth in the ice foot during the next few weeks. It was sometimes difficult to know when the drill had gone all the way through the grounded ice, but since the drill bits were quickly damaged when hitting rocks, it was not desirable to push the drill too hard to be absolutely sure.

Figure 6.7 shows the result of a laser scanning of the snow surface (a) and the measured snow surface from Section 1 (b), both done on March 31. Figure 6.7b is a simplified version of Fig. 5.14b. The scanning was done using a high-accuracy Riegl VZ-1000 laser scanner, which was placed on top of the cabin, mapping the area around the tip of Barryneset from the cabin and several hundred meters out on the ice. The plot is showing the height of the snow surface,

measured along a 1 m wide path going from the cabin and out to the free-floating ice, close to Section 1. It was continuously measuring the ice surface from high to low tide.

The surface of the measured section is fairly similar to the laser scanning where the ice is floating. Features such as the elevation of the ice around Site 1, and the relatively steep descent of the ice at low tide (around 13 m from the bluff in Fig. 6.7a) are visible in both sections. However, in places where the ice was grounded, the differences between the laser scans and the section were bigger. For example, the small ridge that is visible in the laser scan (Fig. 6.7a), around 26 m from the cabin (presumably Crack 1), is not visible in the section. Also, the topography of the hinge zone at low tide is more uneven in the section than in the laser scan. This is probably due to errors in the assumption that the beach was inclining with a constant rate all the way from the lowest point where the ice was grounded at low tide and to the coastal bluff, which was used when plotting the sections. Moreover, since the laser scan was not taken exactly along Section 1, but about 5 m away from it in a line that stretched from the cabin and crossed Site 1 (see Fig. 4.2), spatial variations may have given some differences between the two plots.

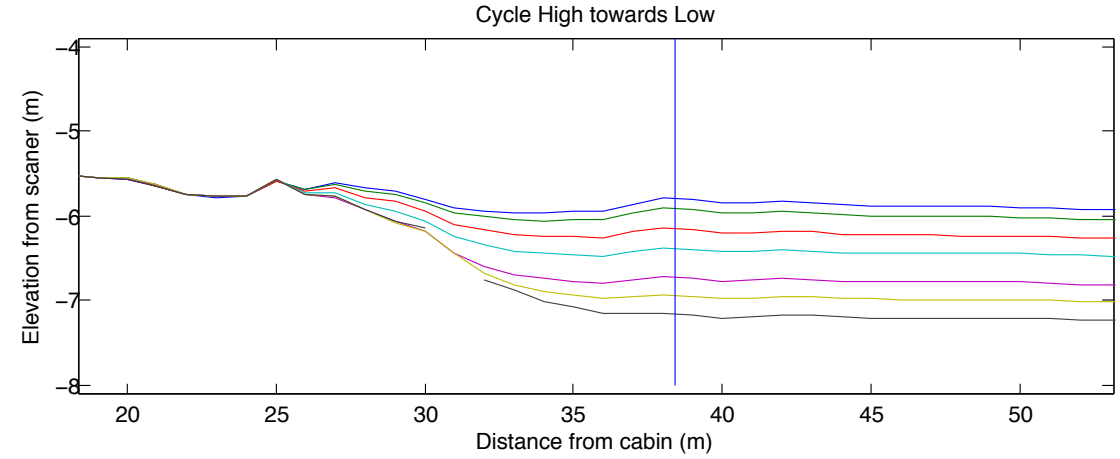

(a) *Laser scanning*

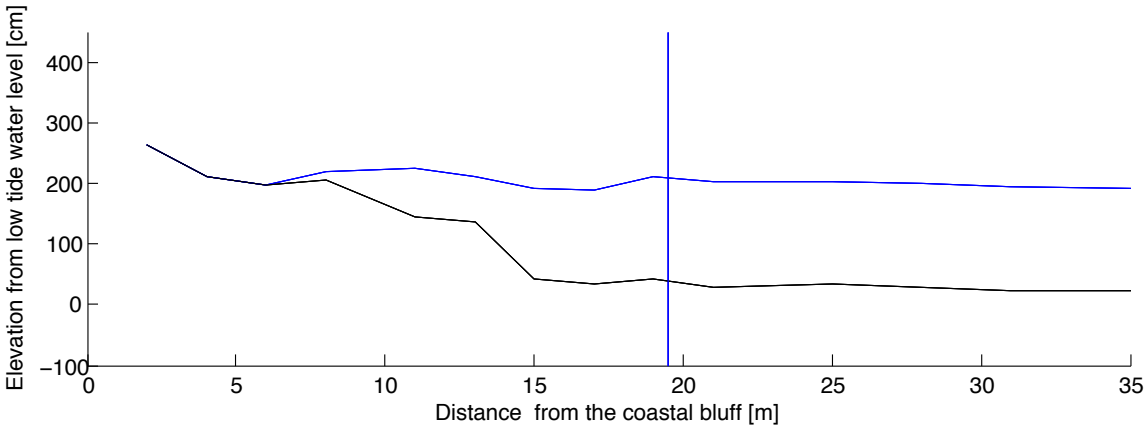

(b) *Section measurements*

Figure 6.7: *Comparison of laser scanning and a measured section, both from March 31. Figure (a) shows a laser scanning of the hinge zone done, with the snow surface at 7 different times from high to low tide, as plotted by David Wrangborg (UNIS). The axes are giving the distance from the scanner, which was placed on the roof of the cabin. Figure (b) shows the snow surface of Section 1 from March 31, at high and low tide (presented in Section 5.3.2). In both plots, the blue vertical lines indicate the position of Site 1*

6.4 Hydrographic Patterns in Sveasundet

As elaborated in Section 5.4, the seawater temperatures varied through the season, and also along with the semi-diurnal tide. As shown in Fig. 5.17 the average seawater temperatures correlated with the air- and ice temperatures through the season, being relatively warm in February/March and May, and colder in April. In the middle of April, higher air temperatures were followed by a period of warmer water. By measurements in Sveasundet and the shallow basin of Braganzavågen, similar results were found in the winter/spring of 2014 by Shestov et al. (2015), which stated that the changes in water temperature were governed by changes in air temperature. They further interpreted the period of relatively warm water (and air) in mid April to be the beginning of the melting season. However, results in this thesis (see e.g. Fig. 5.13) reveal that the free-floating ice in Sveasundet continued to grow at least until May 10.

Figure 5.18 indicates a trend of the sea water temperatures outside Barryneset oscillating with a sharp increase around high tide, followed by a slower decrease during ebb, low tide and flow. This was a trend that was visible through most of the period between February and May. Again, Shestov et al. (2015) had found similar results, and as they had several pressure and temperature sensors deployed on the seafloor in Braganzavågen, they were able to determine that the phase-shift was faster for the ingoing tidal wave than the outgoing, and that the water in general was colder and more saline in the inner parts of Braganzavågen than in Sveasundet. Hence, they concluded that the water floods Braganzavågen faster than leaving it, and one is led to the conclusion that the sharp increase in temperature around high tide is due to rapid inflow of relatively warm water from from the deeper parts of the fjord, whereas the slower decrease is caused by colder and more saline water which had been subject to cooling and brine rejection from freezing sea ice, flowing at a slower pace out of the sound.

6.5 Major Sources of Errors and Uncertainties

Information on accuracy of the different sensors, gauges and tools used to achieve the data presented in this thesis are given in Chapter 4, and in a theoretical world this would have been the accuracy of the measurements. In practice however, many factors are likely to influence the data. This chapter summarizes the most important of them.

Differential GPS-measurements: With its high accuracy in the horizontal plane (Section 4.2), the DGPS measurements were more than accurate enough for its purpose during this field campaign, which was to draw a map of the investigation site and to show the location of the tidal cracks. A misleading factor was the aerial photo from 2008 that was used to plot the data on. Some erosion is likely to have happened since it was taken. It was also tried to map the elevation of the ice surface in the hinge zone by using the DGPS, but the data was found to be way too inaccurate to give a proper picture of it.

Temperature measurements: The thermistor strings used were accurate down to $0.05\,^{\circ}\mathrm{C}$. However, water penetrating the ice close to tidal cracks or by some kind of interaction with the plastic sticks that the strings were fitted into, may have affected the measurements. In periods, the sensors above the ice surface were exposed to sunlight, so after the sun returned by February 16, data from these can be regarded as invalid in the sense of describing air temperatures.

Ice core sampling: The fact that the ice cores had to be collected at different locations every time, in order to avoid disturbance of the ice properties by the hole left after the previous core had been drilled, may have affected the results. Large spatial variations should be expected in the hinge zone in terms of ice thickness and proximity of tidal cracks. This could cause two ice cores collected at different times from "the same" place to be affected not only by temporal changes, but also by spatial variations since they were all collected about 0.5 m from each other. A source of uncertainty for the cores that were collected between Crack 1 and Crack 2 is that the water level was not measured in the holes where they had been collected. Another lack of data is information about the tidal water level when the ice cores from the ice foot were collected.

Calculations of density and salinity: The biggest source of error for the salinity measurements was likely drainage of brine when the ice cores were removed from the ice, especially when the weather was warm. In colder weather, when the temperatures were well below zero, a layer of ice would quickly cover the surface of the ice core, preventing the brine from draining out of the ice cores.

As stated in Section 4.5, the samples were stored in temperatures lower than -15 $^{\circ}$C, in sealed boxes or plastic bags, so any appreciable changes in mass or volume by either dry evaporation or melting is not expected to have taken place. However, since the ice samples often had cracks in them or by other reasons had uneven surfaces, the measurements of their size often became inaccurate which could further have led to errors in the density data. The irregularity in the plots showing density may be an indication of inaccurate volume measurements.

Calculations of permeability: Since the values of salinity used for calculations of permeability in Fig. 5.9 all originated from March 13, the plots of permeability on other dates would be unaffected by any changed salinity in the ice, and possibly misleading. Unfortunately, no other ice cores were collected close to the thermistor string where the permeabilities were of interest neither earlier nor later in the season, since we were unaware of the importance of such data when the measurements were conducted. Further, the formulas used to calculate permeability did not take into account the ice density, which is expected to have led to errors in several of the results (discussed in Section 6.1).

Measurements of ice thickness: When the cross-sections were made, holes were drilled with more or less even distances between them, regardless if there was a crack there or not. This might have given an impression that the ice was more even than it was in reality, since the biggest bends and bucklings of ice were found at the tidal cracks. The holes were never made into a crack, but rather slightly to the side of it. Although the accuracy when measuring ice thickness was sufficiently good ($\pm$1 cm), the data used to plot the cross-sections could have described the ice better if it also had been measured *on* every crack, in addition to on the ice in between them.

Plotting of cross-sections: The assumption that the beach was inclining with a constant rate all the way from the lowest point where the ice was grounded at low tide and to the coastal bluff, was found to be a source of error. It is discussed more thoroughly in Section 6.3.2.

Measurements of upwards ice growth: Exact measurements of upwards ice growth was not done on the first two field trips, as we were not expecting it to be happening to such a great

extent. This caused uncertainties considering the accumulation of superimposed ice, where only minimum amounts could be stated. E.g. an observation of a logger and a pallet that had become submerged in ice, meant that the upwards ice growth had to have been larger than the height of the logger and the pallet.

Chapter 7

Concluding Remarks

7.1 Major Findings

Data from several different tests conducted on the ice outside Barryneset have been presented in this thesis. Together the data sets have formed the basis for a discussion which had to be relatively independent; not much work has been done on these topics earlier. The major findings of this thesis are:

- During a period of around 10 days, temperatures were oscillating with a period similar to the semi-diurnal tide, within the ice in the hinge zone. It was likely due to a combination of hydrostatic pressure variations and high permeability of the ice.

- The ice was growing more rapidly in the hinge zone than in the free-floating ice. It was probably a result of ice growth on top of the ice, caused by large amounts of surface water becoming superimposed ice.

- By the end of the ice season, the ice started to melt in the hinge zone while it continued to grow in the free-floating ice for several days. The free-floating ice was colder than the ice in the hinge zone, and a suggested explanation is conserved thermal energy driving the continued freezing.

- Multiple C-profiles of ice salinity were found both at Site 1 and Site 2 in March. At Site 1 the profiles turned into a single C-shape by the end of April, whereas at Site 2 the double C-profile remained until the end of season. The double C-profiles are expected to be caused by surface water turning into superimposed ice, and gravity drainage of brine is likely the reason why the profile at Site 1 turned into a single C-shape, since the ice generally was warmer at Site 1 than at Site 2.

- At the end of the season, the ice in the hinge zone was bent at high tide, while at low tide it was not. On May 10, the ice across the sound outside Barryneset seemed to be stretched at low tide and compressed at high tide. Several explanations are feasible. Increased lateral extent of the ice in Sveasundet, due to a combination of thermal expansion and freezing

of seawater in the tidal cracks through the season, is suggested as a factor influencing the stresses in the ice and thereby the ice buckling. Further, tidal-induced pressure variations are likely an important factor. Since the shortest distance between two points is a straight line, the ice is more likely to be buckled at high tide than at low tide when it is lowered in the middle of the sound.

- A large spatial variation in ice thickness was found in the hinge zone, not only perpendicular to the shore, but also along the shore. Uneven beach surface and distribution of surface water along the shore are expected to be the major causes.

- The seawater temperatures in Sveasundet correlated with the air temperatures. A trend of increasing water temperatures at high tide followed by a decrease at low tide was observed outside Barryneset. This is presumably related to relatively warm water from the deeper parts of the fjord flowing into the shallow Bragazavågen at high tide, and outflow of cold water at low tide.

7.2 Further Work

To conduct such a fieldwork and process the collected data is time-consuming, and unfortunately there was no time to conduct more experiments this time. More investigations are needed to make the conclusions listed above more specific. Also, comparable investigations over several subsequent years would give valuable information of perennial trends. If the measurements presented in this thesis were to be repeated or continued in a future work, I would recommend the following:

- Repeat measurements of ice thickness along Section 1, Section 2 and the shore parallel section at different times, to get a better understanding of the spatial variability of ice thickness through the season.

- When measuring the cross-sections, determine ice thickness *on* all the tidal cracks in addition to in between them.

- Carefully note the position of the ice surface relative to e.g. plastic sticks inserted in the ice, to get accurate measures of the growth of superimposed ice.

- When collecting ice cores in the hinge zone, note the water level in the holes after they have been removed if possible, or at least note the time when they were collected so that the corresponding tidal level can be determined.

- Make sure that all loggers and cables are elevated high enough above the ice so that they are not submerged in superimposed ice.

- Start the measurements earlier in the season.

To complement the experiments presented in this thesis, data from the following experiments would be useful:

- Thin section investigations of the ice in the hinge zone would give information of its crystal size and orientation at different depths, and thereby tell if there is superimposed ice there, as done by Gabrielsen et al. (2008). This would further help understanding the coastal ice growth processes.

- Stress in the ice across the sound seemed to play an important role for bending of the ice and surface water, causing increased ice growth close to shore. More stress measurements like those that were conducted this year (they are presented in Vindegg (2014)), would give a clearer picture of the stress mechanisms in the sound.

- Measurements on Littrowneset, which is the peninsula opposing Barryneset, on the other side of the sound (see Fig. 3.1), to investigate if the mechanisms governing the ice in the hinge zone and the ice foot there are comparable to Barryneset.

- Combine data from the laser scans and the cross-sections to get better plots of the ice in the hinge zone. By using the laser scan to define the snow surface of the section plots, the assumption that the beach is inclining at a constant rate (which was suspected not to be entirely true) would not have to be used.

Bibliography

Assur, A. (1958). Composition of sea ice and its tensile strength. *Arctic sea ice 598*, 106–138.

Barrault, S. and K. Høyland (2007). Mechanisms and measurements of generation of stresses in first-year landfast sea ice. In *Proceedings of the 19th International conference on Port and Ocean Engineering under Arctic Conditions, Dalian, China*, Volume 7, pp. 685–694.

Bentham, R. (1934). The ice-foot. *Appendix III in Shackleton: Arctic Journeys. The story of the Oxford University Ellesmere and Land Expedition 5*.

Butkovich, T. (1959). Thermal expansion of ice. *Journal of Applied Physics 30*(3), 350–353.

Caline, F. (2010). *Coastal-sea-ice action on a breakwater in a microtidal inlet in Svalbard*. Ph. D. thesis, Norwegian University of Science and Technology, Department of Civil and Transport Engineering.

Caline, F. and S. Barrault (2008). Measurements of stresses in the coastal ice on both sides of a tidal crack. In *19 th IAHR International Symposium on Ice, Vancouver, British Columbia, Canada, July 6 to 11, 2008*, Volume 1, pp. 526– 536.

Comiso, J. C., C. L. Parkinson, R. Gersten, and L. Stock (2008). Accelerated decline in the arctic sea ice cover. *Geophysical Research Letters 35*(1).

Cota, G., S. Prinsenberg, E. Bennett, J. Loder, M. Lewis, J. Anning, N. Watson, and L. Harris (1987). Nutrient fluxes during extended blooms of arctic ice algae. *Journal of Geophysical Research: Oceans (1978–2012) 92*(C2), 1951–1962.

Cox, G. F. (1983). Thermal expansion of saline ice. *Journal of Glaciology 29*(103), 425–432.

Cox, G. F. and W. F. Weeks (1975). Brine drainage and initial salt entrapment in sodium chloride ice. Technical report, DTIC Document.

Cox, G. F. N. and W. F. Weeks (1983). *Equations for determing the gas and brine volumes in sea-ice samples*. Journal of Glaciology, vol 29.

Eicken, H., H. Krouse, D. Kadko, and D. Perovich (2002). Tracer studies of pathways and rates of meltwater transport through arctic summer sea ice. *Journal of Geophysical Research: Oceans (1978–2012) 107*(C10), SHE–22.

Eicken, H. and M. Salganek (2010). *Field Techniques for Sea-Ice Research*. University of Alaska Press.

eKlima (2014). Meteorological and climatological database, the norwegian meteorological institute. http://eklima.met.no.

Fetterer, F. and N. Untersteiner (1998). Observations of melt ponds on arctic sea ice. *Journal of Geophysical Research: Oceans (1978–2012) 103*(C11), 24821–24835.

Freitag, J. (1999). Untersuchungen zur hydrologie des arktischen meereises: Konsequenzen für den kleinskaligen stofftransport= the hydraulic properties of arctic sea-ice: implications for the small scale particle transport. *Berichte zur Polarforschung (Reports on Polar Research) 325*.

Freitag, J. and H. Eicken (2003). Meltwater circulation and permeability of arctic summer sea ice derived from hydrological field experiments. *Journal of glaciology 49*(166), 349–358.

Fukusako, S. (1990). Thermophysical properties of ice, snow, and sea ice. *International Journal of Thermophysics 11*(2), 353–372.

Gabrielsen, M., S. Barrault, F. Caline, and K. V. Høyland (2008). Comparison of physical and mechanical properties of coastal ice and level ice. In *Proceedings of 19th IAHR International Symposium on Ice*, Volume 2, pp. 956–974.

Høyland, K. V. (2009). Ice thickness, growth and salinity in van mijenfjorden, svalbard, norway. *Polar Research 28*(3), 339–352.

Instanes, A., O. Anisimov, L. Brigham, D. Goering, L. N. Khrustalev, B. Ladanyi, J. O. Larsen, O. Smith, A. Stevermer, B. Weatherhead, et al. (2005). Infrastructure: buildings, support systems, and industrial facilities. *Arctic climate impact assessment*, 908–944.

ISO (2010). Iso19906. petroleum and natural gas industries — arctic offshore structures. *International Organization for Standardization*.

Johannessen, O., M. Miles, L. Bengtsson, L. Bobylev, and S. Kuzmina (2003). Arctic climate change. *Arctic Environment Variability in the Context of Global Change (eds. Bobylev, LP, K. Ya. Kondratyev and OM Johannessen), Springer–Praxis Publishing*.

Johannessen, O. M., E. V. Shalina, and M. W. Miles (1999). Satellite evidence for an arctic sea ice cover in transformation. *Science 286*(5446), 1937–1939.

Kovacs, A. (1997). The bulk salinity of arctic and antarctic sea ice versus thickness. In *Proceedings of the International Conference on Offshore Mechanics and Arctic Engineering*, pp. 271–282. American Society of Mechanical Engineers.

Kovacs, A. and D. S. Sodhi (1980). Shore ice pile-up and ride-up: Field observations, models, theoretical analyses. *Cold Regions Science and Technology 2*, 210–288.

Lantuit, H. and W. Pollard (2008). Fifty years of coastal erosion and retrogressive thaw slump activity on herschel island, southern beaufort sea, yukon territory, canada. *Geomorphology 95*(1), 84–102.

Løset, S., K. Shkhinek, and K. Høyland (1998). Ice physics and mechanics. *Norwegian University of Science and Technology*.

Marchenko, A., I. Langen, and A. Shestov (2009). Hydrological characteristics of a narrow and shallow part of van mijen fjord on spitsbergen. In *19th International Offshore and Polar Engineering Conference - ISOPE 2009 :*.

Mettler-Toledo (2015). Mettler toledo's webpage: $http://us.mt.com/us/en/home/$ (2015).

Michel, B. (1978). *Ice mechanics*. Laval University Press Cite Universitaire Laval University Press, Cite Universitaire, Quebec, Quebec G1K 7P4 Canada.

Michel, B. and R. Ramseier (1971). Classification of river and lake ice. *Canadian Geotechnical Journal 8*(1), 36–45.

Moslet, P. O. and K. V. Høyland (2003). Ice stress measurements adjacent to a wide structure in land-fast ice. In *Proceedings of the 17th International conference on Port and Ocean Engineering under Arctic Conditions, Trondheim, Norway*.

Nansen, F. (1922). *The strandflat and isostasy*. Number 11. I kommission hos J. Dybwad.

Nelson, W. G. (1981). Oil migration and modification processes in solid sea ice. In *International Oil Spill Conference*, Volume 1981, pp. 191–198. American Petroleum Institute.

Notz, D. (2005). *Thermodynamic and fluid-dynamical processes in sea ice*. Ph. D. thesis, University of Cambridge.

Notz, D. (2009). The future of ice sheets and sea ice: Between reversible retreat and unstoppable loss. *Proceedings of the National Academy of Sciences 106*(49), 20590–20595.

Notz, D. and M. G. Worster (2009). Desalination processes of sea ice revisited. *Journal of Geophysical Research: Oceans 114*(C5), C05006.

NPI (2014). Toposvalbard - norwegian polar institute's topographical svalbard map. http://toposvalbard.npolar.no.

Ragner, C. L. (2008). The northern sea route. *The Barents: A Nordic Borderland, ed. T. Hallberg*, 114–127.

Rosenberg, A. and W. Tiller (1957). The relationship between growth forms and the preferred direction of growth. *Acta Metallurgica 5*(10), 565–573.

SBE-39 (2013). *SBE 39 user manual p. 9-11*. Website: www.seabird.com: Sea-Bird Electronics, Inc.

Shestov, A., D. Wrangborg, and A. Marchenko (2015). Hydrology of braganzavågen under ice-covered conditions (under preparation). In *Proceedings of the 23rd International conference on Port and Ocean Engineering under Arctic Conditions june 14-18, 2015 Trondheim, Norway*.

Stefan, J. (1891). On the theory of ice formation, in particular on the ice formation in the polar sea. *Ann Phys Chem 42*, 269–286.

Stroeve, J. C., M. C. Serreze, M. M. Holland, J. E. Kay, J. Malanik, and A. P. Barrett (2012). The arctic's rapidly shrinking sea ice cover: a research synthesis. *Climatic Change 110*(3-4), 1005–1027.

Sysselmannen (2012). Information on the agency's webpage: Om svalbard; bosetninger på svalbard. http://sysselmannen.no/toppmeny/om-svalbard/bosetninger/.

Teigen, S., K. Høyland, and P. Moslet (2005). Thermal stresses in first-year sea ice. In *Proceedings: 18th International Conference on Port and Ocean Engineering under Arctic Conditions*, Volume 2, pp. 893–903.

Thuelsen, N. P. (25th November, 2014). Svalbard. in store norske leksikon. *Downloaded 13nd May 2015 from https://snl.no/Svalbard.*.

Untersteiner, N. (1975). Sea ice and ice sheets and their role in climatic variations. *WMO The Phys. Basis of Climate and Climate Modelling p 206-224(SEE N 76-19675 10-47)*.

USACE (2002). Coastal engineering manual. *Engineer Manual 1110*, 2–1100.

Vindegg, C. M. (2014). Stress measurements in landfast sea ice in van mijenfjorden, svalbard.: A survey of internal stress in landfast sea ice winter 2014. Master's thesis, Norwegian University of Science and Technology.

Wadhams, P. (1981). The ice cover in the greenland and norwegian seas. *Reviews of Geophysics and Space Physics 19*(3), 345–393.

Weeks, W. (2010). *On sea ice*. University of Alaska Press.

Weeks, W. F. and S. F. Ackley (1986). *The growth, structure, and properties of sea ice*. Springer.

WMO (1970). *WMO Sea-ice Nomenclature: Terminology, Codes, Illustrated Glossary and Symbols*. Secretariat of the World Meteorological Organization.

Wrangborg, D., R. Grady, A. Marchenko, and E. Karulin (2013). Analysis of tidal deformations of land fast ice in shallow arctic fjord. In *Proceedings of the 22nd International conference on Port and Ocean Engineering under Arctic Conditions june 9-13, 2013 Espoo, Finland*.

Appendices

Appendix A

Additional Plots of Temperature

A.1 Recordings Between Crack 1 and Crack 2

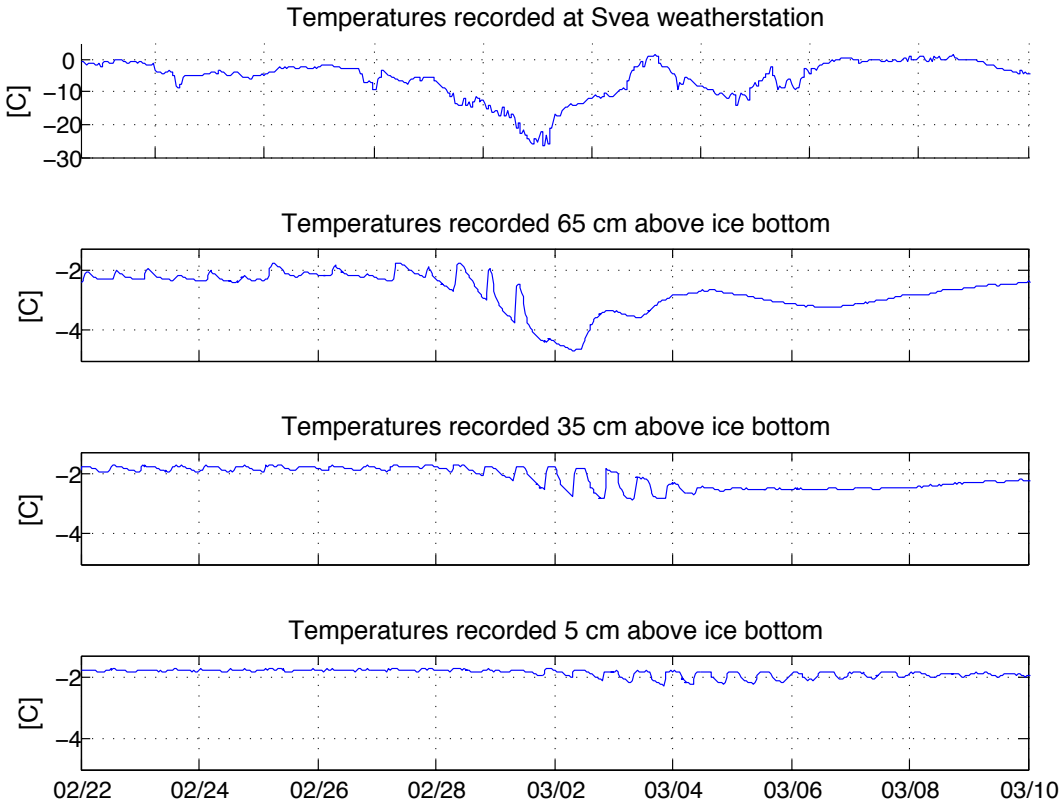

Figure A.1: *Plot showing the oscillations in ice temperature between Crack 1 and Crack 2 in the period February 20-March 10. Distance from ice bottom was measured on March 30*

A.2 Recordings Between Crack 4 and Crack 5, at ”Old” Site 1

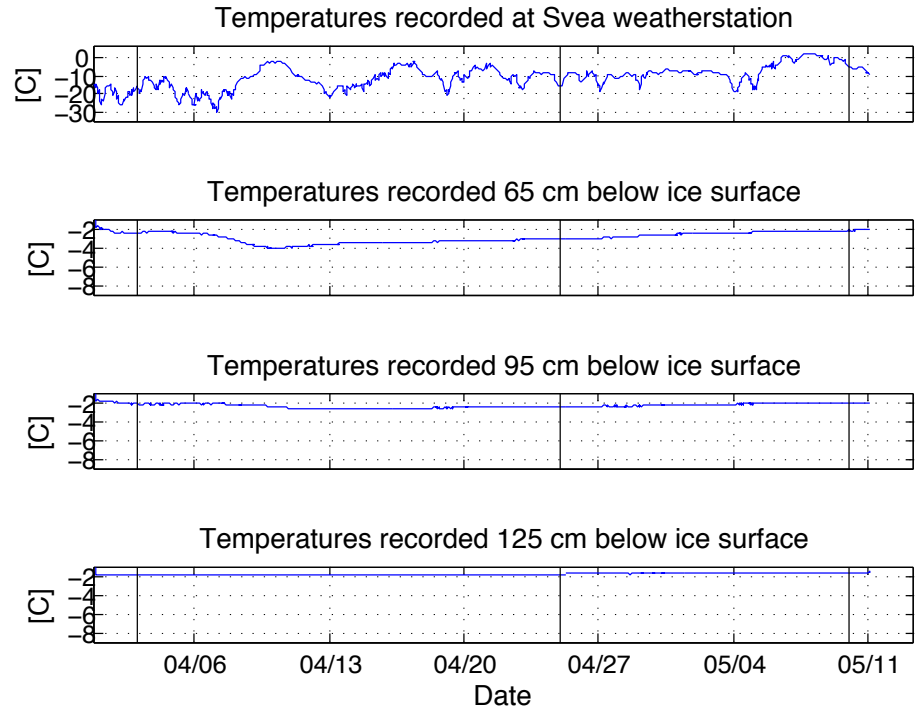

(a)

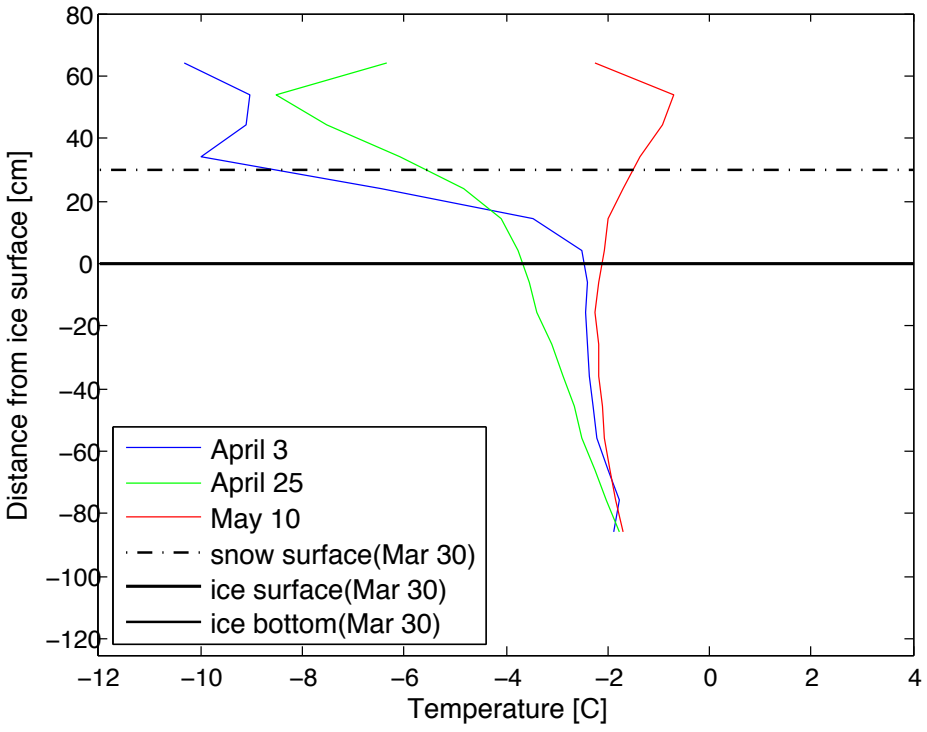

(b)

Figure A.2: *Plots showing temperatures between Crack 4 and Crack 5 between April 1 and May 11 (a), with vertical profiles at three different times, April 3, April 25 and May 10 (b). The black vertical lines in Fig. (a) represent the times when the vertical temperature profiles in Fig. (b) are made.*

Appendix B

Additional Plots of Salinity and Density

B.1 Ice foot

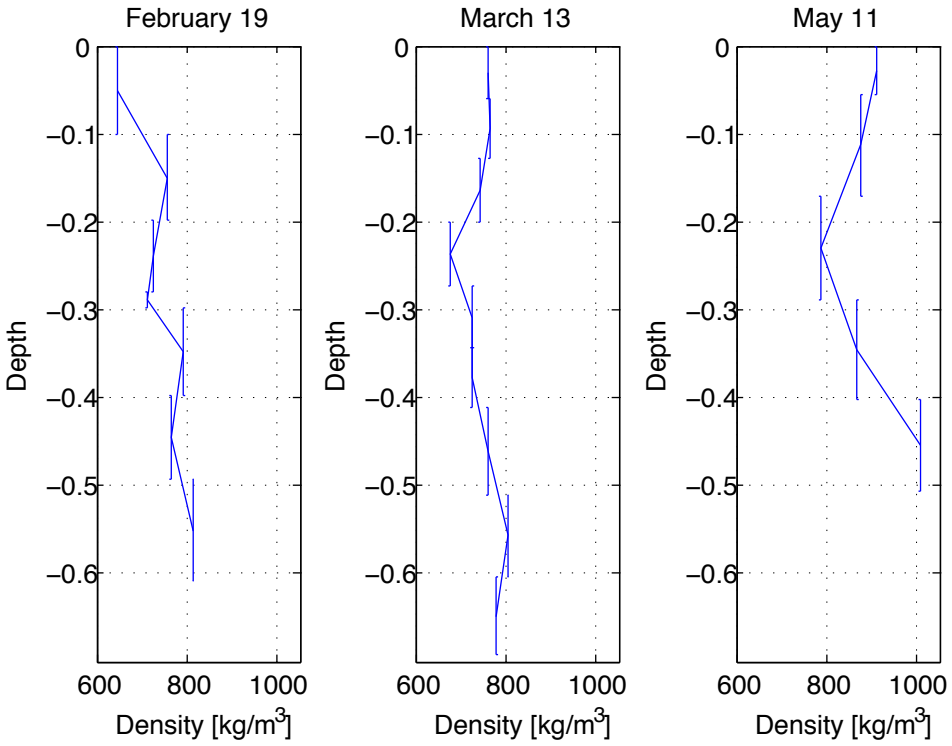

Figure B.1: *Densities recorded in the ice foot, on February 19, March 13 and May 11*

B.2 Hinge Zone

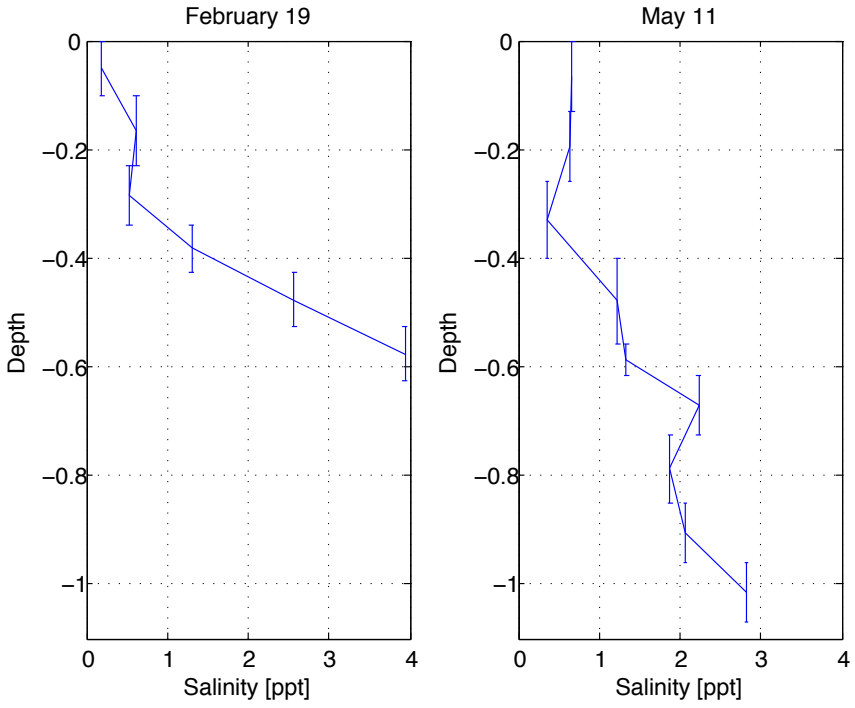

(a)

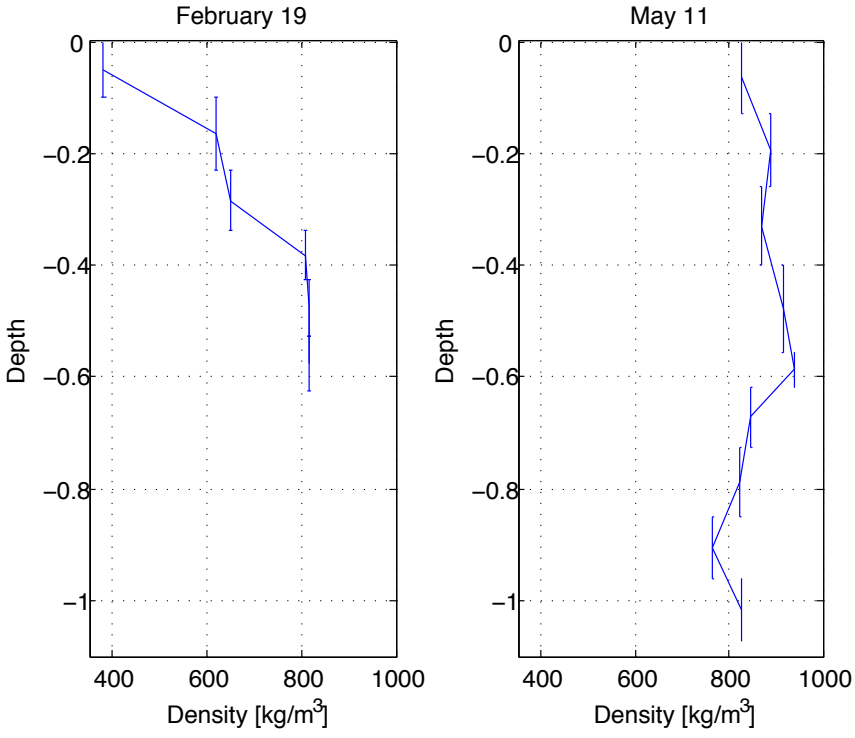

(b)

Figure B.2: *Salinity (a) and density (b) measurements between Crack 1 and Crack 2 in the hinge zone, from February 19 and May 11*

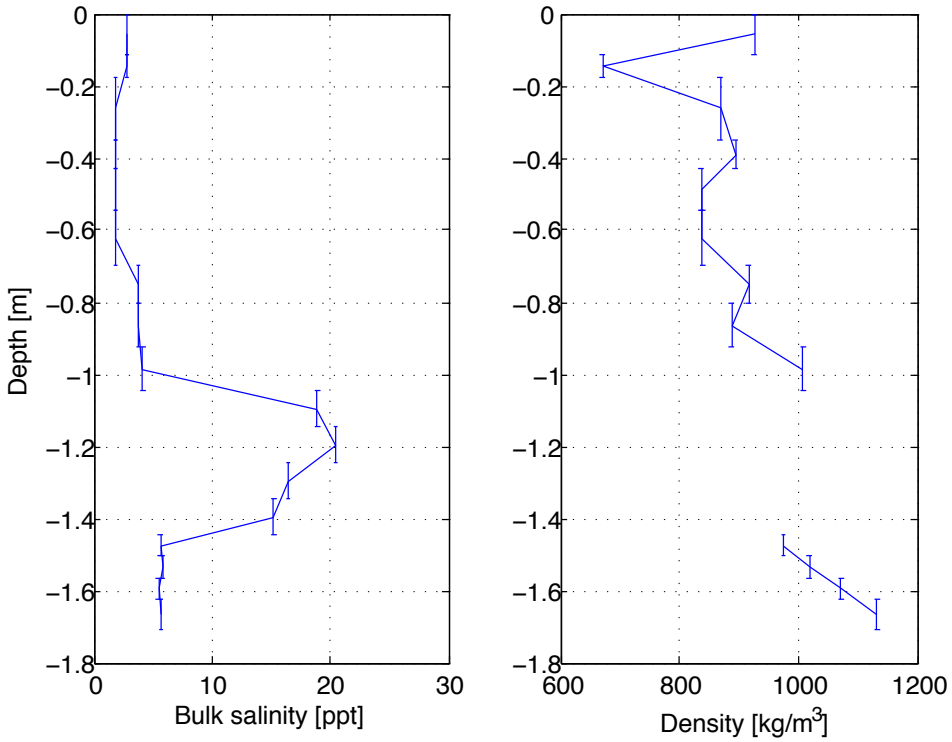

Figure B.3: *Salinity and density of a core taken between Section 1 and Section 2, between Crack 3 and Crack 4 on April 1. A slushy layer inside the ice caused the high salinities and the lack of density data between 1 and 1.4 m depth. Note the ice thickness.*

B.3 Densities at Site 1 and Site 2

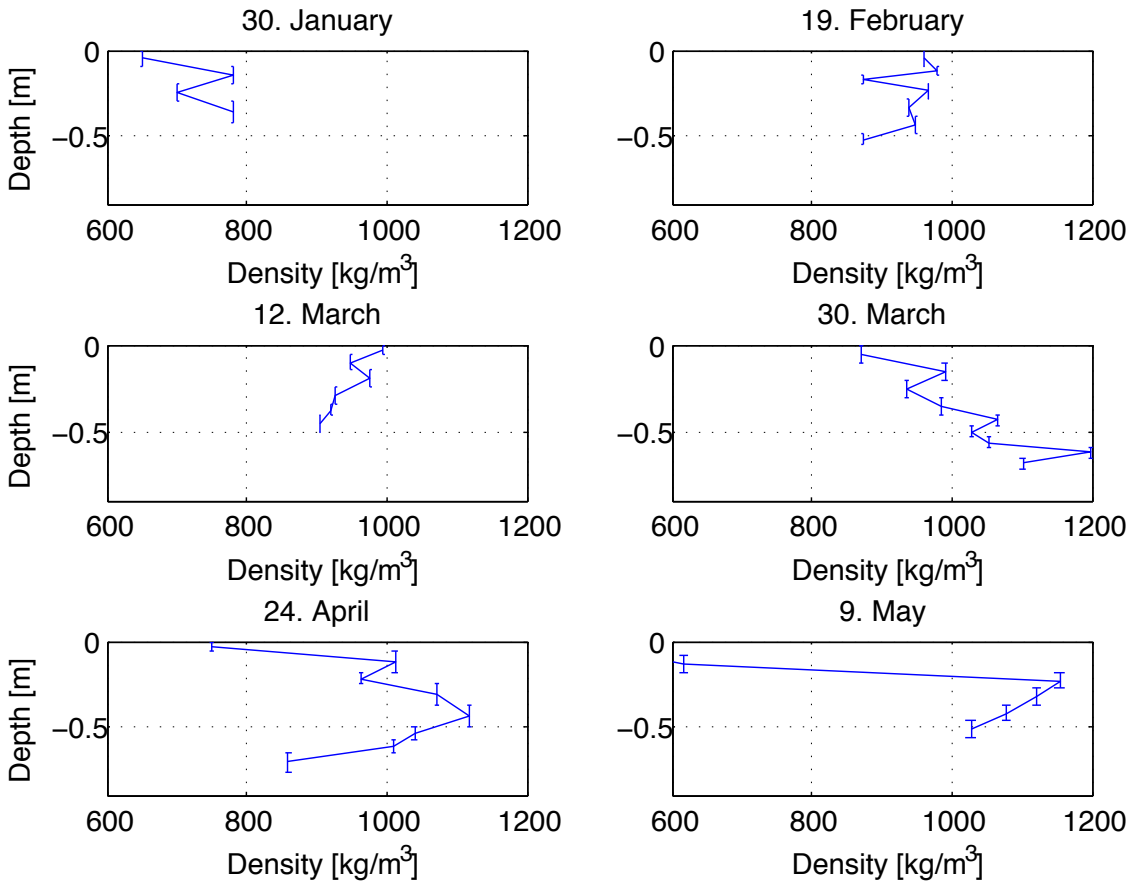

Figure B.4: *Densities recorded at Site 1*

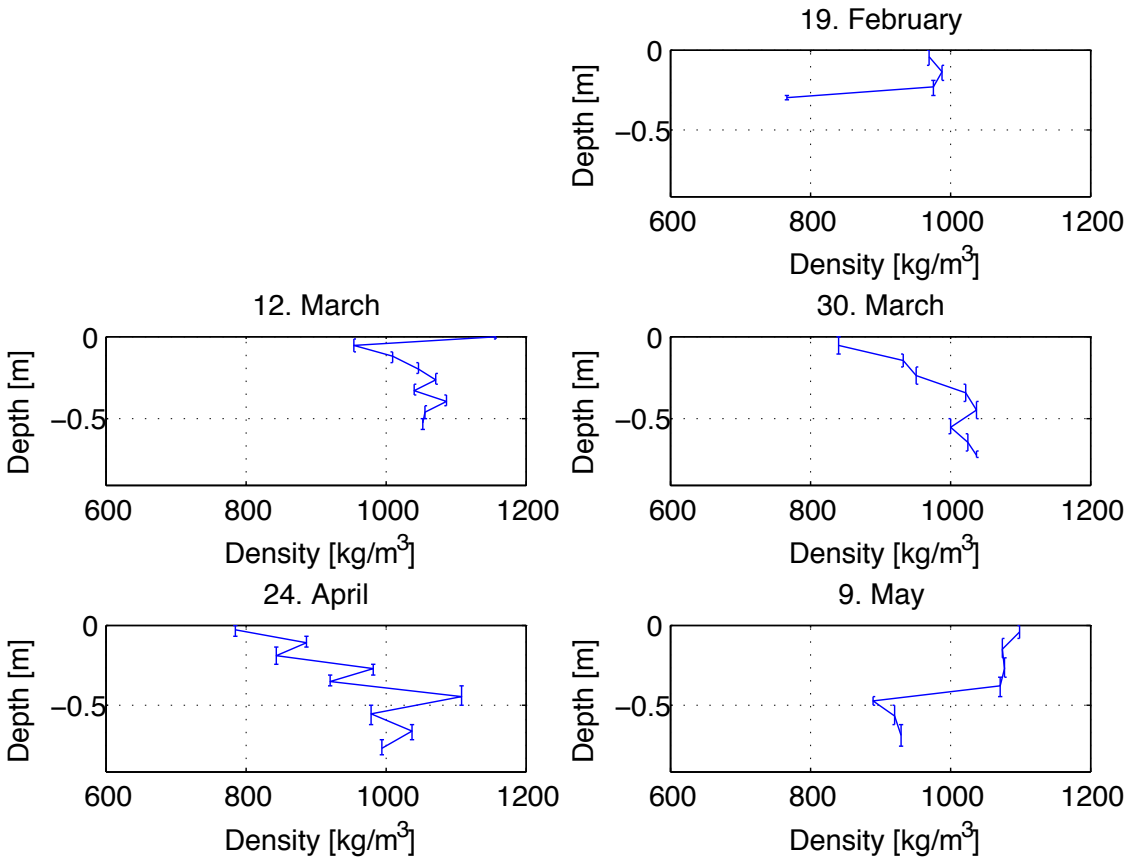

Figure B.5: *Densities recorded at Site 2*

Appendix C

Section 1 Mapped with the DGPS

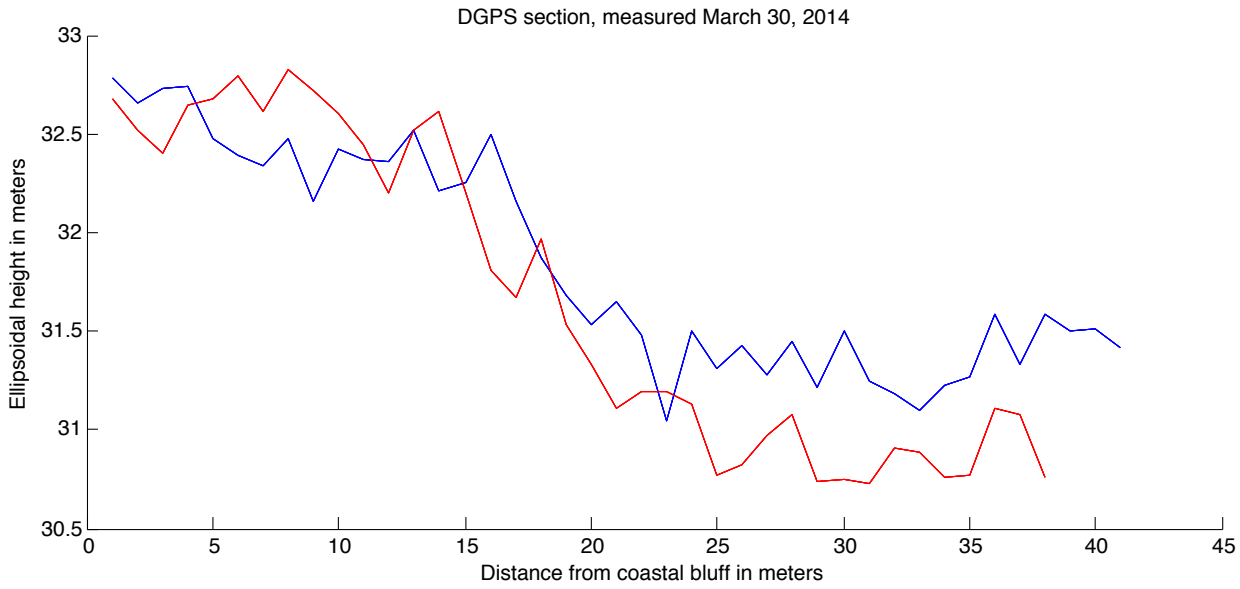

Figure C.1: *Mapping of the ice surface along Section 1 at high and low tide, using DGPS data. The blue line represents the ice surface at high tide*